BIOMEDICAL

PHOTONICS

Volume 14, #3, 2025

In the issue:

- Study of methylene blue photodynamic activity on erythrocyte suspensions in vitro
- Experimental studies X-ray induced cytotoxicity of aqueous colloidal solutions of UV-C luminescent La_{1-x}Pr_xPO₄ nanoparticles
- In vitro photodynamic efficacy of polycationic photosensitizers based on polycationic phthalocyanines
- Application of the Kubelka–Munk model for fast intraoperative analysis of intestinal optical properties using a fiber optic spectrometer
- Multi-course photodynamic therapy in a patient with malignant tumor of the major duodenal papilla. clinical case
- Photodynamic therapy with 5-aminolevulinic acid for basal squamous cell carcinoma



Российская Фотодинамическая Ассоциация



www.pdt-association.com

BIOMEDICAL PHOTONICS

FOUNDERS:

Russian Photodynamic Association
P.A. Herzen Moscow Cancer Research Institute

EDITOR-IN-CHIEF:

Filonenko E.V., Dr. Sci. (Med.), professor, head of the Centre of laser and photodynamic diagnosis and therapy of tumors in P.A.Herzen Moscow Cancer Research Institute (Moscow, Russia)

DEPUTY CHIEF EDITOR:

Grin M.A., Dr. Sci. (Chem.), professor, chief of department of Chemistry and technology of biological active substances named after Preobragenskiy N.A. in Moscow Technological University (Moscow, Russia)

Loschenov V.B., Dr. Sci. (Phys. and Math.), professor, chief of laboratory of laser biospectroscopy in the Natural Sciences Center of General Physics Institute of the Russian Academy of Sciences (Moscow, Russia)

EDITORIAL BOARD:

Kaprin A.D., Academician of the Russian Academy of Sciences, Dr. Sci. (Med.), professor, general director of National Medical Research Radiological Centre of the Ministry of Health of the Russian Federation (Moscow, Russia)

Romanko Yu.S., Dr. Sci. (Med.), professor of the department of Oncology, radiotherapy and plastic surgery named after L.L. Lyovshina in I.M. Sechenov First Moscow State Medical University (Moscow, Russia)

Stranadko E.Ph., Dr. Sci. (Med.), professor, chief of department of laser oncology and photodynamic therapy of State Research and Clinical Center of Laser Medicine named by O.K.Skobelcin of FMBA of Russia (Moscow, Russia)

Blondel V., PhD, professor at University of Lorraine, joint-Head of the Health-Biology-Signal Department (SBS) (Nancy, France)

Bolotine L., PhD, professor of Research Center for Automatic Control of Nancy (Nancy, France)

Douplik A., PhD, professor in Ryerson University (Toronto, Canada)

Steiner R., PhD, professor, the honorary director of Institute of Laser Technologies in Medicine and Metrology at Ulm University (Ulm, Germany)

BIOMEDICAL PHOTONICS -

research and practice, peer-reviewed, multidisciplinary journal. The journal is issued 4 times per year. The circulation – 1000 copies., on a quarterly basis.

The journal is included into the List of peer-reviewed science press of the State Commission for Academic Degrees and Titles of Russian Federation
The journal is indexed in the international abstract and citation database – Scopus.

The publisher «Agentstvo MORE». Moscow, Khokhlovskiy lane, 9

Editorial staff:

Chief of the editorial staff
Science editor professor
Literary editor
Translators
Computer design
Desktop publishing

Ivanova-Radkevich V.I.
Mamontov A.S.
Misseeva R.N.
Kalyagina N.A.
Kreneva E.I.
Shalimova N.M.

The Address of Editorial Office:

Russia, Moscow, 2nd Botkinskiy proezd, 3

Tel. 8 (495) 945–86–60 www: PDT-journal.com E-mail: PDT-journal@mail.ru

Corresponding to:

125284, Moscow, p/o box 13

Registration certificate ПИ № ФС 77–51995, issued on 29.11.2012 by the Federal Service for Supervision of Communications, Information Technology, and Mass Media of Russia

The subscription index of «Rospechat» agency – 70249

The editorial staff is not responsible for the content of promotional material. Articles represent the authors' point of view, which may be not consistent with view of the journal's editorial board. Editorial Board admits for publication only the articles prepared in strict accordance with guidelines for authors. Whole or partial presentation of the material published in the Journal is acceptable only with written permission of the Editorial board.

BIOMEDICAL PHOTONICS

BIOMEDICAL PHOTONICS -

научно-практический, рецензируемый, мультидисциплинарный журнал. Выходит 4 раза в год. Тираж – 1000 экз., ежеквартально.

Входит в Перечень ведущих рецензируемых научных журналов ВАК РФ.
Индексируется в международной реферативной базе данных Scopus.

Издательство «Агентство МОРЕ». Москва. Хохловский пер.. д. 9

Редакция:

Зав. редакцией Иванова-Радкевич В.И. Научный редактор проф. Мамонтов А.С. Литературный редактор Моисеева Р.Н. Калягина Н.А. Компьютерный дизайн Кренева Е.И. Компьютерная верстка Шалимова Н.М.

Адрес редакции:

Россия, Москва, 2-й Боткинский пр., д. 3 Тел. 8 (495) 945–86–60 www: PDT-journal.com E-mail: PDT-journal@mail.ru

Адрес для корреспонденции:

125284, Москва, а/я 13

Свидетельство о регистрации ПИ
№ ФС 77–51995, выдано 29.11.2012 г.
Федеральной службой по надзору в сфере связи, информационных технологий и массовых коммуникаций (Роскомнадзор)

Индекс по каталогу агентства «Роспечать» — 70249

Редакция не несет ответственности за содержание рекламных материалов.

В статьях представлена точка зрения авторов, которая может не совпадать с мнением редакции журнала.

К публикации принимаются только статьи, подготовленные в соответствии с правилами для авторов, размещенными на сайте журнала.

Полное или частичное воспроизведение материалов, опубликованных в журнале, допускается только с письменного разрешения редакции.

УЧРЕДИТЕЛИ:

Российская Фотодинамическая Ассоциация Московский научно-исследовательский онкологический институт им. П.А. Герцена

ГЛАВНЫЙ РЕДАКТОР:

Филоненко Е.В., доктор медицинских наук, профессор, руководитель Центра лазерной и фотодинамической диагностики и терапии опухолей Московского научно-исследовательского онкологического института им. П.А. Герцена (Москва, Россия)

ЗАМ. ГЛАВНОГО РЕДАКТОРА:

Грин М.А., доктор химических наук, профессор, заведующий кафедрой химии и технологии биологически активных соединений им. Н.А. Преображенского Московского технологического университета (Москва, Россия)

Лощенов В.Б., доктор физико-математических наук, профессор, заведующий лабораторией лазерной биоспектроскопии в Центре естественно-научных исследований Института общей физики им. А.М. Прохорова РАН (Москва, Россия)

РЕДАКЦИОННАЯ КОЛЛЕГИЯ:

Каприн А.Д., академик РАН, доктор медицинских наук, профессор, генеральный директор Национального медицинского исследовательского центра радиологии Минздрава России (Москва, Россия)

Романко Ю.С., доктор медицинских наук, профессор кафедры онкологии, радиотерапии и пластической хирургии им. Л.Л. Лёвшина Первого Московского государственного медицинского университета имени И.М. Сеченова (Москва, Россия)

Странадко Е.Ф., доктор медицинских наук, профессор, руководитель отделения лазерной онкологии и фотодинамической терапии ФГБУ «Государственный научный центр лазерной медицины им. О.К.Скобелкина ФМБА России»

Blondel V., профессор Университета Лотарингии, руководитель отделения Здравоохранение-Биология-Сигналы (SBS) (Нанси, Франция)

Bolotine L., профессор научно-исследовательского центра автоматики и управления Нанси (Нанси, Франция)

Douplik A., профессор Университета Райерсона (Торонто, Канада)

Steiner R., профессор, почетный директор Института лазерных технологий в медицине и измерительной технике Университета Ульма (Ульм, Германия)

4

14

24

30

ORIGINAL ARTICLES

Study of methylene blue photodynamic activity on erythrocyte suspensions in vitro

Markova I.V., Ryabova A.V., Romanishkin I.D., Pominova D.V.

Experimental studies X-ray induced cytotoxicity of aqueous colloidal solutions of UV-C luminescent La_{1-} Pr,PO $_4$ nanoparticles

Shaidulin A.T., Orlovskaya E.O., Uvarov O.V., Silaev G.O., Skopin P.I., Gololobova I.A., Aioub A.A.-K., Yakobson D.E., Chernobay R.A., Vainer Y.G., Orlovskii Yu.V, Makhov V.N.

In vitro photodynamic efficacy of polycationic photosensitizers based on polycationic phthalocyanines

Romanishkin I.D., Meerovich I.G., Bunin D.A., Skobeltsin A.S., Akhlyustina E.V., Levkin V.V., Kharnas S.S., Kogan E.A., Zhi-Long Chen, Meerovich G.A., Gorbunova Yu.G., Reshetov I.V.

Application of the Kubelka-Munk model for fast intraoperative analysis of intestinal optical properties using a fiber optic spectrometer

Savelieva T.A., Krivetskaya A.A., Kustov D.M., Klobukov M.I., Romanishkin I.D., Linkov K.G., Levkin V.V., Kharnas S.S., Loschenov V.B.

CASE REPORTS

Multi-course photodynamic therapy in a patient with malignant tumor of the major duodenal papilla. Clinical case

Tseimakh A.E., Shoikhet Ia.N., Tseimakh E.A., Bedyan N.K., Makarenkov A.S.

REVIEWS OF LITERATURE

Photodynamic therapy with 5-aminolevulinic acid for basal squamous cell carcinoma

Filonenko E.V., Ivanova-Radkevich V.I.

ОРИГИНА ЛЬНЫЕ СТАТЬИ

Исследование фотодинамической активности метиленового синего на суспензиях эритроцитов *in vitro*

И.В.Маркова, А.В. Рябова, 4 И.Д. Романишкин, Д.В. Поминова

Рентген-индуцированная цитотоксичность водных растворов УФ-С рентгенолюминесцентных наночастиц $La_{1...}Pr_{...}P0_{...}$

А.Т. Шайдулин, Е.О. Орловская, О.В. Уваров, Г.О. Силаев, П.И. Скопин, И.А. Гололобова, Аюб А.А.-Х., Д.Э. Якобсон, Р.А. Чернобай, Ю.Г. Вайнер, Ю.В. Орловский, В.Н. Махов

Фотодинамическая эффективность in vitro поликатионных фотосенсибилизаторов на основе длинноволновых фталоцианинов

И.Д. Романишкин, И.Г. Меерович, Д.А. Бунин, А.С. Скобельцин, Е.В. Ахлюстина, В.В. Левкин, С.С. Харнас, Е.А. Коган, Zhi-Long Chen, Г.А. Меерович, Ю.Г. Горбунова,

24 И.В. Решетов

14

30

39

Применение модели Кубелки-Мунка для быстрого интраоперационного анализа оптических свойств стенки кишечника с помощью оптоволоконного спектрометра

Т.А. Савельева, А.А. Кривецкая, Д.М. Кустов, М.И. Клобуков, И.Д. Романишкин, К.Г. Линьков, В.В. Левкин, С.С. Харнас, В.Б. Лощенов

КЛИНИЧЕСКИЕ НАБЛЮДЕНИЯ

Многокурсовая фотодинамическая терапия у пациента со злокачественным новообразованием большого дуоденального сосочка. Клинический случай

А.Е. Цеймах, Я.Н. Шойхет, Е.А. Цеймах, Н.К. Бедян, А.С. Макаренков

ОБЗОРЫ ЛИТЕРАТУРЫ

Фотодинамическая терапия с 5-АЛК больных базальноклеточным раком кожи

43 Е.В. Филоненко, В.И. Иванова-Радкевич

43

39



STUDY OF METHYLENE BLUE PHOTODYNAMIC ACTIVITY ON ERYTHROCYTE SUSPENSIONS IN VITRO

Markova I.V.^{1,2}, Ryabova A.V.^{1,2}, Romanishkin I.D.¹, Pominova D.V.^{1,2}

¹Prokhorov General Physics Institute of Russian Academy of Sciences, Moscow, Russia

²National Research Nuclear University MEPhI (Moscow Engineering Physics Institute), Moscow, Russia

Abstract

In this paper we studied the photodynamic activity (the rate of molecular oxygen utilization during irradiation) of methylene blue (MB) in erythrocyte suspensions in vitro. Using spectroscopy and confocal microscopy with fluorescent sensors for singlet oxygen and other active oxygen species, it was shown that with an increase in the MB concentration (10–100 mg/kg), the molar photodynamic activity decreases. It was found that 5–10% of the MB added to erythrocytes tightly binds to the erythrocyte membranes, and the generation of singlet oxygen ($^{1}O_{2}$) is suppressed in favor of type I reactions (formation of $H_{2}O_{2}$, O_{2} , * , * OH). Another 40% of the MB added to erythrocytes is converted into a colorless leuco form, but is reoxidized back to MB under photodynamic exposure. The maximum relative quantum yield of $^{1}O_{2}$ generation (ϕ_{Δ}) among those measured in erythrocyte suspensions was 0.014 for a 10 mg/kg MB concentration, which is an order of magnitude lower than the values for MB in organic solvents and for the aluminum sulfonated phthalocyanine comparison photosensitizer (PS) (ϕ_{Δ} = 0.38). Interaction with erythrocytes (aggregation, reduction to the leuco form, competition for oxygen) explains the decrease in the MB efficiency under physiological conditions compared to organic solvents. The obtained results are important from the point of view of optimizing the systemic use of MB in photodynamic therapy.

Keywords: methylene blue, spectroscopy, absorption, fluorescence, photobleaching, ROS, singlet oxygen.

Contacts: Pominova D.V., e-mail: pominovadv@gmail.com

For citations: Markova I.V., Ryabova A.V., Romanishkin I.D., Pominova D.V. Study of methylene blue photodynamic activity on erythrocyte suspensions *in vitro*, *Biomedical Photonics*, 2025, vol. 14, no. 3, pp. 4–13. doi: 10.24931/2413–9432–2025–14–3–4–13

ИССЛЕДОВАНИЕ ФОТОДИНАМИЧЕСКОЙ АКТИВНОСТИ МЕТИЛЕНОВОГО СИНЕГО НА СУСПЕНЗИЯХ ЭРИТРОЦИТОВ IN VITRO

И.В.Маркова 1,2 , А.В. Рябова 1,2 , И.Д.Романишкин 1 , Д.В. Поминова 1,2

¹Институт общей физики им. А. М. Прохорова Российской академии наук, Москва, Россия ²Национальный исследовательский ядерный университет «МИФИ», Москва, Россия

Резюме

В работе исследована фотодинамическая активность (по скорости утилизации молекулярного кислорода при облучении) метиленового синего (МС) в суспензиях эритроцитов *in vitro*. Методами спектроскопии и конфокальной микроскопии с флуоресцентными сенсорами на синглетный кислород и другие активные формы кислорода показано, что при увеличении концентрации МС (10-100 мг/кг) молярная фотодинамическая активность снижается. Установлено, что 5-10% от добавленного к эритроцитам МС прочно связывается с мембранами эритроцитов, а генерация синглетного кислорода ($^{1}O_{2}$) подавляется в пользу реакций I типа (образование $H_{2}O_{2}$, O_{2} , $^{-}$, $^{-}$ OH). Еще порядка 40% от добавленного к эритроцитам МС переходит в бесцеетную лейкоформу, однако при фотодинамическом воздействии окисляется обратно до МС. Максимальный квантовый выход генерации $^{1}O_{2}$ (ϕ_{Δ}) в суспензиях эритроцитов составил 0,014 для концентрации МС 10 мг/кг, что на порядок ниже значений для МС в органических растворителях и для фотосенсибилизатора сравнения фотосенс ($\phi_{\Delta} = 0,38$). Взаимодействие с эритроцитами (агрегация, восстановление в лейкоформу, конкуренция за кислород) объясняет снижение эфективности МС в физиологических условиях по сравнению с органическими растворителями. Полученные результаты важны с точки зрения оптимизации системного применения МС в фотодинамической терапии.

Ключевые слова: метиленовый синий, спектроскопия, поглощение, флуоресценция, фотообесцвечивание, АФК, синглетный кислород.

Контакты: Поминова Д.В., e-mail: pominovadv@gmail.com

Для цитирования: Маркова И.В., Рябова А.В., Романишкин И.Д., Поминова Д.В. Исследование фотодинамической активности метиленового синего на суспензиях эритроцитов *in vitro* // Biomedical Photonics. – 2025. – Т. 14, № 3. – С. 4–13. doi: 10.24931/2413–9432–2025–14–3–4–13

Introduction

Photodynamic Therapy (PDT) is a method based on the interaction of a photosensitizer (PS), light of a specific wavelength, and molecular oxygen (3O_2). The interaction of these components results in the formation of cytotoxic reactive oxygen species (ROS). Upon light irradiation, the PS transition from its ground state to an excited singlet state occurs, followed by intersystem conversion to a triplet state. Depending on the ROS generation mechanism, two types of reactions are distinguished: Type I – hydrogen removal or electron transfer between the PS excited triplet state and a substrate, leading to the formation of free radicals (H_2O_2 , •OH, O_2 •-); Type II – energy transfer from the PS triplet state to molecular oxygen, generating highly reactive singlet oxygen (1O_2) [1, 2].

Singlet oxygen generation results in a potent cytotoxic effect and is a more efficient mechanism of photodynamic action. However, although the Type II mechanism is considered dominant in most PDT scenarios, Type I becomes more relevant under the hypoxic conditions, characteristic for tumor tissues [3, 4]. The cytotoxic ROS generated by Type I photodynamic reactions, including H_2O_2 , •OH, and O_2 •¯, can stimulate cell apoptosis or necrosis, vascular damage, and immune system activation [5, 6]. PDT is currently widely used in clinical practice [7–12].

The ratio between Type I and Type II reactions depends on the photophysical properties of the chosen PS. Methylene blue (MB), a cationic thiazine dye, is extensively studied as a PS. MB has been used effectively for PDT of various tumors [13]. According to the literature, MB can generate singlet oxygen with a high quantum yield ($\phi\Delta$ ~0.5 in CH₃OH, 0.52 in EtOH), which, combined with relatively low dark toxicity [14, 15], makes it an attractive PS. However, it should be noted that measurements of singlet oxygen quantum yield are primarily performed in ethanol or organic solvents [15].

Currently, the clinical application of MB is limited by several factors related to its aggregation in aqueous environments and interactions with biological systems, such as erythrocytes. In aqueous solutions at concentrations about 10 µM, MB tends to aggregate, forming dimers, trimers, and higher-order aggregates [16, 17]. Aggregate formation alters absorption and fluorescence spectra, fluorescence lifetime, and the photophysical characteristics of the dye, thereby affecting its photodynamic activity and efficacy as a PS [5, 18]. MB forms H-aggregates, whose fluorescence intensity is lower than that of monomers; consequently, luminescence intensity decreases as the dimer/ monomer ratio increases. A strong correlation has been demonstrated between changes in photophysical properties and solvent polarity, viscosity, and dielectric constant. The critical concentration for MB aggregation is higher in solvents with a greater dielectric constant, and MB aggregation in alcohols differs from that in

aqueous solutions, highlighting the importance of the solvent environment for studies of MB aggregation and photophysical properties in medical applications [17]. Data indicate that MB aggregation and dimerization also alter the type of photodynamic reaction [18]; MB dimers predominantly undergo electron transfer pathways to deactivate the excited state (Type I reaction), with almost complete suppression of singlet oxygen generation [19].

Beyond concentration-dependent aggregation, the positively charged MB can bind to negatively charged cell membranes [19, 20]. The interaction of MB with erythrocytes has been actively investigated in the context of treating methemoglobinemia - a condition caused by oxidative stress where hemoglobin is oxidized to methemoglobin (MetHb), losing its oxygen-carrying capacity [21]. Upon interaction with erythrocytes, MB accumulates within them via a "reductive uptake" mechanism: upon entering the cell, it is reduced by NADPH-dependent enzymes of the pentose phosphate pathway to colorless leuco-methylene blue (LMB), which does not absorb light in the red region, loses its photosensitizing ability, and is retained intracellularly until re-oxidation occurs [22]. During methemoglobinemia, MB within erythrocytes acts as a cofactor for the flavin reductase enzyme (biliverdin reductase B, BLVRB), accelerating the reduction of MetHb to functional hemoglobin: oxidized MB (blue) accepts electrons from NADPH via BLVRB, converting to LMB. LMB directly reduces MetHb, itself being oxidized back to MB and closing the catalytic cycle [21, 23– 26]. This process can limit the photodynamically effective concentration of MB after its systemic administration.

MB enhances the respiratory metabolism of erythrocytes, increasing O_2 consumption, which may lead to hypoxia in the irradiation zone [27]. However, in the case of tumors, systemic administration in vivo may conversely increase oxygenation over time due to a metabolic shift towards oxidative phosphorylation [28, 29].

Thus, numerous factors influence the photodynamic activity of MB. Although the interaction of MB with erythrocytes has been well studied in the context of methemoglobinemia treatment, the impact of this interaction on MB's photodynamic activity has not been studied. Under physiological conditions, MB's behavior fundamentally differs from that in organic solvents and alcohols: interaction with erythrocytes, reduction to the leuco-form, and competition for oxygen radically alter its photophysical properties upon systemic administration.

In this work, we investigated the photodynamic activity of MB in erythrocyte suspensions, assessing the influence of dimerization, reduction to LMB, and interaction with erythrocytes on the type of photodynamic reaction (I or II). The results will enable optimization of PDT parameters for systemic MB administration, explain the limitations of its clinical application, and propose strategies to overcome these limitations.



Materials and methods

Sample Preparation

An erythrocyte suspension was prepared in saline (40% red blood cells, 60% saline). The suspension pH was maintained at physiological level. The erythrocyte suspension was then mixed with the investigated PS in a 1.5 ml Eppendorf tube and incubated at 37°C in complete darkness. A 1% aqueous solution of MB (JSC "Samaramedprom", Russia) was used. The investigated MB concentrations were 0, 1, 10, 20, 40, 60, 80, and 100 mg/kg. For comparison, the aluminum sulfonated phthalocyanine-based PS photosens® (NIOPIK, Russia) was used at a concentration of 1 mg/kg; its singlet oxygen quantum yield is reported to be 0.38.

Detection of ROS and Singlet Oxygen Using Fluorescent Indicators

The fluorescent indicator 6-carboxy-2',7'-dichlorodihydrofluorescein diacetate (c-H₂DCFDA, Lumiprobe, Russia) at 25 µM was used to assess ROS generation (H₂O₂, O₂•-, •OH, ROOH, ONOO-). Singlet Oxygen Sensor Green (SOSG, Lumiprobe, Russia) at 10-100 µM was used to detect singlet oxygen (¹O₂) in aqueous solutions. The erythrocyte suspension was incubated with MB (0-100 mg/kg) in saline for 30 min at 37°C. The fluorescent indicator was then added, followed by another 30 min incubation. To generate ROS, samples were irradiated with a laser (660 nm, 40 mW/cm², dose 50 J/cm²). Fluorescence of the ROS indicators (c-H₂DCFDA and SOSG) was recorded using an inverted confocal microscope LSM-710-NLO (Carl Zeiss, Germany) with 488 nm excitation and detection in the 510-580 nm range. Additionally, PS fluorescence was recorded using 633 nm laser excitation and signal detection in the 650-730 nm range. Fluorescence intensities of the indicators and PS were analyzed, averaged over the image.

Spectrophotometric Analysis of MB Aggregation and Binding to Erythrocytes

Incubation of PS with erythrocyte suspensions was performed for 15 min, after which absorption spectra were measured. To evaluate MB binding to erythrocytes, samples were centrifuged for 5 min at 3570 g, the supernatant was removed and replaced with fresh saline (this procedure was repeated twice), and measurements were repeated.

Absorption spectra were recorded using a Hitachi U3400 spectrophotometer (Japan) in quartz cuvettes (1 mm optical path) over the 200-1000 nm range. To analyze MB aggregation and binding to erythrocytes, the spectra were approximated by the sum of three spectra corresponding to erythrocyte absorption, MB absorption at 10 mg/kg, and background signal (scattering). The shape of the experimental spectrum and the approximation were compared, and differences were analyzed. Since the shape of the MB absorption spectrum depends on concentration, the form of the MB

absorption spectrum was determined by subtracting the approximated erythrocyte absorption spectra and background from the experimentally recorded absorption spectra of erythrocyte suspensions containing MB.

Evaluation of MB Photodynamic Activity and Singlet Oxygen Generation Efficiency by Spectroscopic Methods

The photodynamic activity of MB was assessed spectroscopically by the rate of hemoglobin deoxygenation during PDT [30, 31] with PS (MB or aluminum sulfonated phthalocyanine) on erythrocyte suspensions.

Samples consisted of an erythrocyte suspension with PS in saline, were placed between two coverslips separated by a 200 µm thick plastic spacer. The sample volume was 100 μl. Hemoglobin oxygenation was evaluated based on absorption spectra measured using a LESA-01-Biospec spectrophotometer (Biospec, Russia) with a halogen lamp light source. This was done by approximating the measured absorption spectrum as the sum of the absorption spectra of oxygenated hemoglobin, deoxygenated hemoglobin, and background scattering (linear dependence). Hemoglobin oxygenation was calculated as the ratio of oxygenated hemoglobin absorption to the total (oxyand deoxy-) hemoglobin absorption. For PDT, samples were irradiated within the PS absorption band using a semiconductor laser source (wavelength 660 nm, power density 167 mW/cm²; irradiation duration 8 min). The experimental setup is shown in Fig. 1.

During PDT mediated by a Type II PS, the generated $^{1}O_{2}$ undergoes irreversible reactions with biological molecules, leading to a decrease in dissolved $^{3}O_{2}$ in the sample and, consequently, hemoglobin deoxygenation. Thus, the photodynamic activity of the investigated PS can be evaluated by the rate of hemoglobin deoxygenation.

The relative quantum yield of 1O_2 generation ($\varphi\Delta$) can be quantitatively assessed to evaluate PS efficiency. This requires comparing the hemoglobin deoxygenation rate using the investigated PS with the rate using a PS of known quantum yield. The relative quantum yield of 1O_2 generation for MB concentrations of 10-100 mg/kg can then be calculated using the relationship:

$$\varphi_{\Delta}(MB) = \frac{C(PS) \cdot \tau(PS)}{C(MB) \cdot \tau(MB)} \cdot \varphi_{\Delta}(PS) \tag{1}$$

where C is concentration and τ is deoxygenation time. The τ value was determined from experimentally measured deoxygenation curves using the doseresponse relationship:

$$f(t) = \max -\frac{max - min}{1 + \left(\frac{t}{\tau}\right)^{min}},$$
 (2)

where *t* is time, *max* is the maximum asymptote value, *min* is the minimum asymptote value (Fig. 2).

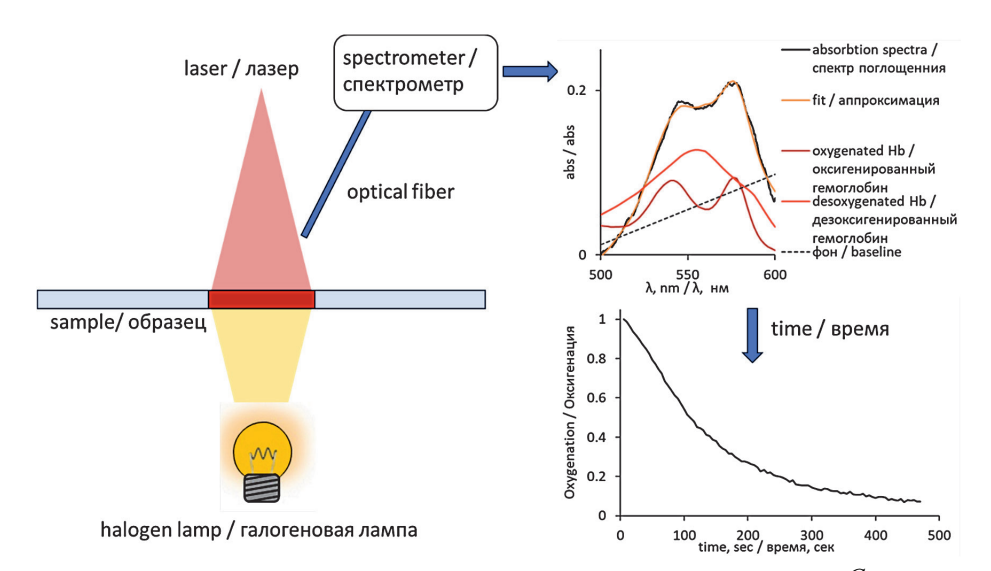


Рис. 1. Схема установки для измерения скорости дезоксигенации гемоглобина.

Fig. 1. Schematic representation of the setup for hemoglobin deoxygenation rate measuring.

The difference between the maximum and minimum asymptotes (delta, the change in oxygenation value over a measured time interval) and the steepness of the curve slope (deoxygenation rate) were also determined from the dependence.

In addition to the relative quantum yield, the photodynamic activity of MB was calculated as a quantitative characteristic of $^{1}O_{2}$ generation efficiency. It is known that during PDT, if oxygen deficiency is not a limiting factor and under low irradiance where ground state PS depletion is negligible, the oxygen consumption rate is expressed by the following equation:

$$\Gamma_{PDT} = \alpha \cdot \varphi_{ch} \cdot C \cdot P, \tag{3}$$

where Γ_{PDT} is the oxygen consumption rate, M/(l·s); α is the singlet oxygen generation efficiency coefficient, cm²/J; φ_{ch} is the quantum yield of chemical (irreversible) quenching of 1O_2 ; C is the molar concentration of PS, M; P is the irradiance, W/cm². The singlet oxygen generation efficiency coefficient (i.e., the number of 1O_2 molecules generated per PS molecule per light dose of 1 J/cm²) is calculated by:

$$\alpha = \frac{\sigma}{E_{loc}} \cdot \varphi_{\Delta} \approx 1.923 \times 10^{-5} \cdot \varepsilon \cdot \lambda \cdot \varphi_{\Delta}, \tag{4}$$

where $\sigma = \frac{ln10 \cdot \varepsilon}{N_{\scriptscriptstyle A}} -$ absorption cross-section of the PS

molecule, cm²; $E_{hv} = \frac{h \cdot c}{\lambda}$ – photon energy, J; ϕ_{Δ} – quantum

yield of $^{1}O_{2}$ formation; λ – irradiation wavelength, nm; ε – extinction coefficient of the PS, L·mol $^{-1}$ ·cm $^{-1}$. We used extinction coefficient values ε in saline at λ =660 nm: for MB 53300 L·mol $^{-1}$ ·cm $^{-1}$ [32], for aluminum sulfo-nated phthalocyanine 82000 L·mol $^{-1}$ ·cm $^{-1}$.

The PDT oxygen consumption rate $\Gamma_{_{PDT}}$ can also be experimentally estimated from the change in hemoglobin oxygen saturation in the sample:

$$\Gamma_{PDT} = -4 \cdot \left[Hb_{tot} \right] \cdot \frac{dS_{O_2}}{dt},\tag{5}$$

where $[Hb_{tot}] = \frac{C_{Hb}}{M_{Hb}}$ – total molar concentration of hemoglobin tetramer in the sample, mol/L; $\frac{dS_{O_2}}{dt}$ – rate

of change of hemoglobin oxygen saturation; C_{Hb} – hemoglobin concentration in blood (typically 130-150 g/L, in our case 152 g/L), g/L; M_{-Hb} = 66,500 g/mol – molecular weight of the hemoglobin molecule (tetramer).

Due to the low probability of chemical quenching of ${}^{1}\text{O}_{2}$ molecules, it is more convenient to evaluate the photodynamic activity Ψ as the probability of chemical quenching of a ${}^{1}\text{O}_{2}$ molecule per 100 photons absorbed by the PS: $\Psi = \varphi_{\Lambda} \cdot \varphi_{ch} \cdot 100. \tag{6}$

Using equations (3 – 5) and substituting the value of $\phi_{_ch'}$ we obtain from the slope of the experimental hemoglobin deoxygenation curve at the initial time point after PDT onset:

$$\Psi = 5.2 \times 10^{6} \cdot \frac{-4 \left[Hb_{tot} \right] \cdot \frac{dS_{O_{2}}}{dt}}{\lambda \cdot \varepsilon \cdot C \cdot P}, \tag{7}$$

where $\frac{dS_{O_2}(0)}{dt} = \frac{S_{O_2}(0)}{\tau}$ – rate of change of hemoglobin

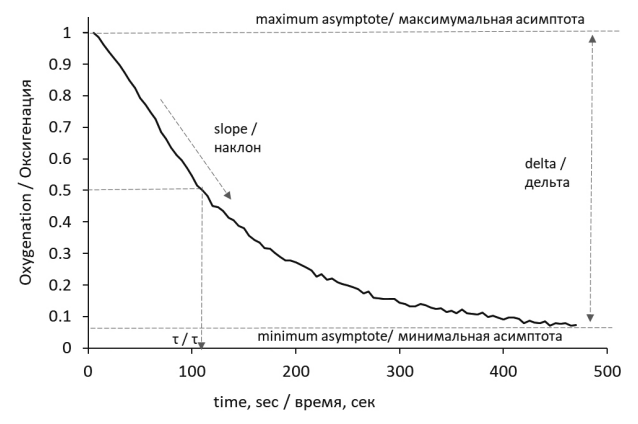


Рис. 2. Зависимость «доза-ответная реакция» и ее основные параметры.

Fig. 2. Dose-response function and its main parameters.



oxygen saturation at the initial moment of irradiation. Substituting PS molar concentrations in μ M, wavelength 660 nm, irradiance 167 mW/cm², and an initial hemoglobin oxygenation level of 0.7 for our samples, we obtain the resulting formula for calculating the photodynamic activity of MB:

$$\Psi = 3.02 \times 10^8 \cdot \frac{1}{\varepsilon \cdot C \cdot \tau}.$$
 (8)

All measurements were performed in triplicate and then averaged. Data are presented as mean \pm standard deviation. Groups were compared using Student's t-test (p < 0.05 considered significant).

Results and discussion

Investigation of Methylene Blue Photodynamic Activity Using Fluorescent Indicators

Results of studying the photodynamic activity of MB and aluminum sulfonated phthalocyanine using fluorescent indicators – SOSG for detecting singlet oxygen ($^{1}O_{2}$) and c-H $_{2}$ DCFDA for detecting ROS other than singlet oxygen ($^{1}O_{2}$) o $_{2}$. •OH) – revealed that irradiation of erythrocyte suspensions with aluminum sulfonated phthalocyanine resulted in increased SOSG fluorescence intensity compared to the control, indicating singlet oxygen generation. The fluorescence intensity of aluminum sulfonated phthalocyanine increased with increasing irradiation dose, Fig. 3.

After 10 min of irradiation, SOSG fluorescence intensity decreased due to erythrocyte lysis and quenching of the indicator's fluorescence by hemoglobin. SOSG fluorescence intensity after irradiation of erythrocyte suspensions with MB was significantly lower than with aluminum sulfonated phthalocyanine and remained unchanged with increasing irradiation dose. It is also noteworthy that at the same irradiation dose, SOSG fluorescence intensity slightly decreased with increasing MB concentration, suggesting suppression of ¹O₂ generation associated with MB aggregation.

The fluorescence intensity of the PS itself as a function of irradiation dose was also assessed, Fig. 4.

The fluorescence intensity of aluminum sulfonated phthalocyanine and MB showed no significant change

with irradiation dose. Probable explanations include dissociation of MB dimers at low doses, followed by photobleaching and conversion of MB to LMB in an oxygen-depleted environment.

When studying erythrocyte suspensions with c-H₂DCFDA and MB, an increase in indicator fluorescence intensity was observed with increasing MB concentration, indicating the role of MB aggregation in shifting towards Type I reactions and ROS generation, Fig. 5.

Interestingly, an increase in c-H₂DCFDA fluorescence intensity after irradiation was observed for both MB and aluminum sulfonated phthalocyanine, the latter being a Type II PS primarily generating singlet oxygen. Although ¹O₂ poorly oxidizes c-H₂DCFDA to its fluorescent form directly, several indirect mechanisms may explain this phenomenon in erythrocyte suspensions [33–36]. Firstly, indirect oxidation of c-H₂DCFDA via secondary ROS is possible. Reactions of ¹O₂ or radicals formed during its interaction can lead to hydrogen peroxide (H₂O₂) formation and increased c-H₂DCFDA fluorescence. The influence of this mechanism is supported by studies in physiological saline without erythrocytes (Fig. 5), where an increase in c-H₂DCFDA fluorescence after irradiation was also observed.

In erythrocyte suspensions with aluminum sulfonated phthalocyanine, the c-H₂DCFDA signal increase was more pronounced compared to physiological saline, likely due to additional indirect oxidation via products of ¹O₂ reactions with cellular components. Singlet oxygen is highly reactive with double bonds in erythrocyte membrane lipids, leading to lipid hydroperoxide (LOOH) formation. Singlet oxygen can also damage heme, releasing iron, a potent catalyst for Fenton/Haber-Weiss reactions generating ROS. Methemoglobin (MetHb, Fe³⁺) or heme itself can decompose LOOH or H₂O₂ (formed from other ROS), generating highly reactive radicals (LO•, •OH) that oxidize c-H2DCFDA. Fe²⁺ ions also catalyze LOOH decomposition via the Fenton reaction:

$$LOOH + Fe^{2+} \rightarrow LO^{-} + OH^{-} + Fe^{3+},$$
 (9)

producing lipid alkoxyl radicals (LO•) that oxidize c-H₂DCFDA and initiate lipid peroxidation chain reactions,

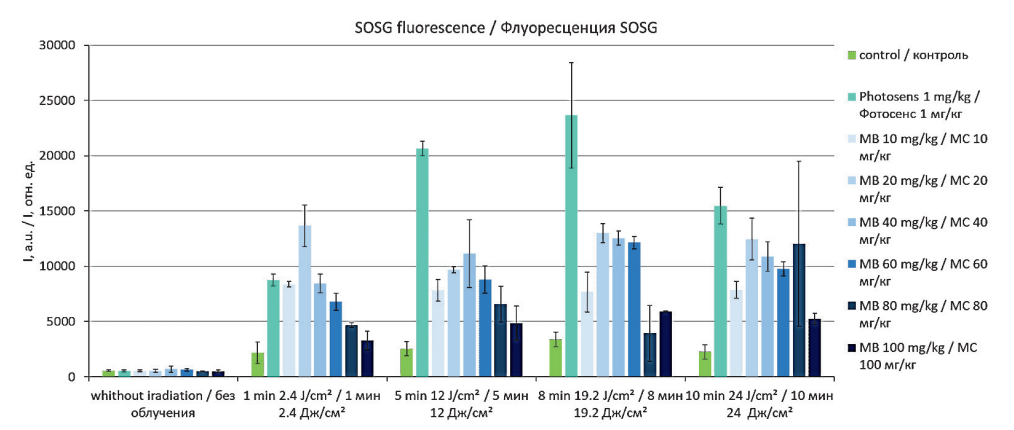


Рис. 3. Зависимость интенсивности флуоресценции индикатора SOSG для выявления синглетного кислорода от дозы облучения при различных концентрациях ФС.

Fig. 3. Dependence of the indicator for detecting singlet oxygen SOSG fluorescence intensity on the radiation dose at different concentrations of PS.

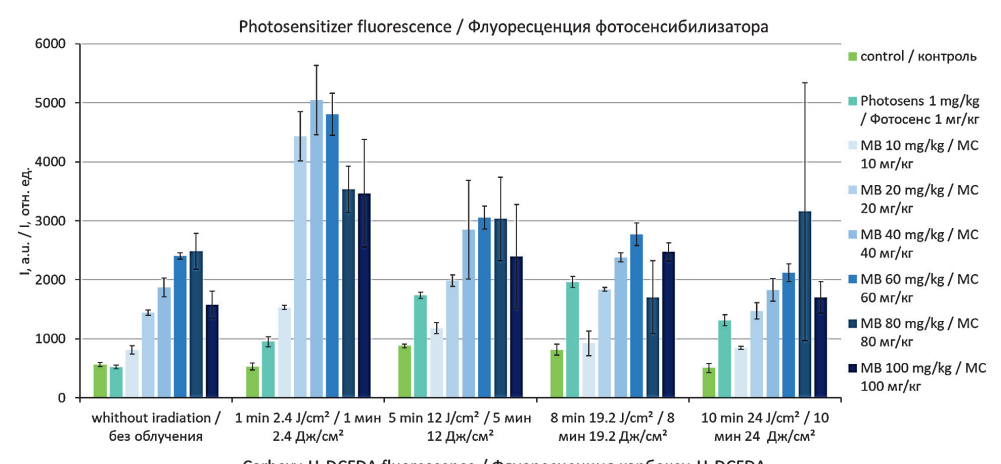




Fig. 4. Dependence of the studied PS fluorescence intensity on the irradiation dose at different concentrations of PS.

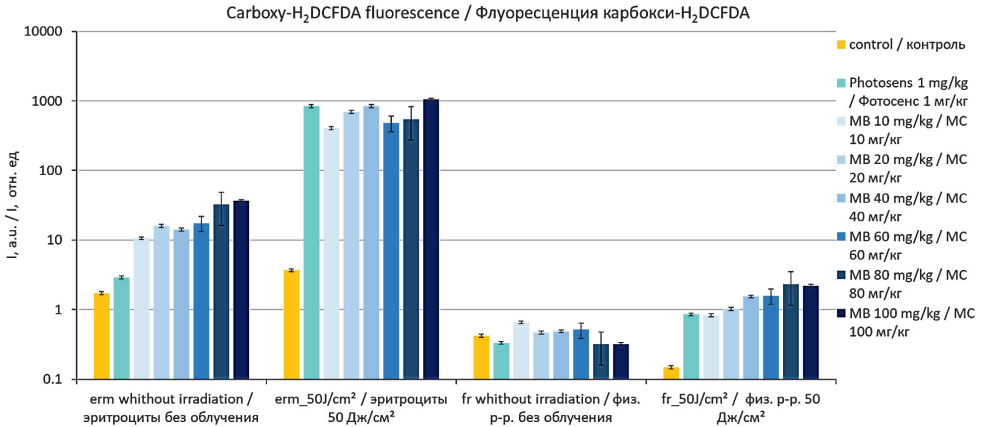


Рис. 5. Зависимость интенсивности флуоресценции индикатора с-H₂DCFDA для выявления АФК, отличных от синглетного кислорода. от дозы облучения при различных концентрациях ФС. Fig. 5. Dependence of the indicator for detecting ROS other than singlet oxygen c-HaDCFDA fluorescence intensity on the irradiation dose at different concentrations of PS.

generating new radicals (L•, LOO•) and peroxides, which can also oxidize c-H₂DCFDA.

эритроциты без облучения

Thus, c-H₂DCFDA fluorescence after irradiating erythro-cyte suspensions with a PS is a direct consequence of potent ¹O₂ generation within the lipid-rich, catalystabundant erythrocyte environment. 102 triggers a cascade of secondary reactions, and c-H2DCFDA detects not the primary ¹O₂ itself, but the total oxidative stress arising from its reaction with key erythrocyte components and subsequent chain reactions catalyzed by hemoglobin and iron. The role of erythrocyte interaction is confirmed by the increased c-H₂DCFDA signal in control erythrocyte suspensions without added PS compared to physiological

When interpreting these results, it is important to consider sensor limitations. SOSG is relatively specific to ${}^{1}O_{2}$ but can react with other oxidants. c-H2DCFDA is oxidized by a broad spectrum of ROS and is non-specific. Moreover, hemoglobin itself can influence indicator fluorescence (absorption quenching) or conversely catalyze their oxidation. However, the contrast between the SOSG fluorescence data (aluminum sulfonated phthalocyanine >> MB) and c-H₂DCFDA data (MB > aluminum sulfonated phthalocyanine) convincingly indicates the predominance of different photodynamic mechanisms: Type II for aluminum sulfonated phthalocyanine and a mixed I/ Il type with dominance of Type I for MB in this system. Spectroscopic methods without additional indicators

may provide more precise results and allow quantitative assessment of ${}^{1}O_{2}$ generation efficiency.

Spectral Analysis of MB Aggregation and Binding to **Erythrocytes**

To evaluate MB aggregation upon interaction with erythrocytes, absorption spectra were recorded and changes in their shape within the 600-700 nm region (corresponding to MB absorption) were analyzed. Absorption spectra recorded for erythrocyte suspensions with various MB concentrations and their approximation as the sum of erythrocyte suspension and MB solution spectra are presented in Fig. 6.

Increasing of MB concentration led to greater divergence between experimentally measured spectra and the approximation. To recover the true absorption spectrum shape corresponding to MB within the erythrocyte suspension, the approximated erythrocyte absorption spectra and background were subtracted from the experimental data. The resulting MB absorption spectra were compared with experimental absorption spectra of the supernatant after centrifuging the MBtreated erythrocyte suspension, Fig. 7.

The shape of the absorption spectrum obtained via decomposition and subtraction completely matched the supernatant absorption spectrum and the shape of the MB spectrum in physiological saline, indicating that no additional MB aggregation occurs upon interaction with erythrocytes.



To assess MB binding to erythrocytes, absorption spectra of erythrocyte suspensions were recorded after centrifugation and three additional washes to remove unbound MB, followed by approximation, Fig. 8.

The MB absorption spectra obtained via approximation show that after washing, the MB absorption peak (~664 nm) is still present in the erythrocyte suspension spectra. Approximately 5% of the initial MB concentration (~5 mg/kg for an initial concentration of 100 mg/kg) remained bound to the erythrocytes.

Thus, it can be concluded that while interaction with erythrocytes does not induce additional aggregation, a portion of MB binds to erythrocyte membranes via electrostatic interactions.

Hemoglobin Deoxygenation Kinetics

Deoxygenation curves recorded for erythrocyte suspensions with different MB concentrations are presented in Fig. 9.

During irradiation, the hemoglobin deoxygenation rate increased with MB concentration. Interestingly, the deoxygenation rate for the sample with an initial MB concentration of 100 mg/kg, after washing to remove

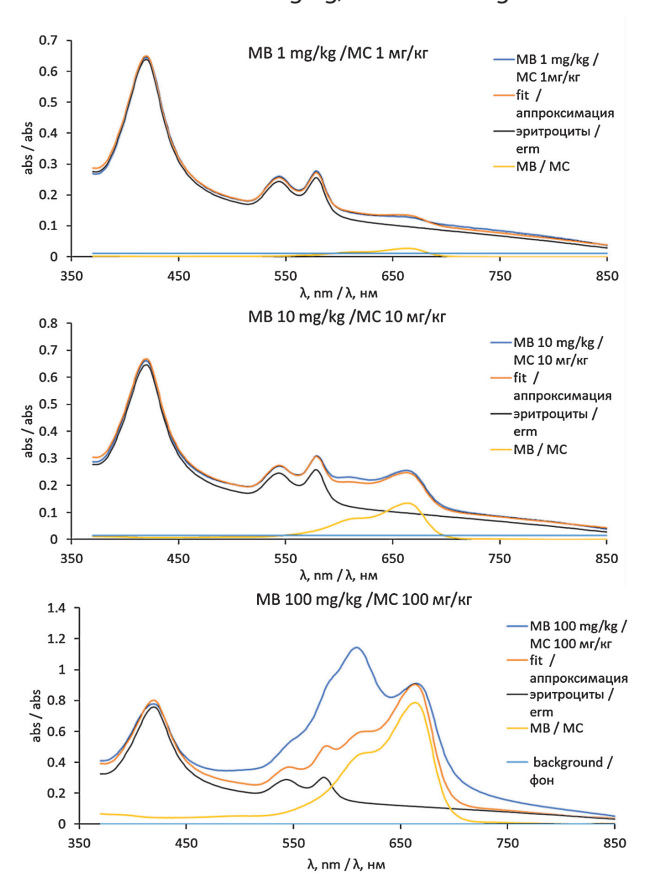


Рис. 6. Спектры поглощения, зарегистрированные для суспензии эритроцитов с концентрациями МС 1, 10 и 100 мг/кг, и их аппроксимация суммой спектров поглощения суспензии эритроцитов и раствора МС.

Fig. 6. Absorption spectra recorded for erythrocyte suspension with 1, 10 and 100 mg/kg MB and their approximation by the sum of the absorption spectra of the erythrocyte suspension and the MB solution.

unbound MB, corresponded to the rate observed at 60 mg/kg MB. This suggests that approximately 50% of the MB remained associated with the erythrocytes – ten times higher than the concentration determined spectrophotometrically. We hypothesize this discrepancy is due to the reduction of MB to LMB within erythrocytes. Erythrocytes possess potent reductive systems (NADPH and reduced glutathione, GSH) capable of reducing MB to LMB. Consequently, during pre-irradiation incubation with erythrocytes, a significant portion of MB may be converted intracellularly to the inactive leuco-form. MB primarily generates ROS via a Type I mechanism upon irradiation. These ROS attack and deplete key erythrocyte antioxidants. GSH is oxidized by radicals (especially •OH, HOCI, ONOO-) and peroxides. The enzyme glutathione peroxidase also consumes GSH to reduce H₂O₂ and lipid hydroperoxides. NADPH is critically required for glutathione reductase, which regenerates oxidized glutathione back to GSH. Under massive oxidative stress, NADPH and GSH reserves are rapidly depleted, diminishing the cell's reducing capacity and hindering the reduction of MB to LMB. Under these conditions, LMB can be oxidized back to MB by oxygen, ROS, or secondary oxidants

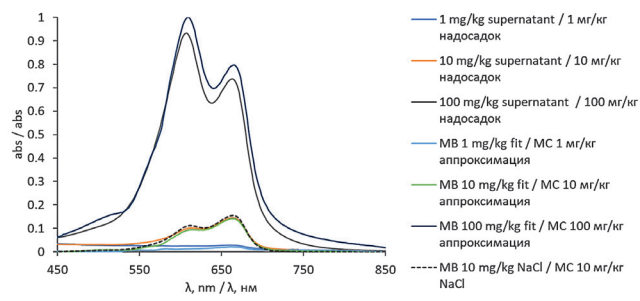


Рис. 7. Сравнение спектров поглощения МС, полученных в результате аппроксимации, с экспериментальными спектрами поглощения супернатанта после центрифугирования. Fig. 7. Comparison of the MB absorption spectra obtained as a result of approximation with the experimental absorption spectra of the supernatant after centrifugation.

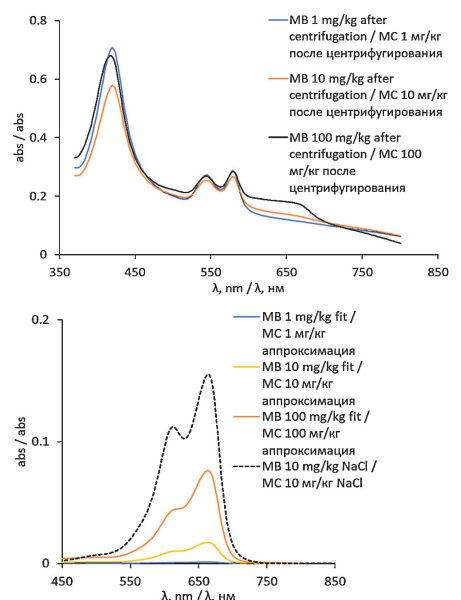


Рис. 8. Спектры поглошения эритроцитов после центрифугирования и дополнительной трехкратной отмывки от МС и спектры поглощения МС, полученные в результате аппроксимации. Fig. 8. Absorption spectra of erythrocytes after centrifugation and additional three-fold washing from MB and absorption spectra of MB obtained as a result of approximation.

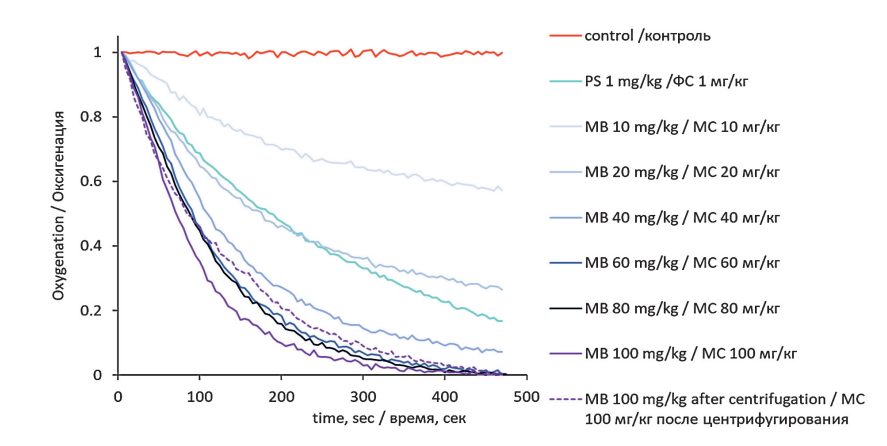


Рис. 9. Кривые дезоксигенации, зарегистрированные для суспензий эритроцитов с различной концентрацией MC. **Fig. 9.** Deoxygenation curves recorded for erythrocyte suspensions with different MB concentrations.

formed during antioxidant depletion. The oxidized MB can then generate new ROS upon further irradiation. Values obtained from deoxygenation curve fitting, along with calculated photodynamic activity (Ψ) and relative singlet oxygen quantum yield ($\varphi\Delta$) values, are presented in Table 1.

With increasing MB concentration, deoxygenation time decreased, while delta and the deoxygenation rate increased. This indicates that the amount of singlet oxygen generated increased with MB concentration. Deoxygenation time decreased from 33.8 sec (MB 10 mg/kg) to 15.8 sec (MB 100 mg/kg). However, photodynamic activity decreased with increasing MB concentration, Fig. 10.

Photodynamic activity represents the probability of chemical quenching of a ${}^{1}O_{2}$ molecule per 100 photons absorbed by the PS. The decrease in photodynamic activity with increasing MB concentration indicates that the number of photons absorbed by the PS grows faster than the number of singlet oxygen molecules generated. Over the concentration range studied, the efficiency of singlet oxygen generation was relatively low. The relative quantum yield of ${}^{1}O_{2}$ generation was 0.014 at 10 mg/kg MB and

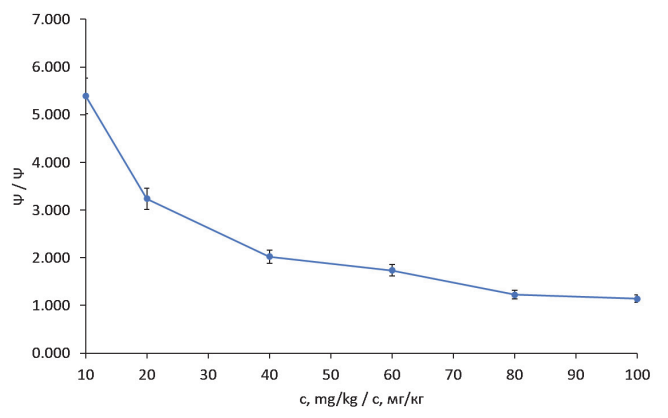


Рис. 10. Зависимость фотодинамической активности от концентрации MC.

Fig. 10. Dependence of photodynamic activity on the MB concentration.

0.003 at 100 mg/kg MB, one to two orders of magnitude lower than for aluminum sulfonated phthalocyanine ($\phi\Delta$ = 0.38), respectively. This supports the hypothesis that the photodynamic reaction for MB proceeds predominantly via Type I, generating ROS other than singlet oxygen.

Таблица 1

Полученные в результате аппроксимации кривых дезоксигенации значения времени дезоксигенации (τ), изменения значения оксигенации за измеренный промежуток времени (дельта), скорости дезоксигенации (наклон) и рассчитанные значения фотодинамической активности (Ψ) и относительного квантового выхода генерации синглетного кислорода ($\phi\Delta$)

Table 1

The values of deoxygenation time (τ) , change in oxygenation value over a measured time interval (delta), deoxygenation rate (slope), and calculated values of photodynamic activity (Ψ) and relative quantum yield of singlet oxygen generation $(\phi\Delta)$ obtained as a result of deoxygenation curve approximation

	c, мг/кг c, mg/kg	c, мκM c, μM	τ, c τ, sec	дельта delta	наклон slope	Ψ	$\phi_{\scriptscriptstyle \Delta}$
MC MB	10	31	33.8	0.56	1.27	5.39	0.014
	20	63	27.7	0.9	1.26	3.24	0.008
	40	125	22.3	0.99	1.75	2.02	0.005
	60	188	17.3	1	1.96	1.74	0.004
	80	250	18.4	1	2.16	1.23	0.003
	100	313	15.8	1	2.27	1.14	0.003
сульфированный фталоцианин алюминия sulfated aluminum phthalocyanine	1	1	37.5	1	1.49	97.99	0.380



Thus, data obtained using fluorescent indicators and spectroscopy on MB-mediated ROS generation and the low quantum yield of singlet oxygen generation confirm the hypothesis of a shift in the photosensitization mechanism from Type II to Type I upon MB interaction with erythrocytes.

Conclusion

It has been established that the interaction of MB with erythrocytes radically alters its photophysical and photodynamic properties compared to those observed in organic solvents. A key finding is the significant suppression of singlet oxygen (102) generation – the relative quantum yield $(\phi\Delta)$ does not exceed 0.014 (at an MB concentration of 10 mg/ kg) and decreases to 0.003 at 100 mg/kg. This is 1-2 orders of magnitude lower than values characteristic of MB in alcohols $(\phi\Delta \sim 0.5)$ and the reference photosensitizer aluminum sulfonated phthalocyanine ($\phi\Delta$ = 0.38). This reduction is attributed to several interrelated factors: aggregation of MB molecules, their specific interaction with erythrocytes, and conversion to the inactive reduced form LMB.

It was experimentally confirmed that approximately 5% of the added MB binds to erythrocyte membranes via electrostatic interactions. Over 40% of MB is reduced to LMB by erythrocyte enzymes (NADPH-dependent

systems). However, under photodynamic action, LMB can be oxidized back to active MB, particularly against the backdrop of depletion of the cell's antioxidant reserves (NADPH, glutathione) induced by the generated ROS.

The combined use of fluorescent indicators (SOSG for ¹O₂ and c-H₂DCFDA for other ROS) and spectroscopic analysis of hemoglobin deoxygenation unequivocally demonstrates a shift in the mechanism of MB's photodynamic action in the presence of erythrocytes from Type II (dominant in organic media) towards Type I. This is manifested by enhanced generation of reactive oxygen species concurrent with suppressed ¹O₂ yield.

An important practical conclusion is the demonstration of an inverse relationship between the molar photodynamic activity (Ψ) of MB and its concentration within the studied range (10–100 mg/kg). Increasing the MB concentration does not overcome for the loss of efficacy associated with its interaction with the biological substrate and may even exacerbate it, likely due to enhanced aggregation and reduction to the leuco-form. These findings are critically important for optimizing the parameters of systemic PDT using MB.

The study was funded by a grant from the Russian Science Foundation (project N 22-72-10117).

REFERENCES

- Foote C. S. Definition of type I and type II photosensitized oxidation, *Photochemistry and Photobiology*, 1991, vol. 54(5), pp. 659–659. doi: 10.1111/j.1751-1097.1991.tb02071.x.
- Baptista M. S., Cadet J., Di Mascio P. et al. Type I and Type II Photosen-sitized Oxidation Reactions: Guidelines and Mechanistic Pathways, Photochemistry and Photobiology, 2017, vol. 93(4), pp. 912–919. doi: 10.1111/php.12716.
- Li X., Kwon N., Guo T. et al. Innovative Strategies for Hypoxic-Tumor Photodynamic Therapy, *Angewandte Chemie International Edition*, 2018, vol. 57(36), pp. 11522–11531. doi: 10.1002/anie.201805138.
- Zhao X., Liu J., Fan J. et al. Recent progress in photosensitizers for overcoming the challenges of photodynamic therapy: from molecular design to application, *Chemical Society Reviews*, 2021, vol. 50(6), pp. 4185-4219. doi: 10.1039/D0CS00173B.
- Xu J., Bonneviot L., Guari Y. et al. Matrix Effect on Singlet Oxygen Gen-
- retain Using Methylene Blue as Photosensitizer, *Inorganics*, 2024, vol. 12(6), pp. 155. doi: 10.3390/inorganics12060155. Lucky S. S., Soo K. C., Zhang Y. Nanoparticles in Photodynamic Therapy, *Chemical Reviews*, 2015, vol. 115(4), pp. 1990–2042. doi: 10.1021/cr5004198.
- Filonenko E. V. Clinical implementation and scientific development of photodynamic therapy in Russia in 2010-2020, Biomedical Photonics,
- 2022, vol. 10(4), pp. 4–22. doi: 10.24931/2413-9432-2021-9-4-4-22. Semyonov D. Yu., Vasil'ev Yu. L., Dydykin S. S. et al. Antimicrobial and antimycotic photodynamic therapy (review of literature), *Biomedical Photonics*, 2021, vol. 10(1), pp. 25–31. doi: 10.24931/2413-9432-2021-
- Trushina O. I., Filonenko E. V., Novikova E. G. et al. Photodynamic therapy in the prevention of HPV-induced recurrences of precancer and initial cancer of the cervix, *Biomedical Photonics*, 2024, vol. 13(3), pp. 42–46. doi: 10.24931/241-9432-2024-13-3-42-46.
- Tseimakh A. E., Mitshenko A. N., Kurtukov V. A. et al. Effectiveness of palliative photodynamic therapy for unresectable biliary cancer. Systematic review and meta-analysis, *Biomedical Photonics*, 2024, vol. 13(2), pp. 34–42. doi: 10.24931/2413-9432-2024-13-2-
- Shanazarov N. A., Zinchenko S. V., Kisikova S. D. et al. Photodynamic therapy in the treatment of HPV-associated cervical cancer: mechanisms, challenges and future prospects, *Biomedical Photonics*, 2024, vol. 13(1), pp. 47–55. doi: 10.24931/2413-9432-2023-13-1-47-55. Panaseykin Y. A., Kapinus V. N., Filonenko E. V. et al. Photodynamic therapy in treatment of squamous cell carcinoma of oral cavity with
- chlorine e6 photosensitizer with long-term follow up, Biomedical Photonics, 2024, vol. 13(1), pp. 28-38. doi: 10.24931/2413-9432-2023-13-1-28-38.

ЛИТЕРАТУРА

- Foote C.S. Definition of type I and type II photosensitized oxidation // Photochemistry and photobiology. 1991. Vol. 54(5). P. 659-659. doi: 10.1111/j.1751-1097.1991.tb02071.x.
- Baptista M.S., Cadet J., Di Mascio Р. и др. Type I and type II photosensitized oxidation reactions: guidelines and mechanistic pathways // Photochemistry and photobiology. – 2017. – Vol. 93(4). – P. 912-919. doi: 10.1111/ php. 12716. Li X., Kwon N., Guo Т. и др. Innovative strategies for hypoxic-tumor pho-
- todynamic therapy // Angewandte chemie international edition. 2018. Vol. 57(36). P. 11522-11531. doi: 10.1002/ anie.201805138.
- Zhao X., liu J., Fan J. и др. Recent progress in photosensitizers for overcoming the challenges of photodynamic therapy: from molecular design to application // Chemical society reviews. – 2021. – Vol. 50 (6). – P. 4185-4219. doi: 10.1039/d0cs00173b.
- Xu J., Bonneviot L., Guari Y. и др. Matrix effect on singlet oxygen generation using methylene blue as photosensitizer // Inorganics. – 2024. – Vol. 12 (6). – P. 155. doi: 10.3390/inorganics12060155.
- Lucky S.S., Soo K.C., Zhang Y. Nanoparticles in photodynamic therapy // Chemical reviews. 2015. Vol. 115 (4). P. 1990-2042. doi: 10.1021/
- Филоненко Е.В. Клиническое внедрение и научное развитие фото-динамической терапии в России в 2010-2020 гг. // Biomedical Photonics. – 2021. – T. 10, № 4. – C. 4-22. doi: 10.24931/2413-9432-2021-9-4-4-22
- Семенов Д.Ю., Васильев Ю.Л., Дыдыкин С.С. и др. Антимикробная и антимикотическая фотодинамическая терапия (обзор литературы)// Biomedical Photonics. - 2021. - T. 10, №1. - C. 25-31. doi: 10.24931/2413-9432-2021-10-1-25-31. Трушина О.И., Филоненко Е.В., Новикова Е.Г. и др. Фотодинамическая
- терапия в профилактике ВТЧ- индуцированных рецидивов предра-ка и начального рака шейки матки // Biomedical Photonics. 2024. Т. 3, № 3. - C. 42-46. doi: 10.24931/241-9432-2024-13-3-42-46.
- Цеймах А.Е., Мищенко А.Н., Куртуков В.А. и др. Эффективность паллиативной фотодинамической терапии нерезектабельных злокачественных новообразований желчевыводящей системы. Систематический обзор и метаанализ // Biomedical Photonics. – 2024. – Т. 13, № 2. – C. 34-42. doi: 10.24931/2413-9432-2024-13-2-34-42.
- Шаназаров Н.А., Зинченко С.В., Кисикова С.Д. и др. Фотодинамическая терапия в лечении ВПЧ-ассоциированного рака шейки матки: механизмы, проблемы и перспективы на будущее // Biomedical Photonics. - 2024. - T. 13, № 1. - C. 47-55. doi: 10.24931/2413-9432-2023-13--47-55
- Панасейкин Ю.А., Капинус В.Н., Филоненко Е.В. и др. Результаты лечения больных раком полости рта при помощи фотодинамической терапии с фотосенсибилизатором на основе хлорина еб // Biomedi-

- Taldaev A., Terekhov R., Nikitin I. et al. Methylene blue in anticancer photodynamic therapy: systematic review of preclinical studies, Frontiers in Pharmacology, 2023, vol. 14, pp. 1264961. doi: 10.3389/ februages 1264961. fphar.2023.1264961.
- DeRosa M. Photosensitized singlet oxygen and its applications, *Coordination Chemistry Reviews*, 2002, vol. 233–234, pp. 351–371. doi: 10.1016/S0010-8545(02)00034-6.
 Redmond R. W., Gamlin J. N. A compilation of singlet oxygen yields from biologically relevant molecules, *Photochemistry and Photobiology*,
- 1999, vol. 70(4), pp. 391–475. doi: 10.1111/j.1751-1097.1999.tb08240.x. Tardivo J. P., Del Giglio A., De Oliveira C. S. et al. Methylene blue in photodynamic therapy: From basic mechanisms to clinical applications, *Photodiagnosis and Photodynamic Therapy*, 2005, vol. 2(3), pp. 175–191. doi: 10.1016/S1572-1000(05)00097-9.
- Medhi D., Hazarika S. Formation of dimer and higher aggregates of methylene blue in alcohol, Spectrochimica Acta Part A: Molecular and Biomólecular Spectroscopy, 2025, vol. 329, pp. 125490. doi: 10.1016/j.
- saa.2024.125490. Junqueira H. C., Severino D., Dias L. G. et al. Modulation of methylene
- Junqueira H. C., Severino D., Dias L. G. et al. Modulation of methylene blue photochemical properties based on adsorption at aqueous micelle interfaces, *Physical Chemistry Chemical Physics*, 2002, vol. 4(11), pp. 2320–2328. doi: 10.1039/b109753a.

 Severino D., Junqueira H. C., Gugliotti M. et al. Influence of negatively charged interfaces on the ground and excited state properties of methylene blue, *Photochemistry and Photobiology*, 2003, vol. 77(5), pp. 459–468. doi: 10.1562/0031-8655(2003)0772.0.co;2.
- Ball D. J., Luo Y., Kessel D. et al. The induction of apoptosis by a positively charged methylene blue derivative, *Journal of Photochemistry* and *Photobiology B:Biology*, 1998, vol. 42(2), pp. 159–163. doi: 10.1016/S1011-1344(98)00061-X.
- Curry S. Methemoglobinemia, Annals of Emergency Medicine, 1982, vol. 11(4), pp. 214–221. doi: 10.1016/S0196-0644(82)80502-7. Sass M. D., Caruso C. J., Axelrod D. R. Accumulation of methylene blue
- by metabolizing erythrocytes, *The Journal of Laboratory and Clinical Medicine*, 1967, vol. 69(3), pp. 447–455.

 Sakai H., Leong C. Prolonged functional life span of artificial red cells in blood circulation by repeated methylene blue injections, *Artificial Communications*, *Artificial Communications*,
- Cells, Nanomedicine, and Biotechnology, 2019, vol. 47(1), pp. 3123–3128. doi: 10.1080/21691401.2019.1645157.
 Sakai H., Li B., Lim W. L. et al. Red Blood Cells Donate Electrons to Methylene Blue Mediated Chemical Reduction of Methemoglobin Com-

- ylene Blue Mediated Chemical Reduction of Methemoglobin Compartmentalized in Liposomes in Blood, *Bioconjugate Chemistry*, 2014, vol. 25(7), pp. 1301–1310. doi: 10.1021/bc500153x.

 May J. M., Qu Z., Cobb C. E. Reduction and uptake of methylene blue by human erythrocytes, *American Journal of Physiology-Cell Physiology*, 2004, vol. 286(6), pp. C1390–C1398. doi: 10.1152/ajpcell.0051.2.2003.

 McDonagh E. M., Bautista J. M., Youngster I. et al. PharmGKB summary: methylene blue pathway, *Pharmacogenetics and Genomics*, 2013, vol. 23(9), pp. 498–508. doi: 10.1097/FPC.0b013e32836498f4.

 Harrop Geo. A., Barron E. S. G. STUDIES ON BLOOD CELL METABOLISM, *Journal of Experimental Medicine*, 1928, vol. 48(2), pp. 207–223. doi: 10.1097/FPC.0b013e328364987.
- Journal of Experimental Medicine, 1928, vol. 48(2), pp. 207–223. doi: 10.1084/jem.48.2.207.
- Pominova D., Ryabova A., Skobeltsin A. et al. The use of methylene blue to control the tumor oxygenation level, *Photodiagnosis and Photodynamic Therapy*, 2024, vol. 46, pp. 104047. doi: 10.1016/j.pdpdt.2024.104047.
- Pominova D. V., Ryabova A. V., Skobeltsin A. S. et al. Spectroscopic Study of Methylene Blue Interaction with Coenzymes and Its Effect on Tumor Metabolism, *Sovremennye tehnologii v medicine*, 2025, vol. 17(1), pp. 18. doi: 10.17691/stm2025.17.1.02.
- Ryabova A. V., Stratonnikov A. A., Loshchenov V. B. Laser spectroscopy technique for estimating the efficiency of photosensitisers in biological media, *Quantum Electronics*, 2006, vol. 36(6), pp. 562–568. doi: 10.1070/QE2006v036n06ABEH013291.
- Stratonnikov A. A., Loschenov V. B. Evaluation of blood oxygen saturation in vivo from diffuse reflectance spectra, *Journal of Biomedical*
- *Optics*, 2001, vol. 6(4), pp. 457. doi: 10.1117/1.1411979. Pominova D. V., Ryabova A. V., Romanishkin I. D. et al. Spectroscopic study of methylene blue photophysical properties in biological media, *Biomedical Photonics*, 2023, vol. 12(2), pp. 34–47. doi: 10.24931/2413-9432-2023- 12-2-34-47.
- Kalyanaraman B., Darley-Usmar V., Davies K. J. A. et al. Measuring reactive oxygen and nitrogen species with fluorescent probes: challenges and limitations, *Free Radical Biology and Medicine*, 2012, vol. 52(1), pp. 1–6. doi: 10.1016/j.freeradbiomed.2011.09.030.

 Marques S., Magalhães L., Tóth I. et al. Insights on Antioxidant Assays for Biological Samples Based on the Reduction of Copper Complex-
- -The Importance of Analytical Conditions, International Journal of Molecular Sciences, 2014, vol. 15(7), pp. 11387-11402. doi: 10.3390/ ijms150711387. George A., Pushkaran S., Li L. et al. Altered phosphorylation of cyto-
- George A., Pushkaran S., Li L. et al. Altered phosphorylation of cytoskeleton proteins in sickle red blood cells: The role of protein kinase C, Rac GTPases, and reactive oxygen species, *Blood Cells, Molecules, and Diseases*, 2010, vol. 45(1), pp. 41–45. doi: 10.1016/j.bcmd.2010.02.006. Gomes A., Fernandes E., Lima J. L. F. C. Fluorescence probes used for detection of reactive oxygen species, *Journal of Biochemical and Biophysical Methods*, 2005, vol. 65(2–3), pp. 45–80. doi: 10.1016/j. ibbm.2015.10.003.
- jbbm.2005.10.003.

- cal Photonics. 2024. T. 13, № 1. C. 28-38. doi: 10.24931/2413-9432-2023-13-1-28-38.
- Taldaev A., Terekhov R., Nikitin I. и др. Methylene blue in anticancer photodynamic therapy: systematic review of preclinical studies // Frontiers in pharmacology. – 2023. – Vol. 14. – P. 1264961. doi: 10.3389/ fphar.2023.1264961.
- DeRosa M. Photosensitized singlet oxygen and its applications // Coordination chemistry reviews. 2002. Vol. 23 (4). P. 351-371. doi: 10.1016/s0010-8545(02)00034-6.
- Redmond R.W., Gamlin J.N. A compilation of singlet oxygen yields from
- hedifiolid K.W., Garnilli J.K. A Compilation of singlet oxyget yields from biologically relevant molecules // Photochemistry and photobiology. 1999. Vol. 70(4). P. 391-475. doi: 10.1111/j.1751-1097.1999.tb08240.x. Tardivo J.P., Del Giglio A., De Oliveira C.S. и др. Methylene blue in photodynamic therapy: from basic mechanisms to clinical applications // Photodiagnosis and photodynamic therapy. 2005. Vol. 2(3). P. 175–191. doi: 10.1016/s1572-1000(05)00097-9.
- Medhi D., Hazarika S. Formation of dimer and higher aggregates of methylene blue in alcohol // Spectrochimica acta part a: molecular and biomolecular spectroscopy. 2025. Vol. 329. P. 125490. doi: 10.1016/j. saa.2024.125490.
- Junqueira H.C., Severino D., Dias L.G. и др. Modulation of methylene blue photochemical properties based on adsorption at aqueous micelle interfaces // Physical chemistry chemical physics. – 2002. – Vol. 4 (11). – P. 2320-
- 2328. doi: 10.1039/b109753a. Severino D., Junqueira H.C., Gugliotti M. и др. Influence of negatively charged interfaces on the ground and excited state properties of methy-
- charged interfaces on the ground and excited state properties of methylene blue // Photochemistry and photobiology. 2003. Vol.77(5). P. 459-468. doi: 10.1562/0031-8655(2003)0772.0.co;2.
 Ball DJ., Luo Y., Kessel D. и др. The induction of apoptosis by a positively charged methylene blue derivative // Journal of photochemistry and photobiology b: biology. 1998. Vol. 42 (2). P. 159-163. doi: 10.1016/s1011-1344(98)00061-x.
- Curry S. Methemoglobinemia // Annals of emergency medicine. 1982. Vol. 11(4), P. 214-221. doi: 10.1016/s0196-0644(82)80502-7.

 Sass M.D., Caruso C.J., Axelrod D.R. Accumulation of methylene blue by metabolizing erythrocytes // The journal of laboratory and clinical medicine. 1967. Vol. 69 (3). P. 447-455.
- Sakai H., Leong C. Prolonged Functional life span of artificial red cells in blood circulation by repeated methylene blue injections // Artificial cells, nanomedicine, and biotechnology. – 2019. – Vol. 47(1). – P. 3123-3128. doi:10.1080/21691401.2019.1645157.
- Sakai H., Li B., Lim W. L. и др. Red blood cells donate electrons to methylene blue mediated chemical reduction of methemoglobin compartmentalized in liposomes in blood // Bioconjugate chemistry. - 2014. - Vol. 25 (7). – P. 1301-1310. doi: 10.1021/bc500153x.
- May J.M., Qu Z., Cobb C.E. Reduction and uptake of methylene blue by human erythrocytes // American journal of physiology-cell physiology. 2004. Vol. 286 (6). P. 1390-1398. doi: 10.1152/ajpcell.00512.2003.
- 2004. Vol. 286 (δ). P. 1390-1398. doi: 10.1152/ajpceli.00512.2005. McDonagh E. M., Bautista J. M., Youngster I. и др. Pharmgkb summary: methylene blue pathway // Pharmacogenetics and genomics. 2013. Vol. 23(9). P. 498-508. doi: 10.1097/fpc.0b013e32836498f4. Harrop Geo. A., Barron E. S. G. Studies on blood cell metabolism // Journal of experimental medicine. 1928. Vol. 48 (2). P. 207-223. doi: 10.1084/
- jem.48.2.207
- Pominova D., Ryabova A., Skobeltsin A. и др. The use of methylene blue to control the tumor oxygenation level // Photodiagnosis and photodynamic therapy. 2024. Vol. 46. P. 104047. doi: 10.1016/j. pdndt 2024 104047
- Pominova D.V., Ryabova A.V., Skobeltsin A.S. и др. Spectroscopic study of methylene blue interaction with coenzymes and its effect on tumor metabolism // Sovremennye tehnologii v medicine. – 2025. – Vol. 17(1). – P.
- табовіят // sovernemy ternnologii v medicine. 2023. vol. 17(1). Р. 18. doi: 10.17691/stm2025.17.1.02. Рябова А.В., Стратонников А.А., Лощенов В. Б. Лазерно-спектроскопический метод оценки эффективности фотосенсибилизаторов в биологических средах // Квантовая электроника. 2006. Т. 36, № 6. C. 562-568. doi: 10.1070/ge2006v036n06abeh013291.
- Stratonnikov A.A., Loschenov V.B. Evaluation of blood oxygen saturation in vivo from diffuse reflectance spectra // Journal of biomedical optics. – 2001. – Vol. 6 (4). – Р. 457. doi: 10.1117/1.1411979. Поминова Д.В., Рябова А.В., Романишкин И.Д. и др. Спектроскопиче-
- ское исследование фотофизических свойств метиленового синего в биологических средах // Biomedical Photonics. 2023. Т. 12, № 2. С.
- 34-47. https://doi.org/10.24931/2413-9432-2023-12-2-34-47. Kalyanaraman B., Darley-Usmar V., Davies K.J.A. и др. Measuring reactive oxygen and nitrogen species with fluorescent probes: challenges and limitations // Free radical biology and medicine. 2012. Vol. 52(1). Р. 1-6. doi: 10.1016/j.freeradbiomed.2011.09.030.
- Marques S., Magálhães L., Tóth I. и др. Insights on antioxidant assays for
- Marques S., Magalhães L., Tóth I. и др. Insights on antioxidant assays for biological samples based on the reduction of copper complexes the importance of analytical conditions // International journal of molecular sciences. 2014. Vol. 15(7). P. 11387–11402. doi: 10.3390/ijms150711387. George A., Pushkaran S., Li L. и др. Altered phosphorylation of cytoskeleton proteins in sickle red blood cells: the role of protein kinase c, rac gtpases, and reactive oxygen species // Blood cells, molecules, and diseases. 2010. Vol. 45 (1). P. 41-45. doi: 10.1016/j. bcmd.2010.02.006. Gomes A., Fernandes E., Lima J.L.F.C. Fluorescence probes used for detection of reactive oxygen species // Journal of biochemical and biophysical methods. 2005. Vol. 65(2-3). P.45-80. doi: 10.1016/j.jbbm.2005.10.003.



X-RAY INDUCED CYTOTOXICITY OF AQUEOUS COLLOIDAL SOLUTIONS OF UV-C LUMINESCENT La_{1-x}Pr_xPO₄ NANOPARTICLES

Shaidulin A.T.^{1,2}, Orlovskaya E.O.¹, Uvarov O.V.¹, Silaev G.O.^{2,3}, Skopin P.I.⁴, Gololobova I.A.⁴, Aioub A.A-K.⁴, Yakobson D.E.⁴, Chernobay R.A.⁴, Vainer Y.G.³, Orlovskii Yu.V.¹, Makhov V.N.⁵

- ¹ Prokhorov General Physics Institute of the Russian Academy of Sciences Moscow, Russia
- ² Higher School of Economics National Research University, Moscow, Russia
- ³ Institute of Spectroscopy of the Russian Academy of Sciences, Moscow, Russia
- ⁴ National Research Ogarev Mordovia State University, Saransk, Russia
- ⁵ P.N. Lebedev Physical Institute of the Russian Academy of Sciences, Moscow, Russia

Abstract

The use of UV-C radiation for the treatment of tumors is a stand-alone therapeutic intervention that can induce cellular apoptosis and is independent of photosensitizer or oxygen concentration in tumor. To explore the potential of using X-ray excited UV-C luminescent nanoparticles as a basis for creating drugs to improve radiation therapy, two colloidal solutions of monoclinic La_{1-x}Pr_xPO₄ nanoparticles with different morphologies of large nanofibers (x = 0.02) or small nanorods (x = 0.05) were prepared using a microwave-assisted hydrothermal method. Comparison of X-ray excited UV-C luminescence of colloidal solutions showed approximately 6.3 times higher brightness for larger nanoparticles. The intrinsic and X-ray-induced cytotoxicity of the prepared colloidal solutions on the viability of cancerous Mh22a and healthy L929 cell cultures were studied using MTT assay and fluorescence microscopy. Fluorescence microscopy showed differences in the types of cell death (apoptosis or necrosis) after incubation with nanofiber or nanorod samples. X-ray irradiation was performed in two modes with different voltage on the X-ray tube (50 and 80 kV) and the same radiation dose (8 Gy). Groups of cells incubated with nanoparticles and irradiated with 50 kV mode showed greater death rate. According to MTT analysis, irradiation of cells incubated with La_{0.98}Pr_{0.02}PO₄ nanofibers at a concentration of 2 mg/mL reduced survival by 20-30%, and at the same time, according to fluorescence microscopy data, the number of cells undergoing apoptosis exceeded the number of cells that died through necrosis and reached 50-70%. Quantitative analysis of the relative number of dead cells caused by X-ray-induced cytotoxicity of La_{0.98}Pr_{0.02}PO₄ nanorods did not reveal statistically significant results in reducing cell viability.

Key words: UV-C luminescence, X-ray excited optical luminescence, aqueous colloidal solution of nanocrystals, X-ray induced cytotoxicity, *in vitro*, fluorescence microscopy, apoptosis.

Contacts: Shaidulin A.T., e-mail: shatarte@yandex.ru

For citations: Shaidulin A.T., Orlovskaya E.O., Uvarov O.V., Silaev G.O., Skopin P.I., Gololobova I.A., Aioub A.A.-K., Yakobson D.E., Chernobay R.A., Vainer Y.G., Orlovskii Yu.V, Makhov V.N. Experimental studies X-ray induced cytotoxicity of aqueous colloidal solutions of UV-C luminescent La_{1...}Pr_.PO₄ nanoparticles, *Biomedical Photonics*, 2025, vol. 14, no. 3, pp. 14–23. doi: 10.24931/2413–9432–2025–14-3–14–23

РЕНТГЕН-ИНДУЦИРОВАННАЯ ЦИТОТОКСИЧНОСТЬ ВОДНЫХ РАСТВОРОВ УФ-С РЕНТГЕНОЛЮМИНЕСЦЕНТНЫХ НАНОЧАСТИЦ La_{1-} , Pr_{p} , Po_{d}

А.Т. Шайдулин^{1,2}, Е.О. Орловская¹, О.В. Уваров¹, Г.О. Силаев^{2,3}, П.И. Скопин⁴, И.А. Гололобова⁴, Аюб А.А.-Х.⁴, Д.Э. Якобсон⁴, Р.А. Чернобай⁴, Ю.Г. Вайнер³, Ю.В. Орловский¹, В.Н. Махов⁵

¹Институт общей физики им. А.М. Прохорова Российской академии наук, Москва, Россия ²Национальный исследовательский университет «Высшая школа экономики», Москва, Россия

³Институт спектроскопии Российской академии наук, Москва, Россия

⁴Национальный исследовательский Мордовский государственный университет им. Н.П. Огарёва, Саранск, Россия

 5 Физический институт им. П.Н. Лебедева Российской академии наук, Москва, Россия



Резюме

Использование УФ-С излучения является отдельно стоящим терапевтическим воздействием на раковые опухоли, которое способно вызывать клеточный апоптоз и не зависит от фотосенсибилизатора или концентрации кислорода в опухоли. Для исследования потенциала использования наночастиц, способных к рентгенолюминесценции в УФ-С области, в качестве основы для создания препарата, направленного на улучшение лучевой терапии, гидротермально-микроволновым методом были приготовлены два коллоидных раствора наночастиц моноклинного $La_{1-x}Pr_xPO_4$ с морфологиями крупных нановолокон (x = 0,02) или мелких наностержней (x = 0,05). Сравнение рентгенолюминесценции в УФ-С области коллоиных растворов показало в 6,3 раз превосходящую яркость для более крупных наночастиц. Собственная и рентген-индуцированная цитотоксичность коллоидных растворов на культуре опухолевых клеток Mh22a и культуре клеток L929 были исследованы при помощи МТТ анализа и флуоресцентной микроскопии. Флуоресцентная микроскопия выявила различия в форме клеточной смерти (апоптоз или некроз) после инкубации клеток с образцами нановолокон или наностержней. Облучение рентгеном проводили в двух режимах с различным напряжением на рентгеновской трубке (50 или 80 кВ) и с одинаковой дозой облучения (8 Гр). Группы клеток, инкубированные с крупными наночастицами и облученные в режиме 50 кВ, показали более высокие показатели гибели. Согласно МТТ анализу, облучение клеток, инкубированных с нановолокнами $La_{0.98}Pr_{0.07}PO_4$ с концентрацией 2 мг/мл, снизило выживаемость на 20-30%, и одновременно по данным флуоресцентной микроскопии, количество клеток, находящихся в апоптозе, превысило число клеток погибших путем некроза и достигло 50-70%. Количественный анализ относительного числа погибших клеток, исследованных на влияние рентген-индуцированной цитотоксичности наностержей $La_{0.95}Pr_{0.05}PO_{4}$, не выявил достоверных результатов по снижению жизнеспособности клеток.

Ключевые слова: УФ-С люминесценция, рентгенолюминесценция, водный коллоидный раствор нанокристаллов, рентген-индуцированная цитотоксичность, *in vitro*, флуоресцентная микроскопия, апоптоз.

Контакты: A.T. Шайдулин, e-mail: shatarte@yandex.ru

Для цитирования: Шайдулин А.Т., Орловская Е.О., Уваров О.В., Силаев Г.О., Скопин П.И., Гололобова И.А., Аюб А.А.-Х., Якобсон Д.Э., Чернобай Р.А., Вайнер Ю.Г., Орловский Ю.В., Махов В.Н. Рентген-индуцированная цитотоксичность водных растворов УФ-С рентгенолюминесцентных наночастиц L_{a_1} Pr_PO_4 // Biomedical Photonics. – 2025. – Т. 14, № 3. – С. 14–23. doi: 10.24931/2413–9432–2025–14–3–14–23

Introduction

A separate mechanism of action on cancer tumors without the use of a photosensitizer (but not excluding it) may be the use of nanoparticles (NPs) exhibiting X-ray excited optical luminescence in the UV-C (200-280 nm) region. It is known that UV-C quanta have the ability to initiate cell apoptosis due to direct photochemical reactions in DNA molecules [1]. This property should help reduce tissue necrosis, which should facilitate the body's recovery. Since body tissues strongly absorb UV-C radiation, to affect deep-seated solid tumors it is necessary to create a localized source of UV-C quanta, which can be excited by X-ray irradiation, which easily penetrates biological tissue. To the best of our knowledge, only one research group has tested the effect of nanoparticles (NPs) capable of X-ray-excited optical luminescence in the UV-C spectral range (lutetium phosphate NPs doped with Pr³⁺ and Nd³⁺ ions) on the deactivation of cancer cells [2-6]. The most significant effects of the combined action of X-ray-excited UV-C fluorescent nanoparticles and X-ray irradiation were demonstrated in vitro in [2, 6]. An increase in the efficiency of radiation exposure under hypoxic conditions [2] and the possibility of strong inhibition of cancer spheroid growth as a result of apoptosis, cell cycle arrest and necrosis [6] were demonstrated.

However, high intensity UV-C radiation can also be observed in other suitable crystalline matrices doped with Pr³⁺ or Nd³⁺ ions due to the presence of interconfigurational electronic transitions in these ions from the excited electron configuration 4fⁿ⁻¹5d¹

to the ground electron configuration $4f^n$ (n = 2 and 3, respectively). Among them is LaPO, nanocrystals with monazite structure (m-LaPO₄, monoclinic system, P2₁/n) doped with Pr³⁺ ions, which also exhibit strong emission in the UV-C range (220–280 nm) due to $4f^15d^1 \rightarrow {}^3H_{4.5.6'}$ ³F₂ transitions in Pr³⁺ ions under high-energy excitation [7-12]. Since La³⁺ and Pr³⁺ ions have close ionic radii and form the same phosphate crystal structure, a higher degree of substitution of cations with lower structural defects can be expected. In addition, the $4f^15d^1 \rightarrow {}^3H_e$ transition in Pr3+ ions has an intensity maximum in the spectral range of 256 nm [7], which practically coincides with the absorption maximum of DNA [3]. Based on this, the aim of this work was to conduct an in vitro study of the intrinsic and X-ray-induced cytotoxicity of aqueous colloidal solutions of m-La,_Pr,PO, NPs.

Two colloidal solutions of La_{1-x}Pr_xPO₄ NPs with different morphologies were synthesized by the hydrothermal microwave-assisted method: nanofibers (La_{0.98}Pr_{0.02}PO₄) with NPs length up to 600 nm and diameter up to 15 nm and nanorods (La_{0.95}Pr_{0.05}PO₄) with length up to 80 nm and diameter up to 10 nm. X-ray excited optical luminescence spectroscopy in the UV-C region of the obtained samples in the form of colloidal solutions using a highly sensitive N₂-cooled CCD camera designed for the UV range. The intrinsic cytotoxicity and X-ray-induced cytotoxicity of the obtained colloidal solutions of La_{1-x}Pr_xPO₄ NPs with different morphologies was investigated *in vitro* by MTT assay. The X-ray-induced cytotoxicity studies were conducted using therapeutic X-ray radiation operating



ORIGINAL ARTICLES

in two different modes of the X-ray tube (accelerating voltage 50 and 80 kV) and a total dose of 8 Gy. Groups of cells irradiated with X-rays under the same conditions without NPs, as well as irradiated with a UV lamp, were used as controls. The nature of cell death of the control groups of cells was studied using double staining of cells and subsequent fluorescence microscopy.

Materials and Methods

Synthesis of colloidal solutions of $La_{1-x}Pr_{x}PO_{4}$ nanoparticles with different morphologies

The initial chemical reagents used in the synthesis without further purification include: Pr(NO₃)₃·6H₂O (Aldrich, 99.9% purity), La(NO₃)₃·6H₂O (Aldrich, 99.999% purity), K₂HPO₄·3H₂O (RusKhim, analytical grade), tartaric acid (hps, analytical grade), 25% aqueous solution of NH₄OH (SigmaTek, analytical grade). Throughout all syntheses, deionized (DI) water (type I) from a water deionizer Crystal EX-1001 (Adrona) was used.

La_{0.98}Pr_{0.02}PO₄ sample consisting of nanofibers (NPs length & diameter not larger than 600 & 15 nm, respectively) was prepared with 0.5 mmol of REIs (0.49 mmol of La(NO₃)₃·6H₂O and 0.01 mmol of Pr(NO₃)₃·6H₂O) and an anion excess ratio of K₂HPO₄ equal to 1.25. The solution of REIs (10 mL) was continuously supplied (0.4 mL/min) using a syringe pump directly into solution containing excess K₂HPO₄ (15 mL) with constant stirring. The formed cloudy solution of gel was diluted with DI water to a volume of 50 mL (resulting pH = 5), transferred to a 100 ml autoclave (DAK-100), sealed and treated at 200 °C for 2 hours under microwave-hydrothermal conditions using a speedwave XPERT (Berghof Products+Instruments GmbH) laboratory device with two magnetrons (2.45 GHz, 2 kW maximum output power). After hydrothermal treatment, the sediment from the bottom of autoclave was washed twice with a weak solution of HNO, and once with DI water (80 mL each time) using a centrifugationredispersion using a centrifuge (14800 rf, 15 min). After the third washing, the suspension ring was redispersed in 5 mL of DI water forming a turbid translucent solution (pH of the final colloidal solution was 5.3). La_{0.95}Pr_{0.05}PO₄ sample consisting of nanorods (NPs length & diameter not larger than 80 & 10 nm, respectively) was prepared with 0.5 mmol of REIs (0.475 mmol of La(NO₃)₃·6H₂O and 0.025 mmol of Pr(NO₃)₃·6H₂O) and anion excess ratio of K₂HPO₄ equal to 2. The pH of the REIs solution was adjusted to pH = 8 using alkaline solution of ammonium tartrate and NH₄OH, which acted as a weak complexing agent, preventing, the formation of hydroxides. After hydrothermal-microwave treatment (200°C, 2 h), the precipitate was washed twice with DI water, then with a weak NH,OH solution using the centrifugationredispersion process, followed by redispersion in 5 mL of DI water, resulting in a transparent colloidal solution (pH of the final colloidal solution was 7.5).

Transmission electron microscopy

TEM images of NPs were obtained on a Zeiss Libra 200 FTHR microscope under accelerating voltage of 200 kV. The colloids were highly diluted and applied onto a TEM grid and dried in vacuum for several hours. ImageJ software was used to measure sizes of individual nanocrystals by approximating the length and diameter of the observed TEM projections with straight perpendicular lines.

X-ray excited optical luminescence spectroscopy of colloidal solutions

X-ray excitation of the studied samples in the form of a colloidal solution was performed using X-ray tube MOX-HPC 150W 60kV equipped with tungsten anode (Moxtek). The X-ray excited optical luminescence in the UV-C spectral region was recorded using a HORIBA iHR-550 Imaging spectrometer (Horiba Scientific) with a diffraction grating of 1800 grooves/mm and a N₂-cooled PyLoN:2KBUV CCD camera (Princeton Instruments) designed for the UV spectral range. A self-made objective based on two planoconvex lenses made of MgF₂ with a light spot diameter of 35 mm and a focus of 70 mm was used to collect the UV-C light. Colloidal solutions were applied to a polytetrafluoroethylene (PTFE) substrate as a 0.2 mL drop with NPs concentration of 7 mg/mL. The operating mode of the X-ray tube for both types of colloidal solutions was: accelerating voltage: 30 kV; anode current: 2.5 mA; exposure time: 60 s.

Cell strains

The research in the work was carried out on the mouse cell cultures of Mh22a hepatoma (Biolot) and L929 fibroblasts (National Research Center of Epidemiology and Microbiology). The cells were grown in flasks with DMEM culture medium (Servicebio) supplemented with 10% fetal bovine serum (FBS, Biosera) and antibiotics: 100 μ g/mL penicillin, 100 μ g/mL streptomycin (Paneco). The incubation of cells was done in cell incubator (Thermoscientific Midi40), and conditions were standard: 5% CO₂, temperature and humidity of the medium 37°C and 5%, respectively. Cell counting was performed using 0.4% trypan blue solution (Paneco) in a Goryaev chamber.

Design of the experimental in vitro study

The cytotoxicity of $La_{1-x}Pr_xPO_4$ NPs was determined using the photocolorimetric MTT assay in accordance with the international protocol ISO SO 10993-5:2009 "Tests for *In Vitro* Cytotoxicity". Cell cultures were seeded at 5000 cells per well and incubated in a 96-well plate for 24 hours under standard conditions. Then the culture medium was removed and replaced with a new medium (DMEM with 1% FBS) containing NPs at a concentration of 0.0625, 0.125, 0.25, 0.5, 1, 2, 4 mg/mL (n=3). The viability of the cell cultures was determined after 24 hours. After the time had elapsed, the medium with the studied samples was removed, the wells were washed twice with phosphate buffer, then 100 μ l of fresh medium (DMEM with 1% FBS) and 10 μ l of MTT solution (3-(4,5-dimethylthiazol-2-yl)-2,5-diphenyl) tetrazolium bromide) at a concentration

of 5 mg/mL were added to each well. After 3.5 hours of incubation, the formed formazan crystals were dissolved using a DMSO solution, which was added in 150 μ l to each well. The plates were then placed in a thermostatic shaker (ELMI ST-3L) for 20 min at 37°C, 400 rpm. Optical density was measured using a Varioscan Lux multimodal reader (Thermoscientific) at an analytical wavelength of 570 nm versus a reference wavelength of 650 nm. Cell viability was assessed by the ratio of the optical density of the samples to the optical density of the control cells (untreated cells incubated without additional components or external influences), expressed as a percentage.

The effect of La_{1-x}Pr_xPO₄ NPs on the viability of Mh22a and L929 cell cultures irradiated with X-rays was studied using a Terad 200 X-ray therapy apparatus (LINEV ADANI) equipped with a tungsten anode. The study was conducted in two modes: 1) the accelerating voltage, anode current, and Al filter thickness: 50 kV, 20 mA, and 0.5 mm, respectively; 2) the accelerating voltage, anode current, and Al filter thickness: 80 kV, 15 mA, and 2 mm, respectively. In both modes, the irradiation dose was 8 Gray. La_{1-x}Pr_xPO₄ NPs at concentrations of 1 and 2 mg/mL (n=8) were incubated with Mh22a and L929 cell culture in a 96-well plate (5000 cells per well) for 12 hours. Cell viability was determined using the MTT assay 24 h after X-ray exposure according to the protocol described above.

The type of cytotoxicity after incubation of Mh22a and L929 cells with NPs and exposure to X-ray radiation was determined using the double staining method and fluorescence microscopy using an Axio Zeiss Imager A1 microscope (Carl Zeiss Jena). As an additional control, groups of Mh22a and L929 cells were irradiated with a UV lamp at 60 J/cm² for 8 min. Selected control groups of Mh22a and L929 cells were stained with a mixture of acridine orange (AO) and propidium iodide (PI) dyes and then analyzed according to the protocol [13]. AO penetrates living, apoptotic and dead cells and stains their nuclei green or orange. In the case of intact DNA, AO fluoresces green. In early apoptosis, with the initial chromatin condensation, AO fluorescence appears yellow-green, and with DNA fragmentation, it appears

orange. In the late stage of apoptosis, when condensed chromatin disintegrates and the nucleus fragments, the binding of AO to DNA fragments weakens and the cell is stained green again. Propidium iodide penetrates only into dead cells with a damaged membrane (necrotic or late apoptotic) and stains the nucleus red. Thus, separation of cells into groups of viable, apoptotic, and necrotic cells was performed based on the morphological appearance of the cells. Viable cells (VC) were determined by uniform green staining and a fusiform shape. The early apoptotic cells (AC) were determined by cell shrinkage and DNA fragmentation which appears as bright orange staining of nuclei, with the borders of the nuclei clearly visible. The late AC were determined by nuclear disintegration, resulting in cells with bright green nuclei and cytoplasm. Additionally, signs of AC included rounding of cells and small fragments around them – apoptotic bodies. Necrotic cells (NC) were determined by a damaged membrane, a red or red-orange nucleus and cytoplasm, and a rounded shape. The cells that have completed the apoptotic cycle are then poorly distinguishable from necrotic cells, and therefore they were also included in the group of NC. Differentiation of the VC, AC and NC was performed by counting at least 100 cells in each independent group. The results were expressed in percentages.

Calculation of cell viability was performed in Excel. Normality of distribution of the feature by groups was estimated using the Shapiro-Wilk criterion. It was found that the distribution of features corresponds to normality, therefore, comparisons between the groups were performed using analysis of one-way ANOVA. Statistical processing and calculation of IC50 were performed in GraphPad Prism 8.0 (San Diego). Values of P < 0.05 were considered to be significant for both cytotoxicity and X-ray induced cytotoxicity of $La_{1-x}Pr_xPO_4$ NPs. Results were presented as mean \pm SD.

Results and discussion

Transmission electron microscopy

As can be seen from the TEM images (Fig. 1), NPs with different aspect ratios (AR) were obtained: nanofibers

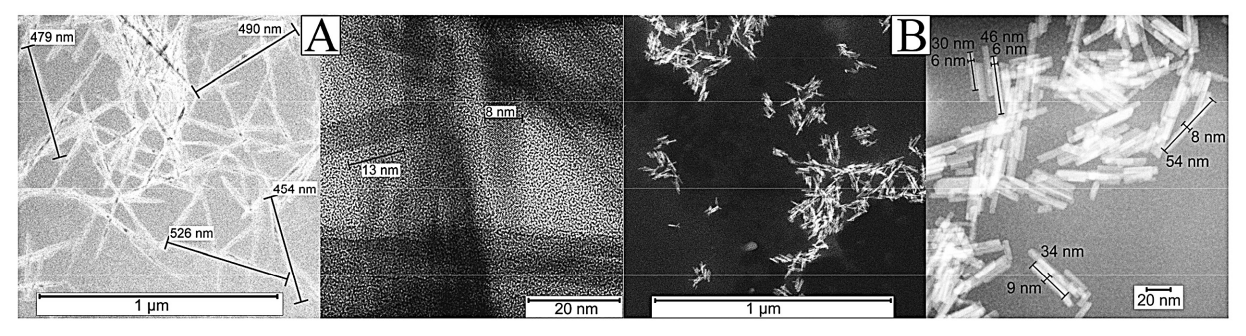


Рис. 1. Различные морфологии и размеры НЧ $La_{1-x}Pr_xPO_4$, синтезированных гидротермально-микроволновым методом (200 °C, 2 ч): А – нановолокна $La_{0.98}Pr_{0.02}PO_4$; В – наностержни $La_{0.98}Pr_{0.05}PO_4$. **Fig. 1.** Different morphologies and sizes of $La_{1-x}Pr_xPO_4$ NPs prepared by microwave-assisted hydrothermal method (200 °C, 2 hours): A – $La_{0.98}Pr_{0.02}PO_4$ nanofibers; В – $La_{0.95}Pr_{0.05}PO_4$ nanorods.

ORIGINAL ARTICLES

(nanofiber sample, AR > 30) (Fig. 1a) and nanorods (nanorod sample, AR \approx 5) (Fig. 1b). The measured sizes of the NPs from the nanofiber sample do not exceed 600 nm in length and 15 nm in diameter, and the NPs from the nanorod sample do not exceed 80 nm in length and 10 nm in diameter. As follows from the TEM analysis, the sizes of the obtained NPs strongly depend on the synthesis conditions: pH and the ratio of excess anions. With an increase in these parameters, the sizes of the NPs decrease significantly.

X-ray excited optical luminescence spectroscopy of La₁_ Pr_PO_n colloidal solutions

The X-ray optical luminescence spectra in the UV-C region of the obtained colloidal solutions consist of three broad luminescence bands of the transitions $4f^15d^1 \rightarrow {}^3H_4$, 3H_5 , 3H_6 (3F_2) in Pr^{3+} ions (Fig. 2). The noise vertical lines observed in the spectra are a consequence of the penetration of X-ray quanta into the CCD camera, which was located in the path of the X-ray tube window.

The transition from nanofibers to nanorods caused a strong weakening of the fluorescence intensity. The observed UV-C luminescence brightness is about 6.3 times higher for the nanofiber sample (Fig. 2, curve A) than that for nanorod sample (Fig. 2, curve B). For nanofibers, the intensities of long-wave transition (4f¹5d¹ \rightarrow ³H₆) predominate, whereas for nanorods, the intensities of transitions from 4f¹5d¹ to the levels of the ground triplet ³H₁ are practically the same.

Intrinsic cytotoxicity of nanoparticles according to MTT assay

The viability of Mh22a and L929 cell cultures (Fig. 3) was assessed using the MTT assay after 24 h of incubation with $La_{0.95}Pr_{0.05}PO_4$ nanorod and $La_{0.98}Pr_{0.02}PO_4$ nanofiber samples at different concentrations of NPs (0.0625 – 4 mg/mL) in DMEM culture medium. Cytotoxicity for all samples was observed at a NPs concentration of 4 mg/mL.

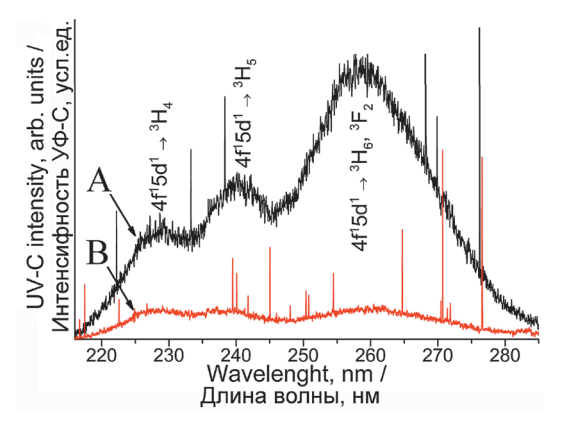
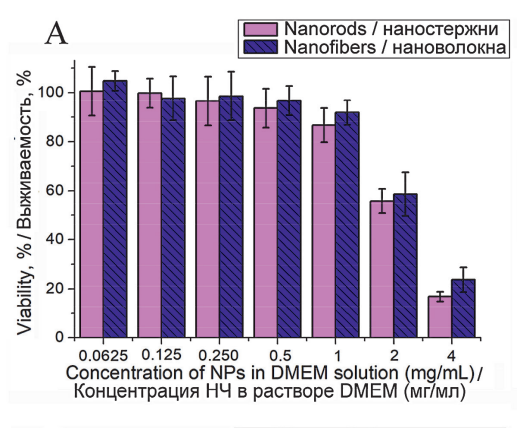


Рис. 2. УФ-С спектры рентгенолюминесценции коллоидных растворов (7 мг/мл): А – нановолокна $La_{0.98}Pr_{0.02}PO_4$; В – наностержни $La_{0.95}Pr_{0.05}PO_4$. Режим работы рентгеновской трубки: ускоряющее напряжение 30 кВ, анодный ток 2,5 мА, время экспозиции 60 с.

Fig. 2. X-ray excited UV-C spectra of colloidal solutions (7 mg/mL) samples: $A - La_{0.98}Pr_{0.02}PO_4$ nanofibers; $B - La_{0.98}Pr_{0.02}PO_4$ nanorods. X-ray tube operating mode: accelerating voltage 30 kV, anode current 2.5 mA, exposure time 60 s.



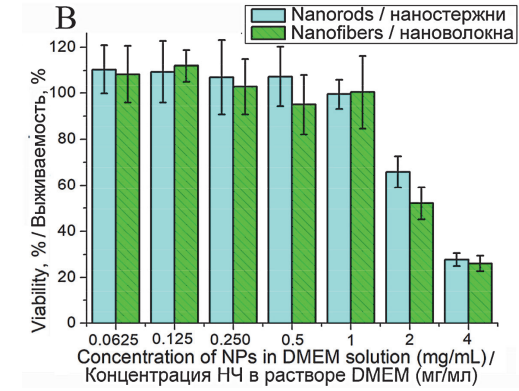


Рис. 3. Результаты МТТ анализа по выживаемости клеток Mh22a (A) и L929 (B) после 24 часов инкубации с наностержнями $La_{0.95}Pr_{0.05}PO_4$ (сплошные столбцы) и нановолоконами $La_{0.98}Pr_{0.02}PO_4$ (штрихованные столбцы) при разных концентрациях HЧ.

Fig. 3. Results of MTT assay for viability of Mh22a (A) and L929 (B) cells after 24 hours of incubation with La $_{0.95}$ Pr $_{0.05}$ PO $_4$ nanorods (solid bars) and La $_{0.98}$ Pr $_{0.02}$ PO $_4$ nanofibers (hatched bars) at different NPs concentrations.

At concentrations in the range of 0.0625 – 1 mg/mL, cell viability was more than 90% for both types of NPs.

For the studied samples of colloidal solutions, the calculated IC50 parameters (Table 1) indicate that they can be classified as low cytotoxic compounds for Mh22a and L929 cell cultures (according to the international standard ISO SO 10993-5:2009). As can be seen for the Mh22a cell line, the nanofiber sample has a slightly higher IC50 value than the nanorod sample. For the L929 cell line, IC50 is slightly higher for the nanorod sample. This may be due to the fact that the nanorod and nanofiber samples were treated differently at the washing stage (washings with addition of NH₄OH or HNO₃, respectively), which may cause different cell responses to NPs depending on the cell line. However, the observed difference in IC50 values is quite small.

Cytotoxicity after X-ray irradiation according to MTT assay

The X-ray irradiation modes on the cell samples were selected to cause low cell death of the control groups of Mh22a and L929 cells (about 10%) (Figs. 4A and 5A, respectively). The irradiation dose was based on previously



Таблица 1 Л $\mathsf{Д}_{50}$ для исследованных образцов по результатам МТТ анализа

Table 1 IC₅₀ of the studied samples according to MTT assay

Культура клеток Cell culture	Образец НЧ NPs sample	ЛД ₅₀ , мг/мл IC ₅₀ , mg/mL
Mh22a	La _{0.95} Pr _{0.05} PO ₄ наностержни La _{0.95} Pr _{0.05} PO ₄ nanorods	2.082
	La _{0.98} Pr _{0.02} PO ₄ нановолокна La _{0.98} Pr _{0.02} PO ₄ nanofibers	2.556
L929	La _{0.95} Pr _{0.05} PO ₄ наностержни La _{0.95} Pr _{0.05} PO ₄ nanorods	2.354
	La _{0.98} Pr _{0.02} PO ₄ нановолокна La _{0.98} Pr _{0.02} PO ₄ nanofibers	2.025

conducted experiments was 8 Gy. As an additional control, groups of Mh22a and L929 cells were irradiated with a UV lamp at 60 J/cm² for 8 min, which resulted in a strong decrease in viability (74% and 68%, respectively) (Fig. 4A and 5A, respectively).

The results of the MTT assay for the X-ray-induced cytotoxicity of the studied colloidal solutions on the viability of Mh22a cells demonstrate a significant decrease in viability only in the group of cells incubated with the sample of La_{0.98}Pr_{0.02}PO₄ nanofibers at a concentration of 2 mg/mL. In this case, the cell viability decreased by 28%

and 25% (for irradiation modes 1 and 2, respectively) compared to the group of cells incubated with the same conditions without exposure to X-rays (Fig. 4E). For the group of L929 cells incubated with the sample of La_{0.98}Pr_{0.02}PO₄ nanofibers at a NPs concentration of 2 mg/mL, the cell viability decreased by 24% and 17% (for irradiation modes 1 and 2, respectively) compared to the group of cells incubated with the same conditions without exposure to X-rays (Fig. 4J). Thus, the results of the MTT assay after the addition of NPs and X-ray irradiation showed a slightly stronger effect on Mh22a cancer cells than on L929 healthy fibroblasts. Unfortunately, MTT results for X-ray irradiation of both cell cultures incubated with 1 and 2 mg/mL of $La_{0.95}Pr_{0.05}PO_4$ nanorod or 1 mg/mL of La_{0.98}Pr_{0.02}PO₄ nanofiber samples showed little change in cell viability compared to incubation with the same NPs at the same concentrations without X-ray irradiation (Figs. 4B-D and G-I).

Study of the type of cell death according to fluorescence microscopy

To study the type of cytotoxicity under various influences, the double staining method with fluorescent dyes of acridine orange (AO) and propidium iodide (PI) with the subsequent fluorescence microscopy and morphological analysis were performed. The selected control groups of Mh22a and L929 cells from previous experiments were studied: untreated, treated with X-ray in mode 1 and mode 2, UV irradiated, incubated with 2 mg/mL of the La $_{0.95}$ Pr $_{0.05}$ PO $_{4}$ nanorod sample without and with X-ray treatment in mode 1 and mode 2, incubated with 2 mg/mL of the La $_{0.98}$ Pr $_{0.02}$ PO $_{4}$ nanofiber sample without

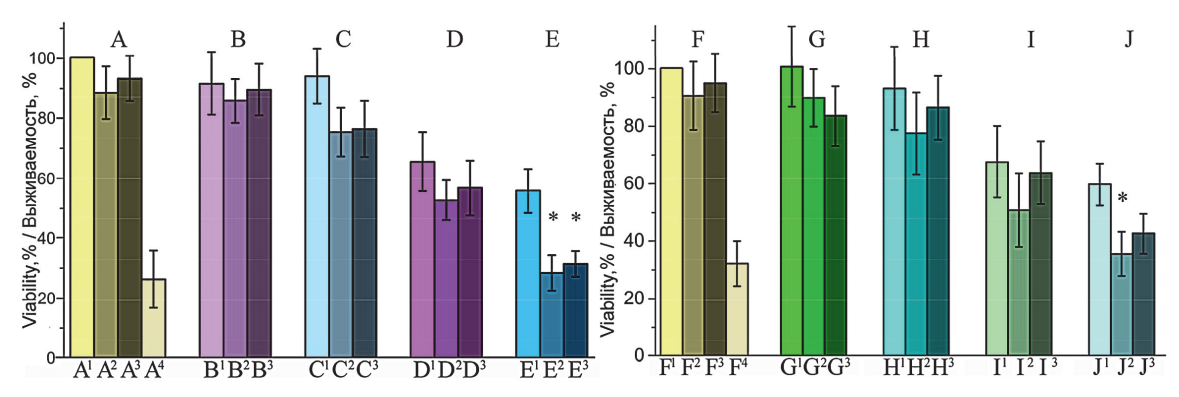


Рис. 4. Результаты МТТ теста по эффекту цитотоксичности на клетки Mh22a (A-E) и L929 (F-J) при различных воздействиях с последующей инкубацией в течении 24 ч. Группы столбцов соответствуют различным контрольным выборкам: А и F — отдельные эффекты: контрольные клетки (A^1 , F^1), клетки облученные рентгеном в режиме 1 (A^2 , F^2) и режиме 2 (A^3 , A^3), клетки облученные УФ лампой (A^4 , A^4 , A^4) и С — образец наностержней La_{0.95}Pr_{0.05}PO₄ (1 мг/мл) без облучения (A^1) и с облучением рентгеном в режиме 1 (A^2 , A^2) и режиме 2 (A^3 , A^3); С и H — образец наностолокон La_{0.98}Pr_{0.02}PO₄ (1 мг/мл) без облучения (A^2 , A^3) и с облучением рентгеном в режиме 1 (A^2 , A^2) и режиме 2 (A^3 , A^3); С и J — образец наностержней La_{0.95}Pr_{0.05}PO₄ (2 мг/мл) без облучения (A^2 , A^3) и режиме 2 (A^3 , A^3); Е и J — образец нановолокон La_{0.98}Pr_{0.05}PO₄ (2 мг/мл) без облучения (A^2 , A^3) и с облучением рентгеном в режиме 1 (A^2 , A^3) и режиме 2 (A^3 , A^3); Е и J — образец нановолокон La_{0.98}Pr_{0.02}PO₄ (2 мг/мл) без облучения (A^3 , A^3) и с облучением рентгеном в режиме 1 (A^3 , A^3) и режиме 2 (A^3 , A^3); A^3 , A^3 0 и с облучением рентгеном в режиме 1 (A^3 , A^3) и режиме 2 (A^3 , A^3 0 и режиме 2 (A^3 , A^3 0 и режиме 2 (A^3 0 и режиме 2

Fig. 4. MTT assay results on cytotoxicity effect on Mh22a (A-E) and L929 (F-J) cells under the influence of various treatments followed by incubation for 24 hours. The groups of columns correspond to the different control groups: A – individual effects: control cells (A¹, F¹), cells treated with X-ray mode 1 (A², F²) and mode 2 (A³, F³), cells irradiated with UV lamp (A⁴, F⁴); B – La $_{0.95}$ Pr $_{0.05}$ PO $_4$ nanorod sample (1 mg/mL) without (B¹, G¹) and with X-ray treatment in mode 1 (B², G²) and mode 2 (B³, G³); C and H – La $_{0.95}$ Pr $_{0.02}$ PO $_4$ nanorod sample (1 mg/mL) without (C¹, H¹) and with X-ray treatment in mode 1 (C², H²) and 2 mode (C³, H³); D and I – La $_{0.95}$ Pr $_{0.05}$ PO $_4$ nanorod sample (2 mg/mL) without (D¹, I¹) and with X-ray treatment in mode 1 (D², I²) and mode 2 (D³, I³); E and J – La $_{0.98}$ Pr $_{0.02}$ PO $_4$ nanofiber sample (2 mg/mL) without (E¹, J¹) and with X-ray treatment in mode 1 (E², J²) and mode 2 (E³, J³). * – P < 0.05



ORIGINAL ARTICLES

and with treatment with X-ray in mode 1 and mode 2 (see caption to Fig. 4A, D, E, F, I, J). The analysis of the number of viable (VC), apoptotic (AC) and necrotic (NC) cells was carried out according to their morphological features described in the in vitro study methodology.

The untreated groups of Mh22a and L929 cells had an intact membrane with uniform green staining of the cytoplasm and nucleus (Fig. 5A). In addition, spotted local orange fluorescence, which is more pronounced for Mh22a cells is characteristic of AO associated with active lysosomes or acidic cellular vesicles [14, 15]. The exposure to X-rays at a dose of 8 Gray in mode 1 and 2 modes did not lead to noticeable morphological changes in both cell

lines (Fig. 5B and C). Exposure of Mh22a and L929 to UV irradiation caused a strong change in cell morphology (Fig. 5D) indicating significant cell death with signs of apoptosis. Most Mh22a cells exposed to UV had disrupted membranes and a rounded shape with no evidence of active lysosomes, and their nuclei were stained orange (Fig. 5D, left side). However, in the case of L929, completely green cells with apoptotic bodies around them were observed (Fig. 5D, right side). This difference may be due to different kinetics of apoptosis depending on the cell line.

Images of Mh22a cells incubated with the nanorod and nanofiber samples without exposure to X-rays (Fig. 5E and F,

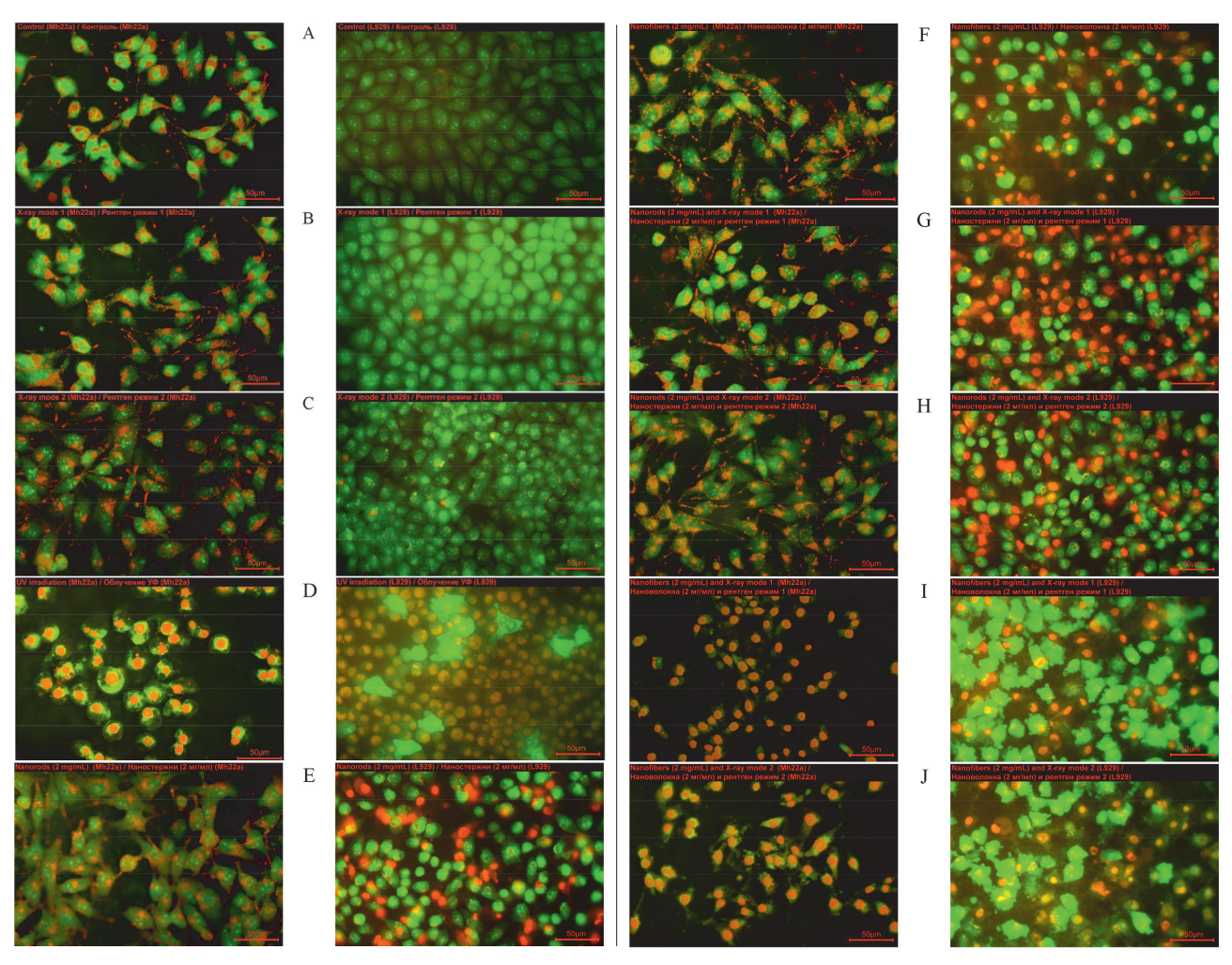


Рис. 5. Флуоресцентные изображения различных групп клеток Mh22a (слева) и L929 (справа) окрашенных акридиновым оранжевым и пропидий йодидом (увеличение: \times 400). А – контрольная группа (без дополнительных воздействий); В – облучение рентгеном в режиме 1; С – облучение рентгеном в режиме 2; D – облучение УФ лампой; Е – инкубация с 2 мг/мл наностержней La $_{0.95}$ Pr $_{0.05}$ PO $_4$; F – инкубация с 2 мг/мл нановолокон La $_{0.98}$ Pr $_{0.02}$ PO $_4$; G – инкубация с 2 мг/мл наностержней La $_{0.95}$ Pr $_{0.05}$ PO $_4$ и облучение рентгеном в режиме 1; H – инкубация с 2 мг/мл нановолокон La $_{0.98}$ Pr $_{0.05}$ PO $_4$ и облучение рентгеном в режиме 2; I – инкубация с 2 мг/мл нановолокон La $_{0.98}$ Pr $_{0.02}$ PO $_4$ и облучение рентгеном в режиме 2; и облучение рентгеном в режиме 2; и облучение рентгеном в режиме 2; и облучение рентгеном в режиме 2.

Fig. 5. Fluorescence images of different groups of Mh22a (left) and L929 (right) cells stained with AO and PI dyes (magnification: $\times 400$). A – control cells (untreated); B – irradiation with X-ray in mode 1; C – irradiation with X-ray in mode 2; D – irradiation with UV; E – incubation with 2 mg/mL of La_{0.98}Pr_{0.05}PO₄ nanorods; F – incubation with 2 mg/mL of La_{0.98}Pr_{0.05}PO₄ nanorods and irradiation with X-ray in mode 1; H – incubation with 2 mg/mL of La_{0.95}Pr_{0.05}PO₄ nanorods and irradiation with X-ray in mode 2; I – incubation with 2 mg/mL of La_{0.98}Pr_{0.02}PO₄ nanorods and irradiation with X-ray in mode 2; I – incubation with X-ray in mode 2.

left side, respectively) showed signs of apoptosis and, to a lesser extent, signs of necrosis, but a fairly large number of viable cells were preserved. Also, of note is the increase in spotted local orange fluorescence, indicating higher lysosomal activity of cells, possibly caused by oxidative stress induced by NPs). In fact, NPs containing REIs may exhibit catalytic properties and participate in oxidationreduction reactions, causing cell death [16]. However, the majority of cells were uniformly stained green by AO, indicating the integrity of the cell membranes. For L929 cells incubated with the nanorod sample (Fig. 5E, right side), a higher number of necrotic cells with red staining of the nucleus and cytoplasm were observed. However, the response of L929 cells to incubation with the nanofiber sample (Fig. 5F, right side) resulted in an increase in the number of AC with orange staining of nuclei or green staining with apoptotic bodies around them.

Exposure to X-rays (in both irradiation modes) of Mh22a cells incubated with the nanorod sample caused rounding of some of the cells, single apoptotic and necrotic cells were also observed (Fig. 5G, H, left side). For L929 cells incubated with the nanorod sample and irradiated with X-rays (in both modes), slightly higher numbers of necrotic cells were observed (Fig. 5G, H, right side). In contrast, in the groups of Mh22a cells incubated with 2 mg/mL nanofiber and treated with X-rays in mode 1 and 2 (Fig. 5I and J, left side), a decrease in the number of VC and a significant increase in the number of AC was observed. The apoptotic Mh22a cells were determined by the shrinkage and rounding of cells and intense orange fluorescence of the nucleus, which is caused by the destruction of the

native DNA structure and the binding of DNA fragments to AO dye. Single necrotic Mh22a cells, appearing as red nucleus, were also seen in this case. Similar visual effects were observed for L929 cells incubated with the nanofiber sample and treated with X-rays in mode 1 and 2 (Fig. 5I and J, right side). However, in the case of L929 cells, more cells with apoptotic bodies around them were observed, which again may be due to different apoptosis kinetics depending on the cell line.

Based on morphological analysis of fluorescence microscope images, statistics of the distribution of viable (VC), apoptotic (AC) and necrotic (NC) cells were obtained for Mh22a and L929 cell cultures (Fig. 6A and B, respectively). In general, the pattern for X-ray and UV (Fig. 6A²-A⁴, B²-B⁴) exposure is similar for both types of cell cultures and in good agreement with MTT results (Fig. 4A, F). However, for Mh22a cells irradiated with a UV lamp (Fig. 6A4), an almost complete absence of VC was observed, which differs from the MTT results (Fig. 4A). The obtained statistics on VC after incubation of cells with NPs with or without subsequent X-ray irradiation (Fig. 6A⁵-A¹⁰ and B⁵-B¹⁰) are also in good agreement with MTT data (Fig. 4D, E, I, J). Additionally, control groups of Mh22a cells incubated with NPs solutions at a concentration of 2 mg/mL demonstrated higher cell survival according to fluorescence microscopy data (Fig. 6A) compared to the MTT assay (Fig. 4D, E). The observed differences in AC/ NC ratio between the UV irradiated control groups of the Mh22a and L929 cell lines (Fig. A⁴ and B⁴, respectively) are likely due to the faster kinetics of apoptosis for L929 cells, making them less distinguishable from necrotic cells.

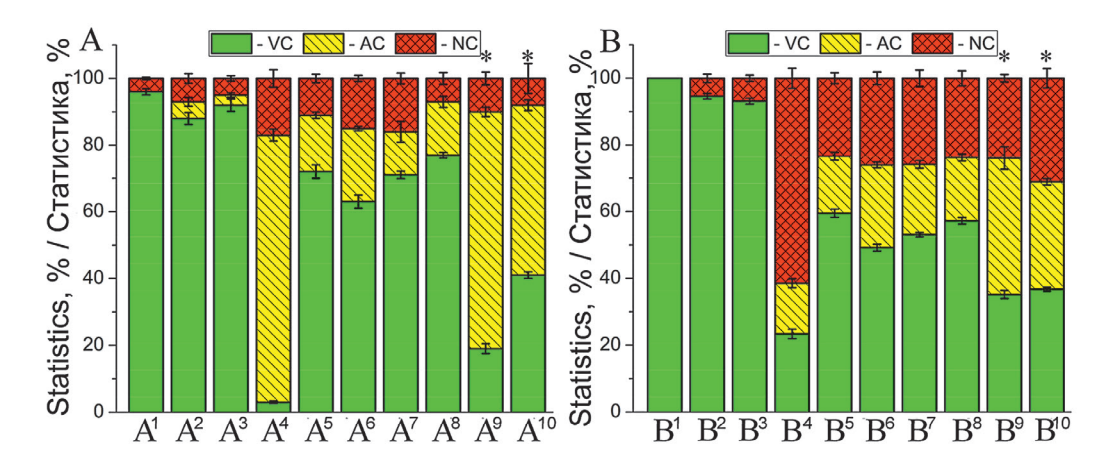


Рис. 6. Морфологический анализ изображений с флуоресцентного микроскопа живых (VC), апоптотических (AC) и мертвых (NC) клеток для A-Mh22a и B-L929 клеточных культур при различных воздействиях: клетки без дополнительных воздействий (A^1 , B^1), облучение рентгеном в режиме 1 (A^2 , B^2) и режиме 2 (A^3 , B^3), облучение $Y\Phi$ лампой (A^4 , B^4), инкубация клеток с 2 мг/мл наностержней $La_{0.95}Pr_{0.05}PO_4$ без облучения (A^5 , B^5) и с облучением рентгеном в режиме 1 (A^6 , B^6) и режиме 2 (A^7 , B^7), инкубация клеток с 2 мг/мл нановолокон $La_{0.98}Pr_{0.02}PO_4$ без облучения (A^8 , B^8) и с облучением рентгеном в режиме 1 (A^9 , A^9) и режиме 1 (A^9) и режиме 1 и режиме 1 (A^9) и режиме 1 и режим

Fig. 6. Morphological analysis of fluorescence microscope images of viable (VC), apoptotic (AC) and necrotic and death (NC) cells for A – Mh22a and B – L929 cell cultures under various influences: untreated cells (A^1 , B^1), X-ray irradiation in mode 1 (A^2 , B^2) and mode 2 (A^3 , B^3), UV irradiation (A^4 , A^4), incubation with 2 mg/mL of the La_{0.95}Pr_{0.05}PO₄ nanorod sample without (A^5 , A^5) and with X-ray irradiation in mode 1 (A^6 , A^6) and mode 2 (A^7 , A^7), incubation with 2 mg/mL of the La_{0.98}Pr_{0.02}PO₄ nanofiber sample without (A^8 , A^8) X-ray and with X-ray irradiation in mode 1 (A^9 , A^9) and mode 2 (A^{10} , A^{10}). * – P < 0.05



ORIGINAL ARTICLES

The apoptotic cycle of Mh22a cells probably takes longer, resulting in better distinguishability and an increased AC/

The obtained statistics of morphological distributions (Fig. 6) indicated a significant decrease in the survival rate of the studied cell lines due to apoptosis after incubation with the La_{0.98}Pr_{0.02}PO₄ nanofiber sample (2 mg/mL) and irradiation with X-rays. This effect becomes more noticeable when the cells are irradiated with X-rays in mode 1 than in mode 2, which is consistent with the MTT assay results (Fig. 4). In addition, the microscopy results indicated a higher sensitivity of Mh22a cancer cells to the studied effects compared to L929, which is also in agreement with the MTT assay results (Fig. 4). Unfortunately, the obtained statistics on the effect of the La_{0.95}Pr_{0.05}PO₄ nanorod sample (2 mg/mL) and X-ray irradiation showed that the effect is practically absent for both cell cultures (Fig. 6A⁵-A⁷ and B⁵-B⁷), which is also in full agreement with the results of the MTT assay (Fig. 4D, I).

Presumably, the decrease in viability of Mh22a and L929 cells was influenced by UV-C generated by nanofiber sample under the influence of X-rays, since in this case cell apoptosis is observed. At the same time, other effects acting on the cell under the influence of NPs reacting with X-rays are also possible, for example, the formation of secondary electrons by NPs or heating of NPs, which can also lead to the deactivation of irradiated cells. The mentioned catalytic activity of NPs doped with REI can also enhance the effect of X-rays. Some studies also report increased cytotoxicity due to apoptosis of NPs with a positively charged surface [17, 18]. Thus, part of the intrinsic cytotoxicity of nanofiber sample may be due to the positively charged adsorption and diffusion layers after washing with HNO₃ solution. In addition, nanorods obtained in an alkaline medium with ammonium tartrate solution can desorb molecules and ions under the influence of X-rays, such as hydroxyl groups, ammonia ions or tartaric acid residues, which can also lead to additional cell death by necrosis. However, despite this, we believe that the main cytotoxic effect was caused by UV-C radiation, since in this case the morphology of the cells is similar to cells irradiated with a UV lamp. Moreover, in [4] it was shown that LuPO, NPs without an activator have virtually no effect on X-ray-induced cytotoxicity relative to LuPO₄:Pr³⁺ NPs.

It should also be noted that for the successful use of NPs in cancer therapy it is necessary to reduce the concentration of the applied NPs and reduce the effect of intrinsic necrosis. Therefore, more experiments on optimization of synthesis and washing procedure of NPs and their surface functionalization are required to further improve their therapeutic potential. In addition, more extensive studies are needed to examine the mechanisms of cytotoxicity by which NPs act on different cell types under different X-ray irradiation regimens.

Conclusion

Two colloidal solutions of La, Pr, PO, NPs with nanofiber (length & diameter not larger than 600 & 15 nm, respectively) and nanorod (length & diameter not larger than 80 & 10 nm, respectively) morphologies were prepared by the hydrothermal microwaveassisted method. Measurement of X-ray excited optical luminescence spectra in the UV-C range from the obtained colloidal solutions showed a large difference in brightness: for larger NPs, the brightness was 6.3 times higher.

According to the MTT assay, the prepared colloidal solutions were classified as low-cytotoxic compounds (IC50 > 2 mg/mL) for Mh22a and L929 cell lines. A significant decrease in cell viability under the influence of X-rays was achieved only for groups of cells incubated with 2 mg/mL of colloidal solutions consisting of NPs having nanofiber morphology with 2 mole-% doping of Pr³⁺ ions. After X-ray irradiation, groups of Mh22a and L929 cells incubated with colloidal solutions of La_{0.08}Pr_{0.02}PO₄ nanofiber NPs showed pronounced cell apoptosis, which may indicate the successful effect of UV-C quanta generated under the influence of X-rays on controlled cell death. According to MTT assay and fluorescence microscopy, the effect of X-ray-induced NPs cytotoxicity is more pronounced for cancer cells and increases with decreasing accelerating voltage of the X-ray tube. Therefore, the potential for therapeutic use of La, Pr.PO, NPs has been shown. Unfortunately, the use of NPs with nanorod morphology did not significantly enhance the X-ray irradiation effect, indicating the need to increase their X-ray excited UV-C brightness. Fluorescence microscopy showed that the intrinsic and X-ray induced cytotoxicity of La_{0.95}Pr_{0.05}PO₄ colloidal solutions consisting of NPs with nanorod morphology is mostly due to cell necrosis for L929 and Mh22a cell lines. Further research is needed to clarify the cause and type of cell death for various cell cultures incubated with La,__,Pr,PO, NPs and irradiated with X-rays. For medical application of La_{1-x}Pr_xPO₄ NPs, it is still necessary to increase their UV-C luminescence intensity under X-ray excitation and modify their surface, which should lead to an increase in X-ray induced cytotoxicity, a decrease in the practical concentration of the NPs in colloids, and a decrease in intrinsic cytotoxicity.

Acknowledgments

V.Y.G., S.G.O., O.E.O. and S.A.T. are grateful for a support of the Russian Science Foundation (grant number 22-22-00998 for small scientific groups). Authors are grateful to Nikolay Pyatayev for organizing the in vitro studies. G.I.A., A.-k.A.A.M., C.R.A. and Y.D.E. are grateful to Nikolay A. Pyatayev and Mikhail N. Zharkov for their help in writing the text of the in vitro results analysis and formulating the conclusions to them.

ORIGINAL ARTICLES

REFERENCES

- Miwa S., Yano S., Hiroshima Y., Tome Y., Uehara F., Mii S., Efimova E.V., Kimura H., Hayashi K., Tsuchiya H., Hoffman R.M. Imaging UVC-induced DNA damage response in models of minimal cancer. J. Cell. Biochem, 2013, vol. 114(11), pp. 2493-2499.
- Müller M., Espinoza S., Jüstel T., Held K.D., Anderson R.R., Purschke M. UVC-Emitting LuPO₄:Pr³⁺ Nanoparticles Decrease Radiation Resistance of Hypoxic Cancer Cells. Radiat. Res, 2020, vol. 193(1), pp.
- Squillante M. R., Jüstel T., Anderson R.R., Brecher C., Chartier D., 3. Christian J.F., Cicchetti N., Espinoza S., McAdams D.R., Müller M., Tornifoglio B., Wang Y., Purschke M. Fabrication and characterization of UV-emitting nanoparticles as novel radiation sensitizers targeting hypoxic tumor cells. Opt. Mater, 2018, vol. 80, pp. 197-
- Espinoza S., Müller M., Jenneboer H., Peulen L., Bradley T., Purschke M., Haase M., Rahmanzadeh R., Jüstel T. Characterization of Micro- and Nanoscale LuPO₄:Pr³⁺, Nd³⁺ with Strong UV-C Emission to Reduce X-Ray Doses in Radiation Therapy. Part. Part. Syst. Charact, 2019, vol. 36(10), pp. 1900280.
- Espinoza S., Volhard M.-F., Kätker H., Jenneboer H., Uckelmann A., Haase M., Müller M., Purschke M., Jüstel T. Deep Ultraviolet Emitting Scintillators for Biomedical Applications: The Hard Way of Downsizing LuPO,:Pr3+. Part. Part. Syst. Charact, 2018, vol. 35(12), pp. 1800282.
- Tran T. A., Kappelhoff J., Jüstel T., Anderson R.R., Purschke M.U. V emitting nanoparticles enhance the effect of ionizing radiation in 3D lung cancer spheroids. Int. J. Radiat. Biol, 2022, vol. 98(9), pp. 1484-1494.
- Malyy T.S., Vistovskyy V.V., Khapko Z.A., Pushak A.S., Mitina N.E., Zaichenko A.S., Gektin A.V., Voloshinovskii A.S. Recombination luminescence of LaPO,-Eu and LaPO,-Pr nanoparticles. J. Appl. Phys, 2013, vol. 113(22), pp. 224305.
- Srivastava A.M., Setlur A.A., Comanzo H.A., Beers W.W., Happek U., Schmidt P. The influence of the Pr^{3+} $^4f^{15}d^1$ configuration on the 1S_0 emission efficiency and lifetime in LaPO, Opt. Mater, 2011, vol. 33(3), pp. 292-298.
- Okamoto S., Uchino R., Kobayashi K., Yamamoto H. Luminescent properties of Pr3+-sensitized LaPO,:Gd3+ ultraviolet-B phosphor under vacuum-ultraviolet light excitation. J. Appl. Phys, 2009, vol. 106(1), pp. 013522.
- Srivastava A.M. Aspects of Pr³⁺ luminescence in solids. *J. Lumin,* 2016, vol. 169(B), pp. 445-449.
- Bagatur'yants A.A., Iskandarova I.M., Knizhnik A.A., Mironov V.S., Potapkin B.V., Srivastava A.M., Sommerer T.J. Energy level structure of 4f⁵d states and the Stokes shift In LaPO₄:Pr³⁺: A theoretical study. Phys. Rev. B., 2008, vol. 78(16), pp. 165125.
- Hilario E.G., Rodrigues L.C.V., Caiut J.M.A. Spectroscopic study of the 4f5d transitions of LaPO4 doped with Pr3+ or co-doped with Pr³⁺ and Gd³⁺ in the vacuum ultra violet region. Nanotechnology, 2022, vol. 33, pp. 305703. https://doi.org/10.1088/1361-6528/ ac6679
- McGahon A.J., Martin S.J., Bissonnette R.P., Mahboubi A., Shi Y., Mogil R.J., Nishioka W.K., Green D.R. The end of the (cell) line: methods for the study of apoptosis in vitro. Methods Cell Biol, 1995, vol. 46,
- Kusuzaki K., Murata H., Matsubara T., Satonaka H., Wakabayashi T., Matsumine A., Uchida A. Review. Acridine orange could be an innovative anticancer agent under photon energy. In Vivo, 2007, vol. 21(2), pp. 205-214.
- Qian H., Chao X., Williams J., Fulte S., Li T., Yang L., Ding W. X. Autophagy in liver diseases: A review. Mol Aspects Med, 2021, vol. 82,
- Xu C. and Qu X. Cerium oxide nanoparticle: a remarkably versatile rare earth nanomaterial for biological applications. NPG Asia Mater, 2014, vol. 6(3), pp. e90-e90.
- 17. Goodman C. M., McCusker C. D., Yilmaz T., Rotello V.M. Toxicity of gold nanoparticles functionalized with cationic and anionic side chains. Bioconjugate Chem, 2004, vol. 15(4), pp. 897-900.
- Schaeublin N.M., Braydich-Stolle L.K., Schrand A.M., Miller J.M., Hutchison J., Schlager J.J., Hussain S.M. Surface charge of gold nanoparticles mediates mechanism of toxicity. Nanoscale, 2011, vol. 3(2), pp. 410-420.

ЛИТЕРАТУРА

- Miwa S., Yano S., Hiroshima Y., Tome Y., Uehara F., Mii S., Efimova E.V., Kimura H., Hayashi K., Tsuchiya H., Hoffman R.M. Imaging UVC-induced DNA damage response in models of minimal cancer // J. Cell. Biochem. - 2013. - Vol. 114(11). - P. 2493-2499.
- Müller M., Espinoza S., Jüstel T., Held K.D., Anderson R.R., Purschke M. UVC-Emitting LuPO,:Pr3+ Nanoparticles Decrease Radiation Resistance of Hypoxic Cancer Cells // Radiat. Res. - 2020. - Vol. 193(1). - P. 82-87.
- Squillante M. R., Jüstel T., Anderson R.R., Brecher C., Chartier D., Christian J.F., Cicchetti N., Espinoza S., McAdams D.R., Müller M., Tornifoglio B., Wang Y., Purschke M. Fabrication and characterization of UV-emitting nanoparticles as novel radiation sensitizers targeting hypoxic tumor cells // Opt. Mater. - 2018. -Vol. 80. - P. 197-202.
- Espinoza S., Müller M., Jenneboer H., Peulen L., Bradley T., Purschke M., Haase M., Rahmanzadeh R., Jüstel T. Characterization of Microand Nanoscale LuPO₄:Pr³⁺, Nd³⁺ with Strong UV-C Emission to Reduce X-Ray Doses in Radiation Therapy // Part. Part. Syst. Charact. – 2019. – Vol. 36(10). – P. 1900280.
- Espinoza S., Volhard M.-F., Kätker H., Jenneboer H., Uckelmann A., Haase M., Müller M., Purschke M., Jüstel T. Deep Ultraviolet Emitting Scintillators for Biomedical Applications: The Hard Way of Downsizing LuPO_a:Pr³⁺ // Part. Part. Syst. Charact. – 2018. – Vol. 35(12). – P. 1800282.
- Tran T. A., Kappelhoff J., Jüstel T., Anderson R.R., Purschke M.U. V emitting nanoparticles enhance the effect of ionizing radiation in 3D lung cancer spheroids // Int. J. Radiat. Biol. - 2022. - Vol. 98(9). - P. 1484-1494.
- Malyy T.S., Vistovskyy V.V., Khapko Z.A., Pushak A.S., Mitina N.E., Zaichenko A.S., Gektin A.V., Voloshinovskii A.S. Recombination luminescence of LaPO,-Eu and LaPO,-Pr nanoparticles // J. Appl. Phys. – 2013. – Vol. 113 (22). – P. 224305.
- Srivastava A.M., Setlur A.A., Comanzo H.A., Beers W.W., Happek U., Schmidt P. The influence of the Pr³⁺ 4f¹5d¹ configuration on the ¹S₀ emission efficiency and lifetime in LaPO₄ // Opt. Mater. – 2011. Vol. 33(3). - P. 292-298.
- Okamoto S., Uchino R., Kobayashi K., Yamamoto H. Luminescent properties of Pr3+ -sensitized LaPO₄:Gd3+ ultraviolet-B phosphor under vacuum-ultraviolet light excitation // J. Appl. Phys. – 2009. - Vol. 106(1). - P. 013522.
- Srivastava A.M. Aspects of Pr³⁺ luminescence in solids // J. Lumin. – 2016. – 169(B). – P. 445–449.
- Bagatur'yants A.A., Iskandarova I.M., Knizhnik A.A., Mironov V.S., Potapkin B.V., Srivastava A.M., Sommerer T.J. Energy level structure of 4f⁵d states and the Stokes shift In LaPO₄:Pr³⁺: A theoretical study // Phys. Rev. B. – 2008. – Vol. 78(16). – P. 165125.
- Hilario E.G., Rodrigues L.C.V., Caiut J.M.A. Spectroscopic study of the ${}^4\!f^5\!d$ transitions of LaPO $_4$ doped with Pr $^{3+}$ or co-doped with Pr $^{3+}$ and Gd3+ in the vacuum ultra violet region // Nanotechnology. -2022. - Vol. 33. - P. 305703.
- McGahon A.J., Martin S.J., Bissonnette R.P., Mahboubi A., Shi Y., Mogil R.J., Nishioka W.K., Green D.R. The end of the (cell) line: methods for the study of apoptosis in vitro // Methods Cell Biol. -1995. - Vol. 46. - P. 153-185.
- Kusuzaki K., Murata H., Matsubara T., Satonaka H., Wakabayashi T., Matsumine A., Uchida A. Review. Acridine orange could be an innovative anticancer agent under photon energy // In Vivo. -2007. – Vol. 21(2). – P. 205-214.
- Qian H., Chao X., Williams J., Fulte S., Li T., Yang L., Ding W. X. Autophagy in liver diseases: A review // Mol Aspects Med. – 2021. - Vol. 82. – P. 100973.
- 16. Xu C. and Qu X. Cerium oxide nanoparticle: a remarkably versatile rare earth nanomaterial for biological applications // NPG Asia Mater. - 2014. - Vol. 6(3). - P. e90-e90.
- Goodman C. M., McCusker C. D., Yilmaz T., Rotello V.M. Toxicity of gold nanoparticles functionalized with cationic and anionic side chains // Bioconjugate Chem. - 2004. - Vol. 15(4). - P. 897-
- Schaeublin N.M., Braydich-Stolle L.K., Schrand A.M., Miller J.M., Hutchison J., Schlager J.J., Hussain S.M. Surface charge of gold nanoparticles mediates mechanism of toxicity // Nanoscale. -2011. - Vol. 3(2). - P. 410-420.

IN VITRO PHOTODYNAMIC EFFICACY OF POLYCATIONIC PHOTOSENSITIZERS BASED ON LONGWAVE PHTHALOCYANINES

Romanishkin I.D.^{1,2}, Meerovich I.G.³, Bunin D.A.^{2,4}, Skobeltsin A.S.^{1,2,5}, Akhlyustina E.V.^{2,5}, Levkin V.V.², Kharnas S.S.², Kogan E.A.², Zhi-Long Chen⁶, Meerovich G.A.^{1,2,5}, Gorbunova Yu.G.^{4,7}, Reshetov I.V.²

¹Prokhorov General Physics Institute of the Russian Academy of Sciences, Moscow 119991, Russia

²I.M. Sechenov First Moscow State Medical University (Sechenov University), Moscow, Russia ³A.N. Bach Institute of Biochemistry, Research Center of Biotechnology of the Russian Academy of Sciences, Moscow, Russia

⁴Frumkin Institute of Physical Chemistry and Electrochemistry, Russian Academy of Sciences, Moscow, Russia

⁵Institute of Engineering Physics for Biomedicine, National Research Nuclear University MEPhI, Moscow, Russia

⁶Huadong Hospital, Fudan University, Shanghai, China

⁷Kurnakov Institute of General and Inorganic Chemistry, Russian Academy of Sciences, Moscow, Russia

Abstract

Polycationic photosensitizers have previously demonstrated high *in vitro* efficacy against lung cancer cells, including cancer stem cells, and low dark cytotoxicity. Polycationic phthalocyanines have high quantum yield of singlet oxygen and photostability. In addition, it is possible to relatively simply introduce different metal-complexing agents and substituents into phthalocyanine macrocycles, which enables varying their photophysical characteristics. In this work, we studied photophysical properties of photosensitizers based on polycationic phthalocyanine derivatives with different chemical structure with strong absorption in the long wavelength region (680–690 nm). The studied photosensitizers exhibit negligible aggregation in the 1–100 μM concentration range and show very high phototoxicity in an *in vitro* study on A549 lung carcinoma cells (IC₅₀ of 60–100 nM for ZnPcChol₂ and 100–300 nM for 4α ZnPc⁴⁺ and 4α ZnPc⁴⁺, depending on the light dose), and low dark cytotoxicity.

Keywords: polycationic photosensitizer, A549 lung carcinoma, photodynamic therapy

Contacts: Romanishkin I.D., e-mail: igor.romanishkin@nsc.gpi.ru

For citations: Romanishkin I.D., Meerovich I.G., Bunin D.A., Skobeltsin A.S., Akhlyustina E.V., Levkin V.V., Kharnas S.S., Kogan E.A., Zhi-Long Chen, Meerovich G.A., Gorbunova Yu.G., Reshetov I.V. *In vitro* photodynamic efficacy of polycationic photosensitizers based on polycationic phthalocyanines, *Biomedical Photonics*, 2025, vol. 14, no. 3, pp. 24–29. doi: 10.24931/2413–9432–2025–14–3–24–29

ФОТОДИНАМИЧЕСКАЯ ЭФФЕКТИВНОСТЬ IN VITRO ПОЛИКАТИОННЫХ ФОТОСЕНСИБИЛИЗАТОРОВ НА ОСНОВЕ ДЛИННОВОЛНОВЫХ ФТАЛОЦИАНИНОВ

И.Д. Романишкин 1,2 , И.Г. Меерович 3 , Д.А. Бунин 2,4 , А.С. Скобельцин 1,2,5 , Е.В. Ахлюстина 2,5 , В.В. Левкин 2 , С.С. Харнас 2 , Е.А. Коган 2 , Zhi-Long Chen 6 , Г.А. Меерович 1,2,5 , Ю.Г. Горбунова 4,7 , И.В. Решетов 2

¹Институт общей физики им. А. М. Прохорова Российской академии наук, Москва, Россия ²Первый Московский государственный медицинский университет имени И.М. Сеченова Министерства здравоохранения Российской Федерации (Сеченовский Университет), Москва, Россия

³Институт биохимии им. А.Н. Баха Российской академии наук, Москва, Россия

⁴Федеральное государственное бюджетное учреждение науки Институт физической химии и электрохимии им. А.Н. Фрумкина Российской академии наук, Москва, Россия ⁵Национальный исследовательский ядерный университет «МИФИ», Москва, Россия ⁶Huadong Hospital, Fudan University, Шанхай, Китай

⁷Институт общей и неорганической химии имени Н.С. Курнакова Российской академии наук, Москва, Россия

Резюме

Поликатионные фотосенсибилизаторы ранее продемонстрировали высокую эффективность *in vitro* против клеток рака лёгкого, в том числе против раковых стволовых клеток, при низкой темновой цитотоксичности. Поликатионные фталоцианины имеют высокий квантовый выход фотогенерации синглетного кислорода и фотостабильность. Кроме этого, возможно относительно простое введение различных металлов-комплексообразователей и заместителей во фталоцианиновые макроциклы, что дает возможность варьирования фотофизических характеристик. В данной работе мы изучали фотофизические свойства фотосенсибилизаторов на основе поликатионных производных фталоцианинов с различной химической структурой, обладающих интенсивным поглощением в длинноволновой области (680–690 нм). Исследованные фотосенсибилизаторы проявляют незначительную агрегацию в диапазоне концентраций 1–100 мкМ и демонстрируют очень высокую фототоксичность в исследовании *in vitro* на клетках карциномы лёгкого А549 (IC₅₀ 60–100 нМ для ZnPcChol₈ и 100–300 нМ для 4αZnPc⁴⁺ и 4αβZnPc4⁺ в зависимости от дозы света), а также низкую темновую цитотоксичность.

Ключевые слова: поликатионный фотосенсибилизатор, карцинома лёгкого А549, фотодинамическая терапия.

Контакты: Романишкин И.Д., e-mail: igor.romanishkin@nsc.gpi.ru

Для цитирования: Романишкин И.Д., Меерович И.Г., Бунин Д.А., Скобельцин А.С., Ахлюстина Е.В., Левкин В.В, Харнас С.С., Коган Е.А., Сhen Z.-L., Меерович Г.А., Горбунова Ю.Г., Решетов И.В. Фотодинамическая эффективность *in vitro* поликатионных фотосенсибилизаторов на основе длинноволновых фталоцианинов // Biomedical Photonics. – 2025. – Т. 14, № 3. – С. 24–29. doi: 10.24931/2413–9432–2025–14–3–24–29

Introduction

Photosensitizers (PSs) used in clinical practice for photodynamic therapy (PDT) of tumors usually are anionic or electroneutral compounds; monocationic phenothiazines, in particular, Methylene Blue, are used mainly for antibacterial PDT (for photodynamic treatment of local pathological foci with bacterial lesions) [1–4]. Some works, in particular, [5–7], discuss the influence of charge sign of PS molecules in biological fluids, which are aqueous compositions, on its antitumor efficacy. It was discovered that polycationic chlorin conjugates had a significantly higher photodynamic efficacy against ovarian cancer cells compared to polyanionic ones [7].

Recently, a number of polycationic photosensitizers based on heterocyclic compounds with high antitumor efficacy have been developed [8–16].

The aim of the present work is to comparatively investigate the photophysical properties and phototoxicity of long-wavelength photosensitizers based on polycationic phthalocyanines with different structure and charge.

Materials and methods

Long-wavelength polycationic phthalocyanines with excitation in the spectral range of 680–690 nm with different composition and/or structure, were used as PSs (Fig.1):

- zinc octakis(cholinyl)phthalocyanine (ZnPcChol₈), synthesized at the Institute of Organic Intermediates and Dyes (Russia) [11].
- having the same composition but different structure, symmetric 4αZnPc⁴⁺ tetraiodide 1,8(11),15(18),22(25)-tetrakis(4-((diethylmethylammonium)methyl)phenoxy) zinc phthalocyaninate and asymmetric 4αβZnPc⁴⁺ tetraiodide 1,2,3,4-tetrakis(4-((diethylmethylammonium)methyl)phenoxy)phenoxy) zinc phthalocyaninate, synthesized at Frumkin Institute of Physical Chemistry and Electrochemistry [14, 15].

ZnPcChol $_{\rm g}$ is well soluble in both water and phosphate buffer saline (PBS). Since $4\alpha ZnPc^{4+}$ and $4\alpha\beta ZnPc^{4+}$ have low water solubility, dimethyl sulfoxide (DMSO) was used as their solvent with consideration that DMSO content should not exceed 1% in solutions for intravenous administration. Therefore, PS solutions in PBS containing no more than 1% of DMSO were used in the experiments. PS solutions with concentrations of 1, 3, 10, 30, 100 μM were prepared, as well as samples where inactivated fetal bovine serum (FBS) was used as the solvent and added to 1 mM PBS solution to obtain similar PS concentrations.

Comparative PS studies were performed on solutions of both $4\alpha ZnPc^{4+}$ and $4\alpha\beta ZnPc^{4+}$ pre-dissolved in DMSO, and $ZnPcChol_{\circ}$ in PBS and in its composition with FBS.

Absorption characteristics were investigated in a Hitachi-3410 dual-beam spectrophotometer (Hitachi, Japan) [17].

The shape of spectra and fluorescence intensity of polycationic phthalocyanines were studied using LESA-01-BIOSPEC spectrometer (Biospec, Moscow) with an extended dynamic range of the recorded signal [18] under excitation by a 633 nm laser. The data were analyzed with UnoMomento software (Biospec, Russia). To estimate the fluorescence lifetime, the PSs were excited by picosecond laser pulses with a wavelength of 637 nm, and the fluorescence was recorded using a spectroscopic complex with a streak camera (Hamamatsu, Japan). The fluorescence decay curves of the PSs were analyzed using Maximum Entropy Method to obtain lifetime values of individual fluorescence components [19].

To investigate the effect of PS composition on the survival of A549 human lung cancer cells, the cells were cultured in DMEM medium (PanEco, Russia) containing 2 mM glutamine, 100 U/ml penicillin, 100 μg/ml streptomycin supplemented with 10% fetal calf serum (Capricorn, Germany) at 37°C and 5% CO₂. To study cytotoxicity, cells were seeded into 96-well plates at 8000 cells per 100 μl of growth medium. After 24 h, the growth medium was replaced with the one containing the studied phthalocyanines in chosen concentrations ranging from 10⁻⁴ to 10⁻⁸ M. Cells were incubated with PS for 3 hours, after which they were washed from PS twice with growth medium. The irradiation of cell lines was carried out immediately after washing the cells, using light source with multiple LEDs [20]. After that,

the plate was placed for a day in an incubator with a temperature of 37°C and 5% CO₂ content. Cell plates without irradiation (dark mode) after washing were left for 24 h in incubator at 37°C and 5% CO₂. Cell survival after photodynamic exposure with the studied PS was determined using the MTT test. Optical density of the stained solution was evaluated at 540 nm in multimodal plate spectrophotometer Clariostar plus (BMG, Germany). Statistical data processing was performed using GraphPad software.

Results and discussion

The absorbance dependence of ZnPcChol $_{g'}$, 4α ZnPc $^{4+}$ and $4\alpha\beta$ ZnPc $^{4+}$ solutions in PBS is linear up to 100 μ M (Fig. 2), the shape and full width at half-maximum at high and low concentrations show no notable differences. The values of molar absorption coefficients maxima for these PSs are presented in Table 1.

Studies of PS solutions showed high fluorescence intensity of ZnPcChol $_8$ in water and PBS, while the fluorescence intensity of $4\alpha ZnPc^{4+}$ and $4\alpha \beta ZnPc^{4+}$ was low, presumably due to the aggregation of molecules of these compounds in such compositions. However, the addition of 10% FBS led to a significant increase of fluorescence of $4\alpha ZnPc^{4+}$ and $4\alpha \beta ZnPc^{4+}$. The disaggregation and monomerization of these compounds are also confirmed by measurements of fluorescence lifetime, which does not change in the concentration range < 30 μ M. $ZnPcChol_8$ in water and PBS is characterized at all concentration values by a single fluorescence lifetime value of 2.3 ns, close to that of the

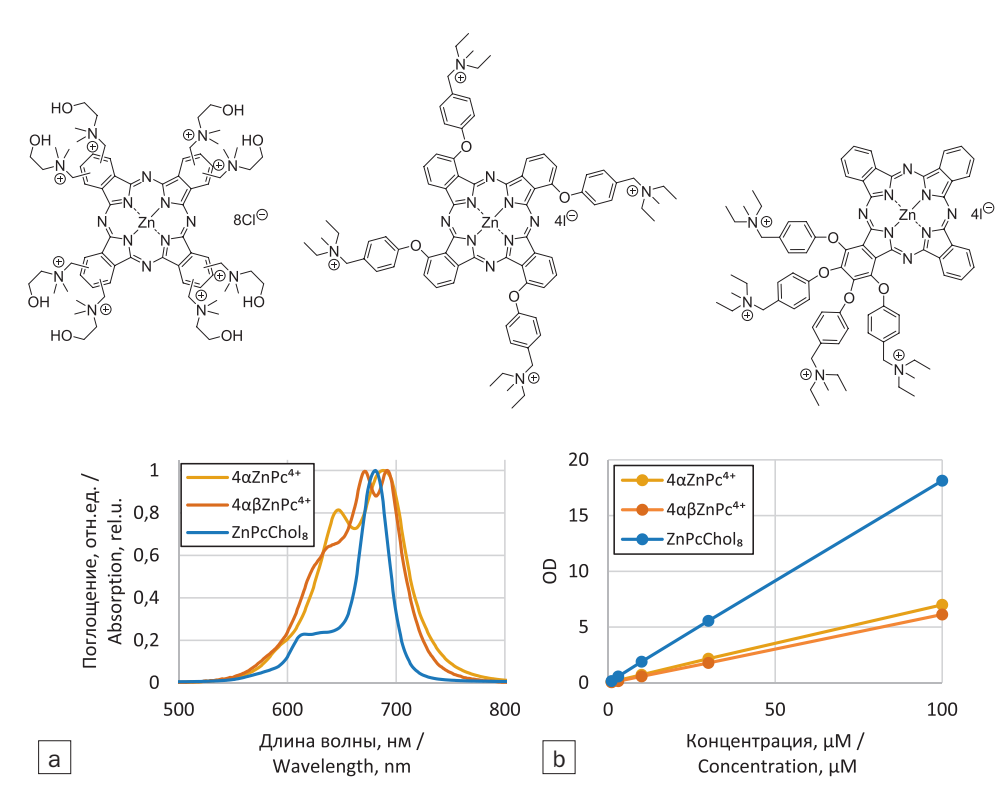


Рис. 1. Структурные формулы исследуемых фталоцианинов: ZnPcChol₈ (слева), 4α ZnPc⁴⁺ (посередине), 4α βZnPc⁴⁺ (справа). **Fig. 1.** Structural formulae of the studied photosensitizers: ZnPcChol₈ (left), 4α ZnPc⁴⁺ (middle), 4α βZnPc⁴⁺ (right).

2. Рис. Характеристики поглощения изучаемых ФС: а нормализованные спектры поглощения; b зависимость оптической плотности растворов ФС от их концентрации. Fig. 2. Absorption characteristics of studied PSs: a - normalized absorptions spectra; b concentration dependency of PS solutions optical density.

Таблица 1

Значение максимума коэффициента молярного поглощения исследуемых фотосенсибилизаторов и его длина волны в фосфатно-солевом буфере

Table 1Molar absorption coefficient maxima of the studied PSs and their wavelengths in PBS

Фотосенсиби- лизатор Photosensitizer	Длина волны максимума, нм Wavelength of maximum, nm	Коэффициент молярного поглощения, см⁻¹·M⁻¹ Molar absorption coefficient, cm⁻¹·M⁻¹		
ZnPcChol ₈	683	12.2×10 ⁴		
4αZnPc⁴⁺	688	7.0×10 ⁴		
4αβZnPc ⁴⁺	682	6.1×10 ⁴		

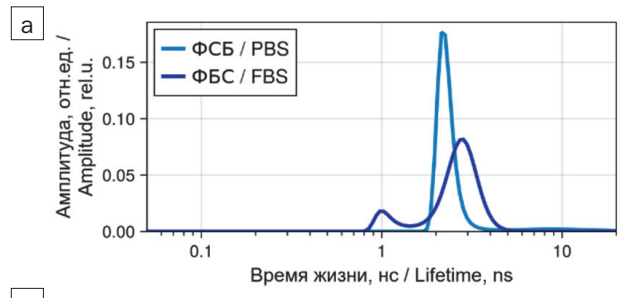
monomeric solution at low concentration. Components with shorter radiative lifetimes (in the range of 0.5-1.3 ns) appear in aqueous compositions of ZnPcChol₈ with FBS (Fig. 3a), but their fraction is negligible, especially in the biologically important range < 30 μ M. Whether this may be a sign of weak aggregation or a result of these PS binding with blood proteins requires additional study.

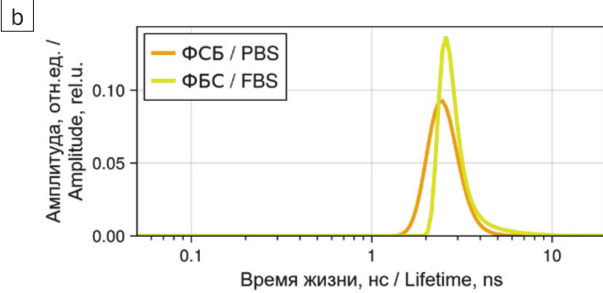
 $4\alpha ZnPc^{4+}$ in PBS with DMSO and in its composition with FBS, besides the main monomeric component with radiative lifetimes in the range of 2.4–3.3 ns, contains components with shorter lifetimes (0.34 and 1.05 ns) corresponding, presumably, to aggregated states, but their fraction is also negligible (Fig. 3b). These results show that $4\alpha ZnPc^{4+}$ slightly aggregates in the studied compositions.

The asymmetric photosensitizer 4αβZnPc⁴⁺ in PBS with DMSO has, in addition to the main monomer component with an emission lifetime of 2.3 ns, a larger fraction of a component with a short lifetime corresponding to the aggregated state (Fig. 3c). However, in the aqueous composition with FBS, this fraction also decreases. The reduction of aggregation in aqueous composition with FBS is due to the disaggregating effect of FBS proteins [21]. Considering that in in vitro studies cell cultures contain up to 10% FBS, and in vivo the PS solution will be administered intravenously (i.e., directly into blood plasma), it can be expected that these PS will be in a predominantly is a disaggregated state, and their photodynamic efficiency will be high.

The photodynamic efficacy of the studied phthalocyanine PSs against A549 lung cancer cells was evaluated by the ratio of cell survival after sensitization with different concentrations of the photosensitizer after irradiation with dose densities of 10 J/cm² and 30 J/cm² (phototoxicity) and without irradiation (cytotoxicity). The phototoxicity was very high, with IC₅₀ values at both light dose densities lying in the submicromole range (Table 2).

In all experiments, cytotoxicity was very low, IC_{50} values for the dark control were not reached even at concentrations of 100 μ M, which allows these photosensitizers to be classified as non-toxic substances.





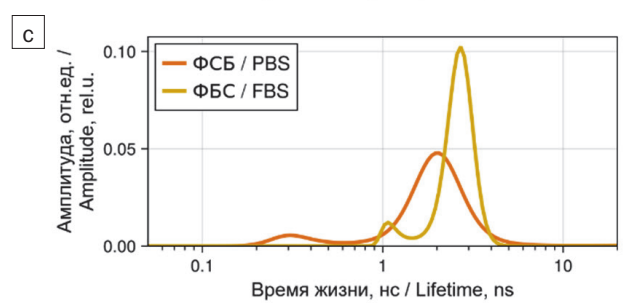


Рис. 3. Распределение времён жизни флуоресценции исследованных фотосенсибилизаторов с концентрацией 10 μ M: a – ZnPcChol $_{\rm g}$; b – 4α ZnPc $^{4+}$; с – 4α βZnPc $^{4+}$ в фосфатно-солевом буфере и в фетальной бычьей сыворотке.

Fig. 3. Distribution of fluorescence lifetimes of the studied photosensitizers with 10 μ M concentration: a – ZnPcChol $_{\rm g}$; b – 4α ZnPc $^{4+}$; c – $4\alpha\beta$ ZnPc $^{4+}$ in phosphate buffer saline and in fetal bovine serum.

Таблица 2

Значения IC_{50} для $ZnPcChol_{g}$, $4\alpha ZnPc4^{+}$ и $4\alpha \beta ZnPc^{4+}$ против клеток рака легкого A549

Table 2

IC $_{50}$ values for ZnPcChol $_{8}$, 4α ZnPc $^{4+}$ and $4\alpha\beta$ ZnPc $^{4+}$ against A549 lung cancer cells

Фотосенсиби- лизатор Photosensitizer	IC ₅₀ (мкМ) при разных плотностях дозы света IC ₅₀ (µM) at different dose densities				
	10 Дж/см² 10 J/cm²	30 Дж/см² 30 J/cm²			
ZnPcChol ₈	0.16±0.03	0.06±0.01			
4αZnPc⁴⁺	0.19±0.01	0.11±0.01			
4αβZnPc ⁴⁺	0.33±0.04	0.25±0.04			

High in vitro photodynamic efficiency of polycationic PSs against cancer cells is due, in our opinion, to several factors:

- high values of extinction and quantum yield of reactive oxygen species [11, 14, 15] in aqueous compositions, maintained in a wide range of concentrations values due to the absence of aggregation because of electrostatic repulsion of the PS ions from each other;
- effective binding of polycationic PS molecules to the surface of tumor cells, which has a significant negative charge due to the Warburg effect [22], internalization of their molecules into cells and photodynamic destruction of their organelles [5–7, 16].

Increasing the light dose density leads to an increase in phototoxicity, but this increase is not proportional to the light dose density. This may be due to the fact that the studies are performed on an adherent culture of A549 cells, which are localized near the bottom of the wells of the plate during irradiation. The study is conducted at high power density (about 50 mW/cm²), and the rate of oxygen utilization in the effective photodynamic process under such exposure is higher than its diffusion rate through the liquid layer in the well. This leads to a significant decrease in the partial pressure of oxygen in the zone of photodynamic action on cells, and the effectiveness of photodynamic reaction will decrease, resulting in lower effect of photodynamic action on the light dose density [23]. The higher phototoxicity of ZnPcChol_o compared to 4α ZnPc⁴⁺ and $4\alpha\beta$ ZnPc⁴⁺ can be explained, similarly to [16], by the fact that the antitumor efficacy of octacationic photosensitizers is higher compared to tetracationic ones. In addition, in in vitro photodynamic efficiency studies in cell culture

monolayers, the fraction of light energy absorbed by $ZnPcChol_8$ -sensitized cells will also be higher [24] compared to $4\alpha ZnPc^{4+}$ and $4\alpha \beta ZnPc^{4+}$ sensitized cells due to the significantly higher extinction of $ZnPcChol_8$. Consequently, the dose-dependent photodynamic cell damage will also be higher.

The photodynamic efficiency of $4\alpha ZnPc^{4+}$ and $4\alpha \beta ZnPc^{4+}$ may in principle be lower compared to $ZnPcChol_8$ due to their partial aggregation in aqueous compositions, but in the range of their concentration values < 30 μ M, the contribution of such aggregation to the IC_{so} value for these PSs is negligible.

Conclusion

Polycationic photosensitizers based on long-wavelength phthalocyanines with high extinction in the spectral range 682–689 nm demonstrate high in vitro phototoxicity in the submicromole range due to effective binding of polycationic PS molecules to the surface of tumor cells possessing significant negative charge, internalization of their molecules into cells and photodynamic destruction of their organelles, and high values of extinction and quantum yield of reactive oxygen species in a wide range of concentration values due to low or no aggregation of polycationic phthalocyanine molecules because of electrostatic repulsion of their ions in aqueous solutions.

Work of Romanishkin I.D., Bunin D.A., Skobeltsin A.S., Akhlyustina E.V., Kogan E.A., Meerovich G.A., Reshetov I.V. was supported by RSF grant N 24-45-00020.

Work of Zhi-Long Chen was supported by NSFC grant N 22361132541.

REFERENCES

- Agostinis P., Berg K., Cengel K. A. et al. Photodynamic therapy of cancer: an update, CA: a cancer journal for clinicians, 2011, vol. 61(4), pp. 250–281. doi: 10.3322/caac.20114.
- Abrahamse H., Hamblin M. R. New photosensitizers for photodynamic therapy, *Biochemical Journal*, 2016, vol. 473(4), pp. 347–364. doi: 10.1042/BJ20150942.
- Kvashnina D. V., Shirokova I. Yu., Belyanina N. A. et al. Study of accumulation of water-soluble asymmetric cationic porphyrins in gram-positive wound infection pathogens during photodynamic inactivation, *Biomedical Photonics*, 2025, vol. 14(2), pp. 4–11. doi: 10.24931/2413-9432-2025-14-2-4-11.
- Suvorov N. V., Shchelkova V. V., Rysanova E. V. et al. New cationic chlorin as potential agent for antimicrobial photodynamic therapy, *Biomedical Photonics*, 2024, vol. 13(3), pp. 14–19. doi: 10.24931/2413-9432-2024-13-3-14-19.
- 5. Governatore M. D., Hamblin M. R., Piccinini E. E. et al. Targeted photodestruction of human colon cancer cells using charged 17.1A chlorine6 immunoconjugates, *British Journal of Cancer*, 2000, vol. 82(1), pp. 56–64. doi: 10.1054/bjoc.1999.0877.
- Hamblin M. R., Miller J. L., Hasan T. Effect of charge on the interaction of site-specific photoimmunoconjugates with human ovarian cancer cells, *Cancer Research*, 1996, vol. 56(22), pp. 5205– 5210.
- 7. Duska L., Hamblin M., Bamberg M. et al. Biodistribution of charged F(ab')2 photoimmunoconjugates in a xenograft model of ovarian

ЛИТЕРАТУРА

- Agostinis P., Berg K., Cengel K. A. et al. Photodynamic therapy of cancer: an update // CA: a cancer journal for clinicians. – 2011. – Vol. 61. – № 4. – P. 250–281.doi: 10.3322/caac.20114.
- Abrahamse H., Hamblin M. R. New photosensitizers for photodynamic therapy // Biochemical Journal. – 2016. – Vol. 473. – № 4. – P. 347–364.doi: 10.1042/BJ20150942.
- Kvashnina D. V., Shirokova I. Yu., Belyanina N. A. et al. Study of accumulation of water-soluble asymmetric cationic porphyrins in gram-positive wound infection pathogens during photodynamic inactivation // Biomedical Photonics. – 2025. – Vol. 14. – № 2. – P. 4–11.doi: 10.24931/2413-9432-2025-14-2-4-11.
- Suvorov N. V., Shchelkova V. V., Rysanova E. V. et al. New cationic chlorin as potential agent for antimicrobial photodynamic therapy // Biomedical Photonics. – 2024. – Vol. 13. – № 3. – P. 14–19.doi: 10.24931/2413-9432-2024-13-3-14-19.
- Governatore M. D., Hamblin M. R., Piccinini E. E. et al. Targeted photodestruction of human colon cancer cells using charged 17.1A chlorine6 immunoconjugates // British Journal of Cancer. – 2000. – Vol. 82. – № 1. – P. 56–64.doi: 10.1054/bjoc.1999.0877.
- 6. Hamblin M. R., Miller J. L., Hasan T. Effect of charge on the interaction of site-specific photoimmunoconjugates with human ovarian cancer cells // Cancer Research. 1996. Vol. 56. № 22. P. 5205–5210.
- Duska L., Hamblin M., Bamberg M. et al. Biodistribution of charged F(ab')2 photoimmunoconjugates in a xenograft model of ovarian

- cancer, *British Journal of Cancer*, 1997, vol. 75(6), pp. 837–844. doi: 10.1038/bjc.1997.149.
- Photosensitizers in Medicine, Environment, and Security ed. T. Nyokong, V. Ahsen, Dordrecht: Springer Netherlands, 2012. doi: 10.1007/978-90-481-3872-2.
- Mantareva V. N., Angelov I., Wöhrle D. et al. Metallophthalocyanines for antimicrobial photodynamic therapy: an overview of our experience, *Journal of Porphyrins and Phthalocyanines*, 2013, vol. 17(06n07), pp. 399–416. doi: 10.1142/S1088424613300024.
- 10. Meerovich G. A., Akhlyustina E. V., Tiganova I. G. et al. Novel Polycationic Photosensitizers for Antibacterial Photodynamic Therapy Cham: Springer, New York, NY, 2019.p. 1–19. doi: 10.1007/5584_2019_431.
- Makarov D. A., Yuzhakova O. A., Slivka L. K. et al. Cationic Zn and Al phthalocyanines: synthesis, spectroscopy and photosensitizing properties, *Journal of Porphyrins and Phthalocyanines*, 2007, vol. 11(08), pp. 586–595. doi: 10.1142/S1088424607000680.
- Yakubovskaya R. I., Plyutinskaya A. D., Plotnikova E. A. et al. Comparative in vitro study of different classes of photosensitizers. Pyropheophorbides and chlorines, *Russian Journal of Biotherapy*, 2015, vol. 14(1), pp. 43–51. doi: 10.17650/1726-9784-2015-14-1-43-51.
- Yakubovskaya R. I., Plotnikova E. A., Plyutinskaya A. D. et al. Photophysical properties and in vitro and in vivo photoinduced antitumor activity of cationic salts of meso-tetrakis(N-alkyl-3-pyridyl)bacteriochlorins, *Journal of Photochemistry and Photobiology B: Biology*, 2014, vol. 130, pp. 109–114. doi: 10.1016/j. jphotobiol.2013.10.017.
- Bunin D. A., Martynov A. G., Safonova E. A. et al. Robust route toward cationic phthalocyanines through reductive amination, *Dyes and Pigments*, 2022, vol. 207, pp. 110768. doi: 10.1016/j. dyepiq.2022.110768.
- Bunin D. A., Akasov R. A., Martynov A. G. et al. Pivotal Role of the Intracellular Microenvironment in the High Photodynamic Activity of Cationic Phthalocyanines, *Journal of Medicinal Chemistry*, 2025, vol. 68(1), pp. 658–673. doi: 10.1021/acs.jmedchem.4c02451.
- Kogan E. A., Meerovich G. A., Karshieva S. Sh. et al. On the mechanisms of photodynamic action of photosensitizers based on polycationic derivatives of synthetic bacteriochlorin against human lung cancer cells A549 (in vitro study), *Photodiagnosis and Photodynamic Therapy*, 2022, vol. 39, pp. 102955. doi: 10.1016/j. pdpdt.2022.102955.
- 17. Pominova D. V., Ryabova A. V., Skobeltsin A. S. et al. Spectroscopic study of methylene blue in vivo: effects on tissue oxygenation and tumor metabolism, *Biomedical Photonics*, 2023, vol. 12(1), pp. 4–13. doi: 10.24931/2413-9432-2023-12-1-4-13.
- Akhlyustina E. V., Lukyanets E. A., Alekseeva N. V. et al. Photosensitizers for the photodynamic inactivation of bacteria, including in biofilms / E. V. Akhlyustina, E. A. Lukyanets, N. V. Alekseeva et al., 2018. Patent RF №2670201.
- Romanishkin I. D., Akhlyustina E. V., Meerovich G. A. et al. On the aggregation of polycationic photosensitizer upon binding to Gram-negative bacteria, *Methods and Applications in Fluorescence*, 2024, vol. 12(3), pp. 035001. doi: 10.1088/2050-6120/ad3892.
- Meerovich G. A., Linkov K. G., Nekhoroshev A. V. et al. Devices for Photodynamic Studies Based on Light-Emitting Diodes, *Journal* of *Biomedical Photonics & Engineering*, 2021, vol. 7(4), pp. 040308. doi: 10.18287/JBPE21.07.040308.
- Tominaga T. T., Yushmanov V. E., Borissevitch I. E. et al. Aggregation phenomena in the complexes of iron tetraphenylporphine sulfonate with bovine serum albumin, *Journal of Inorganic Biochemistry*, 1997, vol. 65(4), pp. 235–244. doi: 10.1016/S0162-0134(96)00137-7.
- Shi D. Cancer Cell Surface Negative Charges: A Bio-Physical Manifestation of the Warburg Effect, Nano LIFE, 2017, vol. 07(03n04), pp. 1771001. doi: 10.1142/S1793984417710015.
- 23. Meerovich I. Photodynamic efficiency of avidin-biotin system including biotinylated antibodies and phthalocyanine photosensitizer derivatives. PhD thesis: 03.00.04.- A.N. Bach Institute of Biochemistry RAS, Moscow, 2001.- 155 p.
- 24. Meerovich G., Romanishkin I., Akhlyustina E. et al. Photodynamic Action in Thin Sensitized Layers: Estimating the Utilization of Light Energy, *Journal of Biomedical Photonics & Engineering*, 2021, vol. 7(4), pp. 040301. doi: 10.18287/JBPE21.07.040301.

- cancer // British Journal of Cancer. 1997. Vol. 75. № 6. P. 837–844.doi: 10.1038/bjc.1997.149.
- Photosensitizers in Medicine, Environment, and Security ed. T. Nyokong, V. Ahsen, Dordrecht: Springer Netherlands, 2012.doi: 10.1007/978-90-481-3872-2.
- Mantareva V. N., Angelov I., Wöhrle D. et al. Metallophthalocyanines for antimicrobial photodynamic therapy: an overview of our experience // Journal of Porphyrins and Phthalocyanines. – 2013. – Vol. 17. – № 06n07. – P. 399–416.doi: 10.1142/S1088424613300024.
- Meerovich G. A., Akhlyustina E.V., Tiganova I. G. et al. Novel Polycationic Photosensitizers for Antibacterial Photodynamic Therapy Cham: Springer, New York, NY, 2019. C. 1–19.doi: 10.1007/5584_2019_431.
- 11. Makarov D. A., Yuzhakova O. A., Slivka L. K. et al. Cationic Zn and Al phthalocyanines: synthesis, spectroscopy and photosensitizing properties // Journal of Porphyrins and Phthalocyanines. 2007. Vol. 11. № 08. P. 586–595.doi: 10.1142/S1088424607000680.
- 12. Yakubovskaya R. I., Plyutinskaya A. D., Plotnikova E. A. et al. Comparative in vitro study of different classes of photosensitizers. Pyropheophorbides and chlorines // Russian Journal of Biotherapy. 2015. Vol. 14. № 1. P. 43–51.doi: 10.17650/1726-9784-2015-14-1-43-51.
- Yakubovskaya R. I., Plotnikova E. A., Plyutinskaya A. D. et al. Photophysical properties and in vitro and in vivo photoinduced antitumor activity of cationic salts of meso-tetrakis(N-alkyl-3-pyridyl) bacteriochlorins // Journal of Photochemistry and Photobiology B: Biology. – 2014. – Vol. 130. – P. 109–114.doi: 10.1016/j. jphotobiol.2013.10.017.
- Bunin D. A., Martynov A. G., Safonova E. A. et al. Robust route toward cationic phthalocyanines through reductive amination // Dyes and Pigments. – 2022. – Vol. 207. – P. 110768.doi: 10.1016/j. dyepig.2022.110768.
- Bunin D. A., Akasov R. A., Martynov A. G. et al. Pivotal Role of the Intracellular Microenvironment in the High Photodynamic Activity of Cationic Phthalocyanines // Journal of Medicinal Chemistry. – 2025. – Vol. 68. – № 1. – P. 658–673.doi: 10.1021/acs.jmedchem.4c02451.
- Kogan E. A., Meerovich G. A., Karshieva S. Sh. et al. On the mechanisms of photodynamic action of photosensitizers based on polycationic derivatives of synthetic bacteriochlorin against human lung cancer cells A549 (in vitro study) // Photodiagnosis and Photodynamic Therapy. – 2022. – Vol. 39. – P. 102955.doi: 10.1016/j. pdpdt.2022.102955.
- 17. Pominova D. V., Ryabova A. V., Skobeltsin A. S. et al. Spectroscopic study of methylene blue in vivo: effects on tissue oxygenation and tumor metabolism // Biomedical Photonics. 2023. Vol. 12. № 1. P. 4–13.doi: 10.24931/2413-9432-2023-12-1-4-13.
- Akhlyustina E. V., Lukyanets E. A., Alekseeva N. V. et al. Photosensitizers for the photodynamic inactivation of bacteria, including in biofilms / E. V. Akhlyustina, E. A. Lukyanets, N. V. Alekseeva et al., 2018. Patent RF №2670201 c.
- Romanishkin I. D., Akhlyustina E. V., Meerovich G. A. et al. On the aggregation of polycationic photosensitizer upon binding to Gramnegative bacteria // Methods and Applications in Fluorescence. – 2024. – Vol. 12. – № 3. – P. 035001.doi: 10.1088/2050-6120/ad3892.
- 20. 20. Meerovich G. A., Linkov K. G., Nekhoroshev A. V. et al. Devices for Photodynamic Studies Based on Light-Emitting Diodes // Journal of Biomedical Photonics & Engineering. 2021. Vol. 7. № 4. P. 040308.doi: 10.18287/JBPE21.07.040308.
- 21. Tominaga T. T., Yushmanov V. E., Borissevitch I. E. et al. Aggregation phenomena in the complexes of iron tetraphenylporphine sulfonate withbovineserumalbumin//JournalofInorganicBiochemistry.−1997.

 Vol. 65. № 4. P. 235–244.doi: 10.1016/S0162-0134(96)00137-7.
- 22. Shi D. Cancer Cell Surface Negative Charges: A Bio-Physical Manifestation of the Warburg Effect // Nano LIFE. 2017. Vol. 07. № 03n04. P. 1771001.doi: 10.1142/S1793984417710015.
- Фотодинамическая эффективность авидин-биотиновой системы, включающей биотинилированные антитела и производные фталоцианиновых фотосенсибилизаторов. Диссертация на соискание ученой степени кандидата химических наук: 03.00.04.- Институт биохимии им. Баха РАН Москва, 2001.- 155 с.: ил. РГБ ОД, 61 02-2/59-0.
- 24. Meerovich G., Romanishkin I., Akhlyustina E. et al. Photodynamic Action in Thin Sensitized Layers: Estimating the Utilization of Light Energy // Journal of Biomedical Photonics & Engineering. 2021. Vol. 7. № 4. P. 040301.doi: 10.18287/JBPE21.07.040301.

APPLICATION OF THE KUBELKA-MUNK MODEL FOR FAST INTRAOPERATIVE ANALYSIS OF INTESTINAL OPTICAL PROPERTIES USING A FIBER OPTIC SPECTROMETER

Savelieva T.A.^{1,2}, Krivetskaya A.A.^{1,2}, Kustov D.M.¹, Klobukov M.I.², Romanishkin I.D.¹, Linkov K.G.¹, Levkin V.V.³, Kharnas S.S.³, Loschenov V.B.^{1,2}

¹Prokhorov General Physics Institute of the Russian Academy of Sciences, Moscow, Russia ²Institute of Engineering Physics for Biomedicine, National Research Nuclear University MEPhI, Moscow, Russia

³Department of Faculty Surgery No. 1, I.M. Sechenov First Moscow State Medical University, Moscow, Russia

Abstract

Intraoperative determination of optical properties of biological tissues is an important task of medical physics, in particular, for photodynamic therapy, because it allows personalizing photodynamic treatment by accurately calculating the required light dose. In this work, we propose a new approach to simultaneous measurement of diffuse reflectance and transmission spectra of the colon wall tissue during intestinal anastomosis, based on the use of two fiber-optic devices to deliver broadband radiation both from the side of the intestinal lumen and from the outer side of the intestinal wall, from which diffuse scattered light is also recorded. To restore the optical properties of these tissues it was proposed to use the Kubelka-Munk model with transformation of the optical parameters of the model into the optical parameters of the diffusion approximation theory with custom equations based on the results of numerical modeling. The proposed approach have been tested *ex vivo* on the biological samples of GIT tissues, allowing us to conclude on its applicability in clinical conditions.

Key words: optical spectroscopy, optical properties, light transport model, gastrointestinal tract.

Contacts: Savelieva T.A., e-mail: savelevat@gmail.com

For citations: Savelieva T.A., Krivetskaya A.A., Kustov D.M., Klobukov M.I., Romanishkin I.D., Linkov K.G., Levkin V.V., Kharnas S.S., Loschenov V.B. Application of the Kubelka-Munk model for fast intraoperative analysis of intestinal optical properties using a fiber optic spectrometer, *Biomedical Photonics*, 2025, vol. 14, no. 3, pp. 30–38. doi: 10.24931/2413–9432–2025–14–3–30–38

ПРИМЕНЕНИЕ МОДЕЛИ КУБЕЛКИ-МУНКА ДЛЯ БЫСТРОГО ИНТРАОПЕРАЦИОННОГО АНАЛИЗА ОПТИЧЕСКИХ СВОЙСТВ СТЕНКИ КИШЕЧНИКА С ПОМОЩЬЮ ОПТОВОЛОКОННОГО СПЕКТРОМЕТРА

Т.А. Савельева^{1,2}, А.А. Кривецкая^{1,2}, Д.М. Кустов¹, М.И. Клобуков², И.Д. Романишкин¹, К.Г. Линьков¹, В.В. Левкин³, С.С. Харнас³, В.Б. Лощенов^{1,2}

¹Институт общей физики им. А.М. Прохорова Российской академии наук, Москва, Россия ²Национальный исследовательский ядерный университет «МИФИ», Москва, Россия ³Университетская Клиническая больница №1 Первого МГМУ им. Сеченова, Москва, Россия

Резюме

Интраоперационное определение оптических свойств биологических тканей является важной задачей медицинской физики, в частности, при планировании фотодинамической терапии, поскольку позволяет персонализировать фотодинамическое воздействие за счет точного расчета необходимой световой дозы. В данной работе предложен новый подход к одновременному измерению спектров диффузного отражения и пропускания света тканью стенки толстой кишки при формировании кишечного анастомоза, основанный на использовании двух волоконно-оптических устройств для подачи широкополосного излучения как со стороны просвета кишки, так и с наружной стороны кишечной стенки, с которой также регистрируется диффузно рассеянный свет. Для восстановления оптических свойств этих тканей предложено использовать модель Кубелки-Мунка с преобразованием оптических параметров моде-

ли в оптические параметры теории диффузионного приближения с использованием собственных уравнений на основе результатов численного моделирования. Предложенный подход апробирован *ex vivo* на биологических образцах тканей желудочно-кишечного тракта, что позволяет сделать вывод о его применимости в клинических условиях.

Ключевые слова: оптическая спектроскопия, оптические свойства, теория переноса излучения, желудочно-кишечный тракт.

Контакты: Savelieva T.A., e-mail: savelevat@gmail.com

Для цитирования: Савельева Т.А., Кривецкая А.А., Кустов Д.М., Клобуков М.И., Романишкин И.Д., Линьков К.Г., Левкин В.В., Харнас С.С., Лощенов В.Б. Применение модели Кубелки-Мунка для быстрого интраоперационного анализа оптических свойств стенки кишечника с помощью оптоволоконного спектрометра // Biomedical Photonics. − 2025. − Т. 14, № 3. − С. 30−38. doi: 10.24931/2413-9432-2025-14-3-30-38

Introduction

Intraoperative determination of optical properties is an important task of medical physics, in particular, for photodynamic therapy [1]. Optical properties also influence the interpretation of the results of diagnostic methods [2]. In connection with the development and widespread use of phototheranostics methods using laser and optical technologies in surgery and therapy, various instrumental and algorithmic approaches are proposed to study the propagation of light in biological tissues, whose complex structure and the natural variability of properties make this task non-trivial. In particular, the effectiveness of photodynamic therapy (PDT) largely depends on the content of the photosensitizer and the distribution of light in the irradiated tissue, and an accurate assessment of the radiation dose absorbed by the tissue makes it possible to determine the mode of photodynamic exposure.

From the point of view of light propagation, biological tissues of the human body are turbid media, i.e. heterogeneous structures with spatial fluctuations in optical properties. These fluctuations and their density cause strong scattering of light by biological tissue. It is important to take into account the effects of multiple scattering which complicate the direct application of electromagnetic theory. Therefore, to describe the propagation of light in such media, the radiation transfer theory (RTT) is used, which ignores some of the wave properties of light, such as interference and polarization, considering only the transfer of light energy in the medium. However, the model implicitly takes into account the wave properties of light due to the optical properties of the tissue included in the basic equation. These properties represent a generalization of optical parameters to an ensemble of particles and were obtained by solving the Maxwell equations proposed by Gustav Mie in 1908. For this purpose optical characteristics averaged over a certain elementary volume are used, such as the absorption coefficient (μ_a) , which is the inverse of the photon's free path before the act of absorption, the scattering coefficient (μ_s) , which is the inverse of the photon's free path between

scattering events, and the anisotropy coefficient (q), which represents the average cosine of the scattering angle. For media characterized by anisotropic scattering, the so-called reduced scattering coefficient ($\mu'_{\epsilon} = \mu_{\epsilon}$ (1g)) is introduced. This coefficient takes into account how many more collisions must occur in an anisotropic medium compared to an isotropic one in order for the light to turn at the same angle as in an isotropic medium. A significant simplification of the theory of radiation transfer is the equation for a stationary state in which the intensity at any point of the medium does not change with time. The diffusion approximation of the RTT also proves useful in the case of small values of the single scattering anisotropy factor and large albedos (close to one). For most biological tissues, the anisotropy coefficient ranges from 0.6 to 0.9, and for blood it reaches 0.995, which significantly limits the applicability of the diffusion approximation [3].

To numerically solve the RTT equation, the Monte Carlo numerical simulation method based on the simulation of photon transport in a scattering medium is widely used. The initial conditions are set and each act of photon scattering on inhomogeneities of the medium is traced until its absorption or exit from the sample. The main disadvantage of the Monte Carlo method is the large expenditure of computer time due to the need of solving the inverse problem consisting of the selection of values of optical properties that correspond to the measured values of transmission and reflection, which complicates the intraoperative determination of the optical properties of tissues. To solve the inverse problem, it is necessary to run the simulation several times for a given set of optical properties; in this case, the search for initial values, optimization method and stopping criteria is also non-trivial [4].

One of the common methods for solving the RTT equation is the Kubelka-Munk method, which has already been used to analyze the optical properties of intestinal tissues [5]. However, in that work, bloodless samples were studied, measured within 2 hours after resection of human small intestine tissue. In work [6], the optical properties of normal and adenomatous human colon

tissues were obtained by the method of two integrating spheres in vitro. The paper [7] presents the optical characteristics of the mucosa and submucosa of human colon tissue obtained in vitro on a spectrophotometer with an integrating sphere LAMBDA 950. The authors of the work [8] in order to assess the kinetics of the optical properties of biological tissues under conditions of optical clearing with glycerol, proposed a simple and indirect method, based on the collimated transmittance (Tc) and thickness d(t) which was measured during processing. The Tc of the sample depends on both the thickness of the sample (d) and the light attenuation coefficient, µt. Assuming that the absorption coefficient remains constant throughout the process, they derive the scattering coefficient from Tc.

As can be seen from the works mentioned above, measurements with two integrating spheres make it possible to determine the optical properties of samples in vitro and ex vivo, but they seem too cumbersome to be used during surgery. At the same time, it is important to know the optical properties of tissues under lightinduced exposure directly at the moment of exposure, not for a similar type of tissue sample measured in the laboratory, since the state of the tissue is variable and critically important for planning and monitoring photodynamic therapy. Therefore, in this work it is proposed to use as measured parameters the values of diffuse transmission and reflection obtained by measuring with a fiber with a given aperture in soft contact with the surface of a biological object. The inevitable decrease in the accuracy of the model in this case is a payment for the ability to analyze optical properties in real time. The purpose of this study was to analyze the possibility of intraoperative assessment of the optical properties of intestinal wall tissues in both diffusely reflected and diffusely transmitted light.

Materials and Methods

Spectroscopic setup for in vivo measurements

The experimental setup (Fig. 1) consisted of a white light source, a spectrum analyzer with a fiber-optic input (LESA-01-BIOSPEC), optical fibers and a personal computer for recording measurements. The diffuse reflection and transmission spectra were recorded in the spectral range of 500-600 nm. An LED lamp with a fiber-optic output was used as a broadband radiation source. The power of the light source is adjustable up to 1 W, the color temperature is 5000K-6500K. The spectrum of the light source in the range of 500-600 nm has sufficient uniformity for analysis. To calculate the diffuse reflectance coefficient $R_d = I/I_o$ and the diffuse transmission coefficient $T_d = I/I_o$ measurements of the diffuse reflection and transmission spectra were carried out relative to a standard sample (BaSO₄) with a reflection coefficient close to unity in the selected spectral range.

Two measurement geometries were used for illumination and registration of radiation: in diffusely reflected (green arrows on Fig. 1) and transmitted light (purple arrows on Fig. 1), therefore, two fiber-optic devices were used as previously for hemoglobin oxygen saturation analysis of colonic wall [10]. A fiber optic diffuser placed inside the Foley catheter was used to uniformly illuminate the intestinal wall from the inside in order to measure the transmitted light passing through the intestinal wall to the outside. The Foley catheter was filled with a fat emulsion (Intralid MCT/LST 10%) diluted to 1% with NaCl 0.9% to ensure a uniform scattering phase function. The length of the diffuser was 10 mm.

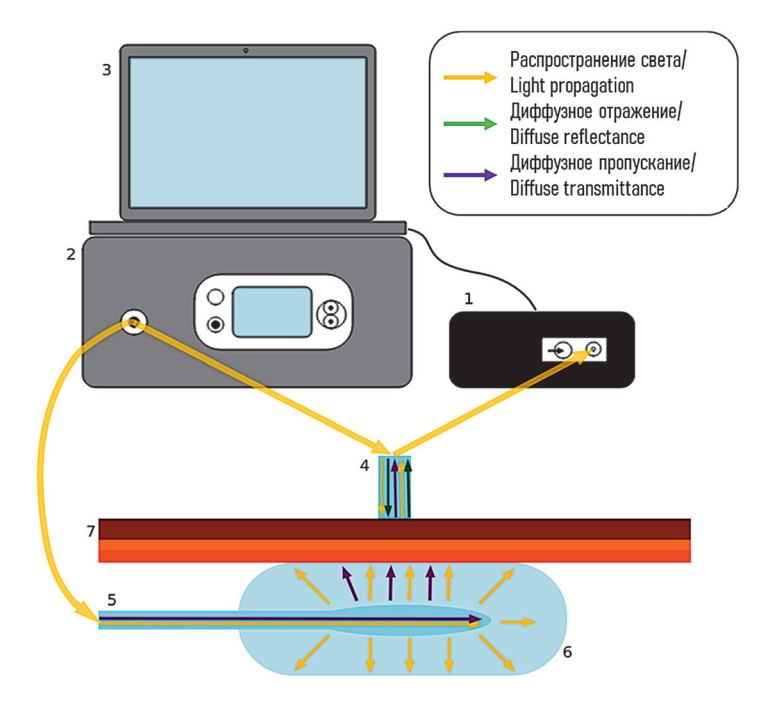
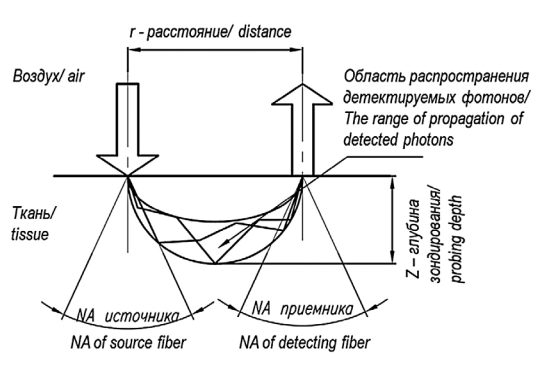
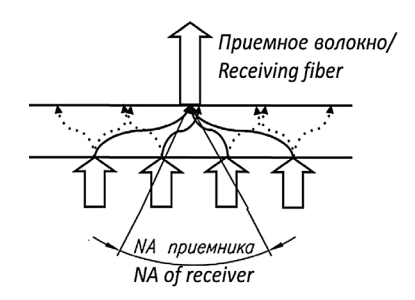


Рис. 1. Схема спектроскопической установки. В состав оборудования входят: 1 - спектрометр «ЛЭСА-01-БИОСПЕК». 2 - широкополосный источник излучения, 3 - компьютер с программой «Uno Momento», 4 - Y-образный оптический световод, 5 - волоконно-оптический диффузор, 6 - катетер Фолея. Исследуемая ткань - стенка кишечника (7). Fig. 1. Scheme of the spectroscopic setup. The equipment includes: 1 - a "LESA-01-BIOSPEC" spectrometer, 2 - a broadband radiation source, 3 - a computer with the program "Uno Momento", 4 - a y-shaped optical fiber, 5 - fiber-optic diffuser, 6 -Foley catheter. The investigated tissue is

the intestinal wall (7).





гурации источника и приемника при проведении численного эксперимента.

Fig. 2. Two configurations of the source and receiver when conducting a numerical experiment.

Рис. 2. Две конфи-

The receiving fibers at the entrance to the spectrometer form a line that serves as the entrance slit of the monochromator, hence they are located perpendicular to the diffraction plane of the dispersing element. The diameter of each fiber is 125 microns, which determines the distance between the centers of closely spaced fibers. The diameter of each fiber including the sheath is 250 microns. The numerical aperture of each fiber is 0.22. The measurements were carried out using an optical fiber with an aperture of 0.22 in contact with biological tissues for both illumination and registration of diffuse reflection spectra and transmission spectra. The light detected in this way is the part of the diffusely scattered light, which can be measured using an integrating sphere. A hypothetical receiving fiber with a numerical aperture of NA = 1 would provide detection of light scattered by tissue at any angle, which can be compared to the total diffuse reflectance signal recorded using an integrating sphere. To estimate the proportion of light received by a real optical fiber with a numerical aperture different from 1, numerical modeling of light propagation in a multilayer medium was performed, the optical parameters of samples corresponded to the optical properties of the intestinal wall layers according to works [6-9].

Monte Carlo simulation of light propagation in tissues In our work, numerical simulation using the Monte Carlo method was used to model the trajectories of photons. Its acceptability is based on the assumption of a large number of acts of light scattering on fluctuations of the refractive index, which makes it possible to neglect the consideration of wave effects. Boundary conditions were set and every act of photon scattering on inhomogeneities of the medium was monitored, up to its absorption or exit from the sample. The value of free path length and the angle of rotation, which are random variables distributed according to a certain law, were determined using the coefficients g, µs and µa. The Henyey-Greenstein (HG) scattering phase function was used to determine the scattering angle. Reflection, refraction, and total internal reflection were taken into account at the boundaries of the media. The receiver with a given numerical aperture was positioned relative to the sample both from the source side (to take into account diffusely reflected photons) and from the opposite side (to account for transmitted photons) (Fig.2).

The optical properties of the intestinal wall layers were used as input parameters for modeling according to works [6-9] (Table 1). The method was implemented using the C# language in the Visual Studio 2019

Таблица 1.Оптические свойства исследуемых тканей стенки кишечника как входные данные для моделирования распространения света методом Монте-Карло, литературные данные [6-9]

Optical properties of the studied intestinal wall tissues as input data for modeling the propagation of light by the Monte Carlo method, literature data from [6-9]

Характеристики Characteristics	Слой Layer				
	Мышечный Muscular	Подслизистый Submucosal	Слизистый Mucosal		
Коэффициент поглощения Absorption coefficient μ _a	6.5 cm ⁻¹	1 cm ⁻¹	3.5 cm ⁻¹		
Koэффициент рассеяния Scattering coefficient µ	100 cm ⁻¹	100 cm ⁻¹	300 cm ⁻¹		
Показатель анизотропии Anisotropy factor g	0.89	0.9	0.9		
Коэффициент преломления Refractive index n	1.36	1.36	1.38		
Толщина Thickness d	1 – 3 mm	0.2 mm	0.8 mm		



Таблица 2.

Содержание цельной крови в оптических фантомах и соответствующие значения коэффициента поглощения на длинах волн 542, 560, 576 нм

The content of whole blood in optical phantoms and the corresponding absorption coefficient values at wavelengths of 542, 560, 576 nm

Коэффициент поглощения µа (см¹) на длине волны	Содержание крови в ткани (% или мл/100 г) Blood in tissue (% or ml/100 g)					
Absorption coefficient µa (cm¹) at wavelength	20	8	4	2	1	0,5
542 nm	53,29	21,32	10,66	5,33	2,67	1,33
560 nm	32,61	13,05	6,52	3,26	1,63	0,82
576 nm	55,35	22,14	11,07	5,55	2,77	1,38

development environment based on the algorithm proposed in [11].

Principle of customization of Kubelka-Munk model

As a rule, during studying of biological tissues in a living organism, the illuminator and light receiver are located on the one side of the sample. Therefore, in most cases, in vivo spectral measurements of biological tissues are performed in diffuse reflectance geometry. Considering the heterogeneity of biological tissues and variations in their physiological characteristics, in the general case the problem of restoring their optical properties does not have a strict solution.

To restore all three optical properties (absorption and scattering coefficients and anisotropy coefficient), it is necessary to measure any three of the following five parameters: total (or diffuse) transmission, total (or diffuse) reflection, absorption of a sample placed in an integrating sphere, collimated transmission coefficient for non-scattered light, angular distribution of light scattered by the sample [3]. Many methods for estimating optical parameters of tissue are also based on a combination of several diffuse reflection measurements with spatial resolution, for example, at several distances from the source.

If in considered case it is enough to determine the absorption coefficient and the reduced scattering coefficient (without decomposing it into the anisotropy factor and the scattering coefficient), then it is enough to measure two of the parameters mentioned above. This paper proposes a method for measuring diffusely scattered light in reflected and transmitted geometry with subsequent restoration of information about the optical properties of an object using the two-stream Kubelka-Munk model with empirically determined conversion coefficients from the optical parameters of the Kubelka-Munk model to the optical parameters of the RTT.

The Kubelka-Munk method is widely used to separate light attenuation into contributions due to absorption and scattering based on measured values of total diffuse reflectance $R_{d'}$ diffuse transmittance $T_{d'}$ and collimated transmittance T_c in turbid media such as biological tissues [12]. This method is based on considering two radiation fluxes propagating inside the tissue: one flow is in the direction of the incident beam L_{ν} and the other is in the backscattering direction L_{2} , which can be described using the following equations [13, 14]:

$$\frac{\partial L_1}{\partial z} = -S \cdot L_1 - A \cdot L_1 + S \cdot L_2,\tag{1}$$

$$\frac{\partial L_1}{\partial z} = -S \cdot L_1 - A \cdot L_1 + S \cdot L_2, \tag{1}$$

$$\frac{\partial L_2}{\partial z} = -S \cdot L_2 - A \cdot L_2 + S \cdot L_1, \tag{2}$$

where S and K are special parameters of the Kubelka-Munk model describing scattering and absorption, which can be calculated as:

$$S = \frac{ln\left(\frac{1 - R_d(a - b)}{T_d}\right)}{b \cdot d} , \tag{3}$$

$$A = S(a-1) , (4)$$

where Rd is the diffuse reflectance coefficient, Td is the diffuse transmittance coefficient, d is the layer thickness

measured in cm, a and b are coefficients defined as:
$$a = \frac{1 - T_d^2 + R_d^2}{2R_J} \ , \eqno(5)$$

$$b^2 = a^2 - 1 {.} {(6)}$$

In this case, it is possible to associate these absorption (A) and scattering (S) parameters of the model with the absorption (μa) and reduced scattering (μ's) coefficients used in the radiation transfer theory, in accordance with the following dependencies [15]:

$$A = 2\mu_a,\tag{7}$$

$$S = \frac{3}{4} \mu_s' - \frac{1}{4} \mu_a. \tag{8}$$

Expression (8) for the scattering parameter in the Kubelka-Munk model through the optical parameters of the RTT has a physical meaning only in the case of an absorption coefficient less than a threefold reduced scattering coefficient. Our work proposes alternative conversion formulas based on the results of numerical modeling of light propagation in a medium with optical

parameters corresponding to ones of the intestinal wall. These conversion formulas were tested on optical phantoms, the optical properties of which are relevant to the intestinal wall.

Therefore, knowing T_a and $R_{d'}$ it is possible to calculate which optical parameters (μ_a and μ'_s) correspond to values of the observed transmittance and reflection coefficients in scattered light through the scattering and absorption parameters of the Kubelka-Munk model (A and S).

Empirical connections of the results of the Kubelka-Munk method and radiative transfer coefficients were used to derive the relationships between them. From the measured total diffuse reflectance (R_d) and diffuse transmittance (T_d), the relation between Kubelka-Munk coefficients and the radiation transfer coefficients of the tissue phantom (μ_a and μ_a') were calculated.

Fig. 3 schematically shows the empirical relationship between the results of the Kubelka-Munk method and radiative transfer coefficients.

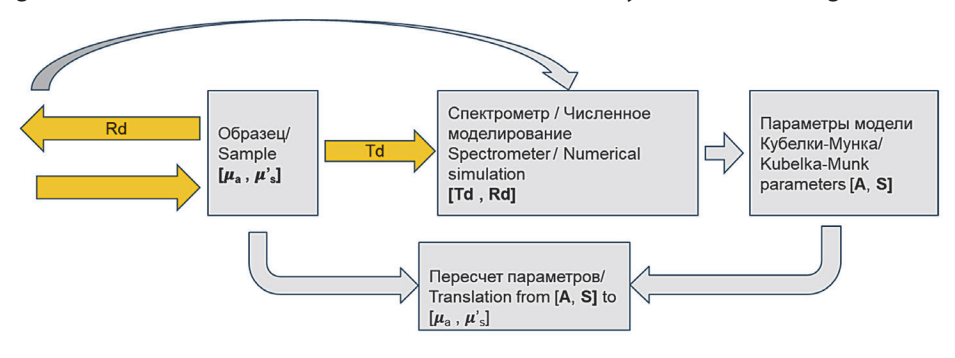
Biological samples

Clinical testing was carried out *ex vivo* on a specimen of intestine obtained as a result of surgical operation of gastrointestinal tumors on the basis of the University Clinical Hospital no. 1 of the I.M. Sechenov First Moscow State Medical University. The reflectance and transmittance spectra of specimen were registered at a distance of + and - 5 cm from the tumor. The thickness of the sample was measured using a caliper.

Results and discussion

The result of using the Monte Carlo method is R_d and T_d values at different concentrations of fat emulsion and blood for each wavelength. The simulation was carried out with values similar to those that were obtained in the experiment (the values of diffuse reflectance and diffuse transmission) for the optical parameters from Table 2. Based on the obtained values of transmission and reflectance, the dependences of the Kubelka-Munk coefficients were calculated at three different wavelengths: 542 nm, 560 nm and 576 nm. Primarily, the dependences of the obtained Kubelka-Munk coefficients for absorption A and scattering S on the known values of the reduced scattering coefficient μ_s' and the absorption coefficient μ_a' were calculated.

Fig.4shows, as an example, the calculated dependences for a wavelength of 560 nm and an anisotropy factor of



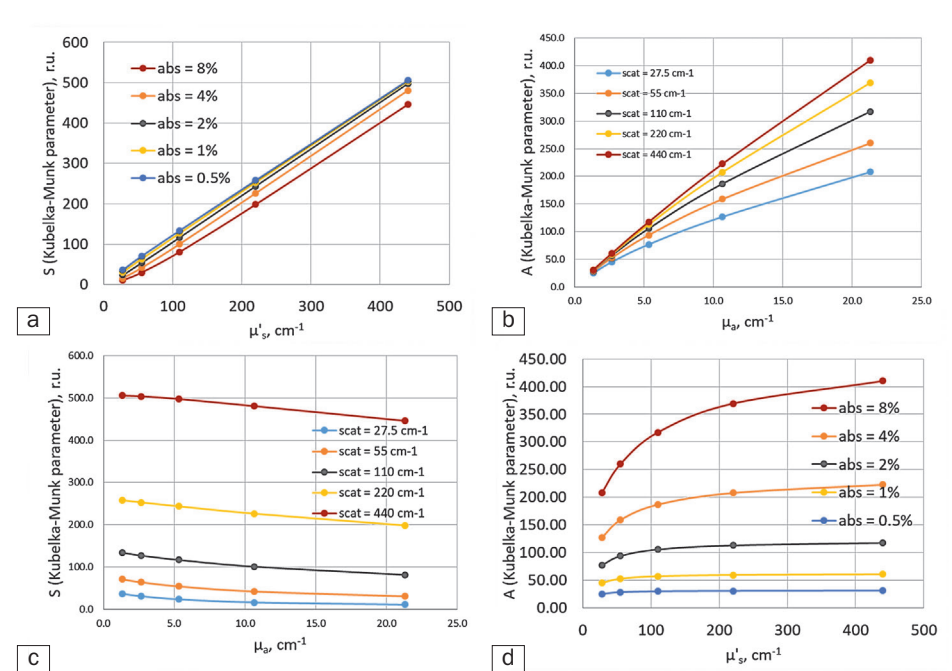


Рис. 3. Схема построения формул для пересчета параметров модели Кубелки-Мунка и оптических параметров теории переноса излучения

Fig. 3. Scheme for constructing formulas for recalculating the parameters of the Kubelka-Munk model and the optical parameters of the radiation transfer theory.

Рис. 4. Зависимости параметров модели Кубелки-Мунка от значений μ'_s и μ_a для длины волны 560 нм: а — взаимная зависимость двух коэффициентов рассеяния; b — взаимная зависимость двух коэффициентов поглощения; с — зависимость параметра рассеяния модели Кубелки-Мунка от коэффициента поглощения модели Кубелки-Мунка от приведенного коэффициента рассеяния.

Fig. 4. Dependences of the parameters of the Kubelka-Munk model on the values of μ'_3 and μ_a for a wavelength of 560 nm: a – muta I dependence of two scattering coefficients; b – mutual dependence of two absorption coefficients; c – dependence of the scattering parameter of the Kubelka-Munk model on the absorption coefficient; d – dependence of the absorption parameter of the Kubelka-Munk model on the reduced scattering coefficient.

0.71: scattering S from the reduced scattering coefficient $\mu'_{s'}$ scattering S from the absorption coefficient $\mu_{o'}$ absorption A from the reduced scattering coefficient μ'_{s} and absorption A from the absorption coefficient μ_{o} .

These results show us the linear dependences of the scattering parameter S of the Kubelka-Munk model on the reduced scattering coefficient μ'_s and the absorption parameter A of the Kubelka-Munk model on the absorption coefficient μ_a , which generally corresponds to the most commonly used conversion formulas (7) and (8). But in the range of optical properties, we are interested in, the other conversion formulas are needed for our ratio of parameters and geometry of measurements.

As a first approximation, we propose the following type of dependence for the parameters under consideration:

$$A(\mu_a.\mu_s') = k(\mu_s') * \mu_a + l, \tag{9}$$

$$S\left(\mu_{a}.\mu_{s}^{'}\right) = m^{*}\mu_{s}^{'} + n\left(\mu_{a}\right). \tag{10}$$

This type of dependence (9) is due to the fact that, as we see in Figure 3, the slope of the mutual absorption dependence depends on the scattering, and not the shift (Figure 3 (b)). For cross-scattering dependence (10), we observe, on the contrary, that its shift depends

on absorption rather than its slope (Figure 3 (a)). For example, for a wavelength of 560 nm, reciprocal terms can be neglected due to the smallness of the coefficients in front of them, in which case more direct relationships will remain:

$$A(\mu_a) = 15.8\mu_a + 35.6,\tag{11}$$

$$S(\mu_a.\mu_s) = 1.2*\mu_s - \mu_a - 14.4.$$
 (12)

This simplicity of the dependencies allows us to reverse them in order to obtain recalculation formulas for solving the inverse problem - restoring optical properties from known transmittance and reflectance through the Kubelka-Munk parameters:

$$\mu_a(A) = (A - l)/k, \tag{11}$$

$$\mu_s(A,S) = (S + n1(A-l)/k + n0)/m.$$
 (12)

On Fig. 5 we can see the example of restoration of optical properties which were used as input parameters for numerical simulation. We see a tendency for the absorption values to be overestimated at higher scattering coefficients, however, this is a second-order effect that we cannot eliminate using the fast linear model. However, the scattering coefficient is recovered with this approximation with a fairly high accuracy. The problem with the upward

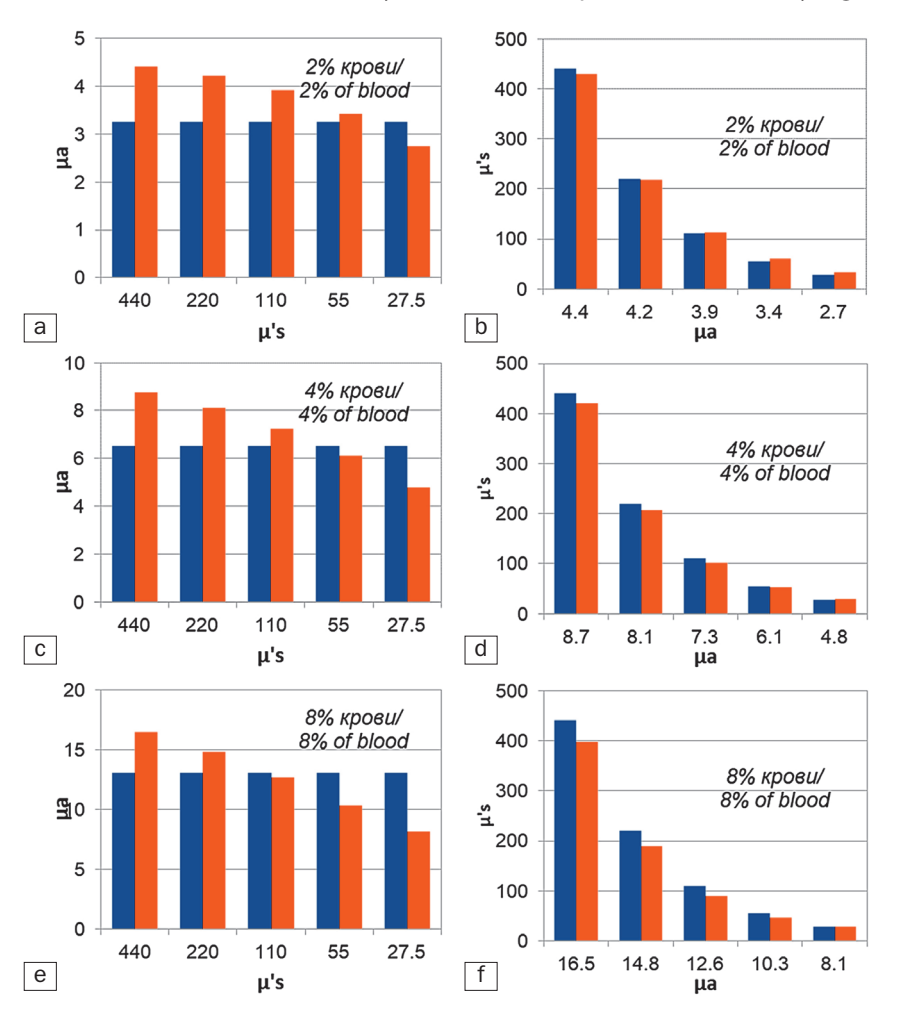


Рис. 5. Результаты восстановления оптических свойств оптических фантомов, содержащих рассеивающие среды (жировую эмульсию) и кровь для 560 нм (красным отмечены восстановленные значения, синим — заданные): а — восстановление μ_a при 2% крови в образце; b — восстановление μ_i при 2% крови в образце; с — восстановление μ_a при 4% крови в образце; d — восстановление μ_i при 4% крови в образце; е — восстановление μ_i при 4% крови в образце; е — восстановление μ_i при 4% крови в образце; f — восстановление μ_i при 4% крови в образце.

Fig. 5. Results of restoration of optical properties of optical phantoms containing scattering media (fat emulsion) and blood for 560 nm (recovered values are marked in red, specified values are marked in blue): $a - \mu_a$ recovery at 2% blood in sample; $b - \mu'_s$ recovery at 2% blood in sample; $c - \mu_a$ recovery at 4% blood in sample; $d - \mu'_s$ recovery at 4% blood in sample; $e - \mu_a$ recovery at 8% blood in sample; $f - \mu'_s$ recovery at 8% blood in sample.

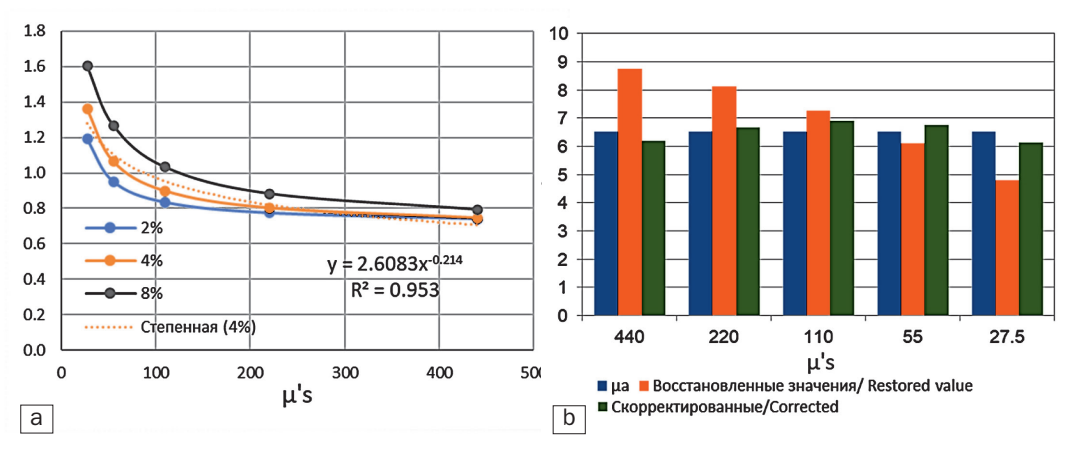


Рис. 6. Зависимость поправочного коэффициента поглошения от рассеяния: а - аналитическое выражение поправочного коэффициента; b - результат применения поправочного коэффициента. Fig. 6. An absorption correction factor dependence on scattering: a the analytic expression of correction factor; b the result of implication

of correction factor.

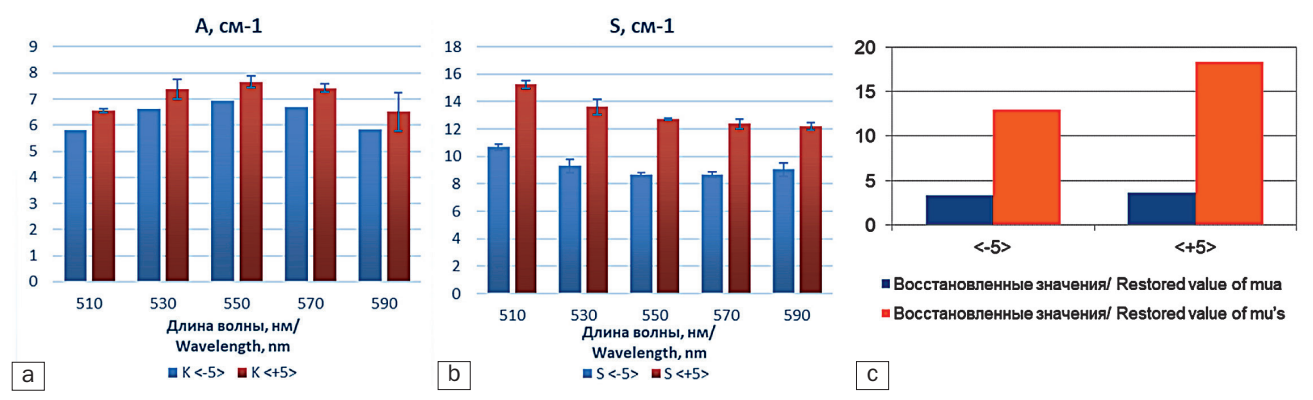


Рис. 7. Клинические испытания модифицированной модели Кубелки-Мунка применительно к восстановлению оптических свойств: а – коэффициент поглощения модели Кубелки-Мунка; b – коэффициент рассеяния модели Кубелки-Мунка; с – восстановленные по значениям коэффициентов модели Кубелки-Мунка оптические свойства тканей.

Fig. 7. Clinical testing of modified Kubelka-Munk model applied to restoration of optical properties: a – absorption coefficient of the Kubelka-Munk model; b – scattering coefficient of the Kubelka-Munk model; c – optical properties of tissues reconstructed from the values of the coefficients of the Kubelka-Munk model.

trend of the reconstructed absorption coefficient can be circumvented either by complicating the algorithm for recalculating the Kubelka-Munk parameters into optical properties according to the RTT, or by introducing a correction factor that takes into account the reconstructed value of the scattering coefficient (Fig. 6).

Results of *ex vivo* colonic wall (thickness 0.2 cm) optical properties assessment with customized formulas are presented on the Fig. 7.

Conclusion

An approach has been proposed for measuring the spectra of diffuse reflection and diffuse transmission of

light through the wall of hollow organs intraoperatively. An algorithm for reconstructing the values of the optical properties of the intestinal wall from the measured spectral dependences is proposed, based on the two-stream Kubelka-Munk model with customized formulas for converting into optical properties based on numerical modeling. The method was tested in a clinical setting, which showed the promise of its use for personalizing the calculation of the dose of light exposure in laser-induced methods of therapy.

The work was funded by the Russian Science Foundation, grant No. 25-25-00516.

REFERENCES

- Krivetskaya A.A., Savelyeva T.A., Kustov D.M., Levkin V.V., Kharnas S.S., and Loshchenov V.B. Automation of Planning and Control of Photodynamic Therapy for the Gastrointestinal Tract. *Biomedical Photonics*, 2025, vol. 14(2), pp. 40-54. doi: 10.24931/2413-9432-2025-14-2-40-54
- Kiryushchenkova N.P., Novikov I.A. Local anisotropy of skin scattering as a possible factor in the distortion of tumor fluorescence boundaries. *Biomedical Photonics*, 2025, vol. 14(2), pp. 12-20. doi: 10.24931/2413-9432-2025-14-2-12-20

ЛИТЕРАТУРА

- 1. Кривецкая А.А., Савельева Т.А., Кустов Д.М., Левкин В.В., Харнас С.С., Лощенов В.Б. Автоматизация планирования и контроля фотодинамической терапии органов желудочно-кишечного тракта // Biomedical Photonics. 2025. Т. 14, № 2. С. 40-54. doi: 10.24931/2413-9432-2025-14-2-40-54
- 2. Кирющенкова Н.П., Новиков И.А. Локальная анизотропия рассеяния кожи как возможный фактор искажения флуоресцентных границ опухоли // Biomedical Photonics. 2025. Т. 14, № 2. С. 12-20. doi: 10.24931/2413-9432-2025-14-2-12-20



- Tuchin V.V. Tissue Optics: Light Scattering Methods and Tools for Medical Diagnostics. SPIE Press: Bellingham, Washington, 2015.
- Macdonald, C.M., Arridge S., Powell S. Efficient inversion strategies for estimating optical properties with Monte Carlo radiative transport models. J. of Biomedical Optics, 2020, vol. 25, pp. 085002. doi: 10.1117/1.JBO.25.8.085002
- Wei H.-J., Xing D., Wu G.-Y., Jin Y., Gu H.-M. Optical properties of human normal small intestine tissue determined by Kubelka-Munk method in vitro. World J Gastroenterol, 2003, vol. 9, pp. 2068-2072. doi: 10.3748/wjg.v9.i9.2068
- Wei H.-J., Xing D., Lu J.J., Gu H.M., Wu G.Y., Jin Y. Determination of optical properties of normal and adenomatous human colon tissues in vitro using integrating sphere techniques. World J Gastroenterol, 2005, vol. 11, pp. 2413-2419. doi: 10.3748/wjg.v11. i16.2413
- Bashkatov A.N., Genina E.A., Kochubey V.I., Rubtsov V.S., Kolesnikova E.A., and Tuchin V.V. Optical Properties of Human Colon Tissues in the Spectral Range 350–2500 nm. *Quantum Electronics*, 2014, vol. 44, pp. 779.
- Carneiro I., Carvalho S., Henrique R., Oliveira L., Tuchin V.V. Kinetics of Optical Properties of Colorectal Muscle During Optical Clearing. IEEE Journal of Selected Topics in Quantum Electronics, 2019, vol. 25, pp. 1-8
- Wiesner W., Mortelé K.J., Ji H., Ros P.R. Normal colonic wall thickness at CT and its relation to colonic distension. J Comput Assist Tomogr, 2002, vol. 26, pp. 102-6. doi: 10.1097/00004728-200201000-00015
- Kustov D.M., Savelieva T.A., Mironov T.A., Kharnas S.S., Levkin V.V., Gorbunov A.S., Shiryaev A.A., Loschenov V.B. Intraoperative Control of Hemoglobin Oxygen Saturation in the Intestinal Wall during Anastomosis Surgery. *Photonics*, 2021, vol. 8, pp. 427. doi: 10.3390/photonics8100427
- 11. Prahl, S.A., Keijzer M., Jacques S.L., Welch A.J. A Monte Carlo model of light propagation in tissue. *In Proc. SPIE of Dosimetry of Laser Radiation in Medicine and Biology*, 1989, vol. 5, pp. 102 111.
- 12. Kubelka P. New contributions to the optics of intensely light-scattering materials. *J. Opt. Soc. Am*, 1948, vol. 38, pp. 448-457.
- Hamdy O., El-Azab J., Al-Saeed T.A., Hassan M.F., Solouma N.H. A Method for Medical Diagnosis Based on Optical Fluence Rate Distribution at Tissue Surface. *Materials*, 2017. vol. 10, pp. 1104. doi: 10.3390/ma10091104
- Van Gemert M.J.C., Welch A.J., Star W.M., Motamedi M., Cheong W. F. Tissue optics for a slab geometry in the diffusion approximation. *Laser Med Sci*, 1987, vol. 2, pp. 295-302. doi:10.1007/BF02594174
- Molenaar R., ten Bosch J.J., Zijp J.R. Determination of Kubelka– Munk scattering and absorption coefficients by diffuse illumination. *Appl. Opt*, 1999, vol. 38, pp. 2068-2077. doi: 10.1364/ ao.38.002068

- Tuchin, V.V. Tissue Optics: Light Scattering Methods and Instruments for Medical Diagnosis // SPIE Press: Bellingham, WA. – 2015.
- Macdonald C.M., Arridge S., Powell S. Efficient inversion strategies for estimating optical properties with Monte Carlo radiative transport models // J. of Biomedical Optics. 2020. Vol. 25. P. 085002. doi: 10.1117/1.JBO.25.8.085002
- Wei H.-J., Xing D., Wu G.-Y., Jin Y., Gu H.-M. Optical properties of human normal small intestine tissue determined by Kubelka-Munk method in vitro // World J Gastroenterol. 2003. Vol. 9. P. 2068-2072. doi: 10.3748/wjg.v9.i9.2068
- Wei H.-J., Xing D., Lu J.J., Gu H.M., Wu G.Y., Jin Y. Determination of optical properties of normal and adenomatous human colon tissues in vitro using integrating sphere techniques // World J Gastroenterol. – 2005. – Vol. 11. – P. 2413-2419. doi: 10.3748/wjg.v11. i16.2413
- Башкатов А.Н., Генина Э.А., Кочубей В.И., Рубцов В.С., Колесникова Е.А., Тучин В.В. Оптические свойства тканей толстой кишки человека в спектральном диапазоне 350–2500 нм // Квантовая электроника. – 2014. – № 44. – С. 779.
- Carneiro I., Carvalho S., Henrique R., Oliveira L., Tuchin V.V. Kinetics of Optical Properties of Colorectal Muscle During Optical Clearing // IEEE Journal of Selected Topics in Quantum Electronics. – 2019. – Vol. 25. – P. 1-8.
- Wiesner W., Mortelé K.J., Ji H., Ros P.R. Normal colonic wall thickness at CT and its relation to colonic distension // J Comput Assist Tomogr. 2002. Vol. 26. P. 102-6. doi: 10.1097/00004728-200201000-00015
- Kustov D.M., Savelieva T.A., Mironov T.A., Kharnas S.S., Levkin V.V., Gorbunov A.S., Shiryaev A.A., Loschenov V.B. Intraoperative Control of Hemoglobin Oxygen Saturation in the Intestinal Wall during Anastomosis Surgery // Photonics. – 2021. - Vol. 8. P. 427. doi: 10.3390/photonics8100427
- Prahl S.A., Keijzer M., Jacques S.L., Welch A.J. A Monte Carlo model of light propagation in tissue // In Proc. SPIE of Dosimetry of Laser Radiation in Medicine and Biology. – 1989. – Vol. 5, P. 102 - 111.
- 12. Kubelka P. New contributions to the optics of intensely light-scattering materials // J. Opt. Soc. Am. 1948. Vol. 38. P. 448-457.
- Hamdy O., El-Azab J., Al-Saeed T.A., Hassan M.F., Solouma N.H. A Method for Medical Diagnosis Based on Optical Fluence Rate Distribution at Tissue Surface // Materials. – 2017. – Vol. 10. – P. 1104 doi: 10.3390/ma10091104
- Van Gemert, M.J.C.; Welch, A.J.; Star, W.M.; Motamedi, M.; Cheong, W. F. Tissue optics for a slab geometry in the diffusion approximation // Laser Med Sci. – 1987. Vol. 2. – P. 295–302. doi:10.1007/BF02594174
- Molenaar R., ten Bosch, J.J., Zijp J.R. Determination of Kubelka– Munk scattering and absorption coefficients by diffuse illumination // Appl. Opt. – 1999. – Vol. 38. P. 2068-2077. doi: 10.1364/ao.38.002068

MULTI-COURSE PHOTODYNAMIC THERAPY IN A PATIENT WITH MALIGNANT TUMOR OF THE MAJOR DUODENAL PAPILLA. CLINICAL CASE

Tseimakh A.E.¹, Shoykhet Ia. N.¹, Tseimakh E.A.¹, Bedyan N.K.², Makarenkov A.S.³

- ¹Altai state medical university, Barnaul, Russia
- ² Altai regional oncological dispenser, Barnaul, Russia
- ³State hospital №5, Barnaul, Russia

Abstract

The article presents a clinical case of successful elimination of mechanical jaundice by means of a course of photodynamic therapy in a patient with a malignant neoplasm of the major duodenal papilla and multimorbid concomitant pathology. The patient, admitted with a clinical picture of mechanical jaundice, after additional examination was given a final diagnosis - moderately differentiated adenocarcinoma of the major duodenal papilla, stage lla (T2N0M0), complicated by moderate mechanical jaundice. After primary stenting, a series of three consecutive courses of combined systemic and local photodynamic therapy were performed with a three-month interval between them. During the last course, stent migration into the duodenum was detected. Nevertheless, the complex therapy allowed to effectively eliminate the manifestations of mechanical jaundice, stabilize the patient's condition, prevent further growth of the primary tumor, restore the patiency of the ducts of the major duodenal papilla and avoid relapses of mechanical jaundice, despite the migration of the stent. This experience demonstrates the promise of the photodynamic approach for solving complex clinical situations associated with tumor damage to the biliary system and allows to consider this method as an alternative in situations of high risk of complications of traditional surgery.

Key words: malignant tumor of the major duodenal papilla; course photodynamic therapy; survival.

Contacts: Tseimakh A.E., e-mail: alevtsei@rambler.ru

For citations: Tseimakh A.E., Shoikhet Ia.N., Tseimakh E.A., Bedyan N.K., Makarenkov A.S. Multi-course photodynamic therapy in a patient with malignant tumor of the major duodenal papilla. Clinical case, *Biomedical Photonics*, 2025, vol. 14, no. 3, pp. 39–42. doi: 10.24931/2413–9432–2025–14–3–39–42

МНОГОКУРСОВАЯ ФОТОДИНАМИЧЕСКАЯ ТЕРАПИЯ У ПАЦИЕНТА СО ЗЛОКАЧЕСТВЕННЫМ НОВООБРАЗОВАНИЕМ БОЛЬШОГО ДУОДЕНАЛЬНОГО СОСОЧКА. КЛИНИЧЕСКИЙ СЛУЧАЙ

А.Е. Цеймах¹, Я.Н. Шойхет¹, Е.А. Цеймах¹, Н.К. Бедян², А.С. Макаренков³

- 1Алтайский государственный медицинский университет, Барнаул, Россия
- ²Алтайский краевой онкологический диспансер, Барнаул, Россия
- ³Городская больница №5, Барнаул, Россия

Резюме

В статье представлен клинический случай успешного устранения механической желтухи посредством проведения курсовой фотодинамической терапии у пациента со злокачественным новообразованием большого дуоденального сосочка и мультиморбидной сопутствующей патологией. Пациенту, поступившему с клинической картиной механической желтухи, после дообследования был поставлен окончательный диагноз – умеренно дифференцированная аденокарцинома большого дуоденального сосочка, стадии lla (T2NOMO), осложненная механической желтухой средней степени тяжести. После первичного стентирования выполнена серия из трёх последовательных курсов комбинированной системной и локальной фотодинамической терапии с трёхмесячным интервалом между ними. Во время последнего курса была выявлена миграция стента в двенадцатиперстную кишку. Тем не менее, комплексная терапия позволила эффективно устранить проявления механической желтухи, стабилизировать состояние пациента, предотвратить дальнейший рост первичной опухоли, восстановить проходимость протоков большого дуоденального сосочка и избежать рецидивов механической желтухи, несмотря на миграцию стента. Данный опыт демонстрирует перспективность фотодинамического под-



хода для решения сложных клинических ситуаций, связанных с опухолевым поражением билиарной системы и позволяет рассматривать этот метод как альтернативное средство в ситуациях высокого риска осложнений традиционной хирургии.

Ключевые слова: злокачественное новообразование большого дуоденального сосочка; курсовая фотодинамическая терапия; выживаемость.

Контакты: Цеймах A.E., e-mail: alevtsei@rambler.ru

Для цитирования: Цеймах А.Е., Шойхет Я.Н., Цеймах Е.А., Бедян Н.К., Макаренков А.С. Многокурсовая фотодинамическая терапия у пациента со злокачественным новообразованием большого дуоденального сосочка. Клинический случай // Biomedical Photonics. – $2025. - T. 14, N^2 3. - C. 39-42$. doi: 10.24931/2413-9432-2025-14-3-39-42

Introduction

Cancer of the major duodenal papilla (MDP) is a rare malignant pathology, which in oncological statistics is considered in combination with other malignant neoplasms of the bile ducts [1, 2, 3, 4]. The structure of morbidity and mortality in biliary cancer is assessed together with hepatocellular cancer [1, 2, 3, 4]. In the overall structure of malignant neoplasms of the digestive tract, the share of MDP cancer is only 0.2%. Being one of the rarest oncological pathologies, estimated together with hepatocellular carcinoma with a prevalence of 6.7 per 100,000 population, malignant neoplasms of the bile ducts have one of the highest overall mortality rates (35.2%) and mortality rates in the first year from the date of diagnosis (66.8%), while MDP cancer in the structure of biliary cancer is only 16.4%, which corresponds to a prevalence of 6 per 1,000,000 population [1, 2, 3, 4].

Despite the development of radiation and chemotherapy methods, the main method of treating MDP cancer remains surgical with a predominance of two types of operations: various modifications of pancreatoduodenal resection and local resection or papillectomy. However, radical surgical treatment is usually difficult due to late diagnosis of the disease: 80.3% of patients have an advanced or locally advanced process [1, 2, 3, 4]. Among the palliative treatment options, the main one remains the chemotherapeutic method, which is difficult to perform in patients with the most common complications of MDP cancer - mechanical jaundice, cholangitis, multiple organ failure, which are the leading clinical manifestations of MDP cancer [5].

One of the methods of palliative treatment, complementing surgical treatment is photodynamic therapy (PDT). PDT is a method of treating malignant neoplasms, in which the tumor is irradiated with light of a certain wavelength, which brings the molecules of a special substance selectively accumulated in the tumor tissue - a photosensitizer, into an excited state in the presence of oxygen. The released singlet oxygen has a direct cytotoxic effect, causing tumor cells to die by apoptosis, necrosis and autophagy. Based on the conducted studies of the effectiveness of PDT of malignant neoplasms of the pancreatobiliary zone,

the authors developed a PDT technique that seems promising for the treatment of patients who are not indicated for radical surgical treatment [6].

Materials and Methods

Developed PDT technique

Algorithm of the developed PDT technique is the following: fluorescence diagnostics on the laser electron-spectral unit "Biospec" (LLC "Novyere Surgical Technologies", Russia) and local and systemic PDT on the software specialized laser dual-wave apparatus "LAMI-Gelios" (LLC "New Surgical Technologies", Russia) according to Technical Specifications 9444-001-53807582-2010. For PDT, a photosensitizer based on chlorin e6 (radachlorin, OOO "RADA-PHARMA", Russia) is used. Systemic PDT is performed through a peripheral intravenous access using an apparatus for intravenous blood irradiation (monochromatic light with a wavelength of 662-665 nm, irradiation time of 30 min, light exposure dose of 1200-1400 J/cm², output power of the light fiber of 0.7 W, radiation power density of 0.22 W/ cm²) with intravenous administration of a photosensitizer at a dose of 1-1.2 mg/kg of body weight according to the instructions for the drug. Local contact PDT is performed after 3 hours (5 hours for solid tumors) from the start of systemic PDT through antegrade percutaneous transhepatic and/or retrograde endoscopic access, depending on the localization of the malignant neoplasm (irradiation with monochromatic light with a wavelength of 662 nm, with an exposure dose of light of 220 J/cm²). To perform local PDT, a specialized dual-wave laser software device with a fiber output power of 0.7 W and a radiation power density of 0.22 W/cm² with a radial diffuser is used.

In the case of pancreatic head cancer, endoscopic ultrasound is used for navigation, and in the case of malignant neoplasms of the intrahepatic and extrahepatic bile ducts, transluminal PDT is used during choledochoscopy on a guiding catheter for direct peroral cholangioscopy with its fixation (Fig. 1). In the case of pancreatic head cancer, if it is possible to install a stent without percutaneous transhepatic drainage, only retrograde endoscopic access is used.

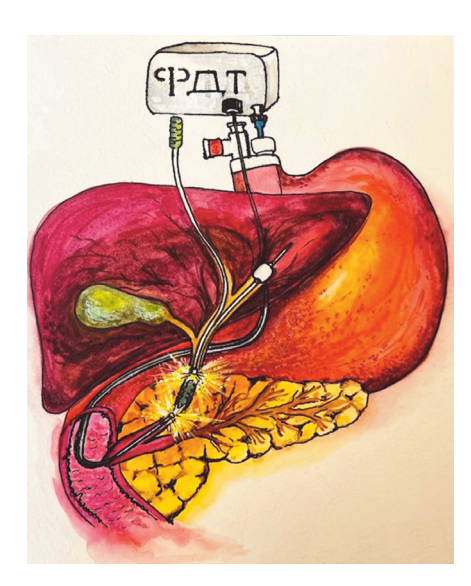


Рис. 1. Схема проведения локальной ФДТ у пациентов со злокачественными новообразования желчевыводяших протоков.

Fig. 1. Scheme of local PDT in patients with malignant tumors of the bile ducts.

The purpose of local PDT is to normalize the outflow through the extrahepatic bile ducts by reducing the volume of tumor tissue. Monitoring is carried out both visually and fluoroscopically and in the laboratory. At the same time, due to one of the advantages of PDT low toxicity of treatment, the method can be carried out as part of a course of therapy to prevent recurrence of mechanical jaundice and increase patient survival, which is especially important for tumors of the pancreatobiliary zone, which have the worst prognosis among tumors of the digestive system [1, 2, 3].

In order to illustrate the method of course PDT, we considered it possible to present a clinical example of a patient with MDP cancer after stenting, in whom, with the help of course PDT, it was possible to prevent recurrence of mechanical jaundice despite the migration of the stent into the duodenum.

Clinical observation

The patient, 87 years old, was hospitalized in the surgical department of the State Healthcare Institution of the Novosibirsk Region "Novosibirsk Regional Clinical Hospital" in July 2024 with complaints of yellowness of the skin for 3 weeks. No other symptoms were noted. The patient underwent an ultrasound examination of the abdominal organs and magnetic resonance imaging of the abdominal organs, where biliary hypertension was detected. The final clinical diagnosis was made after video esophagogastroduodenoscopy with a biopsy from the major duodenal papilla and morphological verification of the diagnosis - moderately differentiated adenocarcinoma of the major duodenal papilla, stage lla (T2N0M0), complicated by moderate mechanical jaundice.

Among the concomitant pathologies, the patient had chronic urinary retention due to prostatic hyperplasia, chronic kidney disease stage IV (stage C4 A1) against the background of acute kidney injury (history of acute tubular necrosis). The patient also had significant concomitant cardiological and endocrine pathologies: hypertension with high cardiovascular risk stage III, degree 3, risk 4; chronic heart failure, functional class IIA; ischemic heart disease with episodes of stable angina pectoris functional, class II; diffuse multinodular goiter with signs of subclinical hyperthyroidism; diverticulosis of the colon; compensated type 2 diabetes mellitus; diabetic nonproliferative retinopathy of both eyes, and polyneuropathy.

Due to multiple concomitant pathologies and high perioperative risk, it was decided to refrain from radical surgery. The patient underwent endoscopic retrocholangiopancreatography, papillosphincterotomy and stenting of the common bile duct with biopsy from the major duodenal papilla. Two months later, before replacing the stent, the patient underwent the first course of local and systemic PDT according to the method described above in the surgery department of the Regional State BBudgetary Institution of Health Care "City Hospital No. 5, Barnaul". A month later, the stent was replaced at the State Healthcare Institution of the Novosibirsk Region "State Novosibirsk Regional Clinical Hospital", followed by two courses of local and systemic PDT with an interval of 3 months between each course. During planned hospitalizations, the patient did not have clinical and laboratory signs of mechanical jaundice. During video esophagogastroduodenoscopy after ultrasound examination of abdominal organs, where no stent was detected, during planned hospitalization for the third course of PDT 6 months after stent placement, stent migration into the duodenum was detected (Fig. 2). At the same time, traces of bile were present in the duodenum, and the lumen of the major duodenal papilla was visualized. When comparing the dynamics according to the data of previous endoscopic studies, it was possible to



Рис. 2. Злокачественное новообразование БСДПК с наличием свободного просвета и следов желчи в двенадцатиперстной кишке.

Fig. 2. Malignant tumor of the major duodenal papilla with visualisation of free lumen and signs of bile in the duodenum.



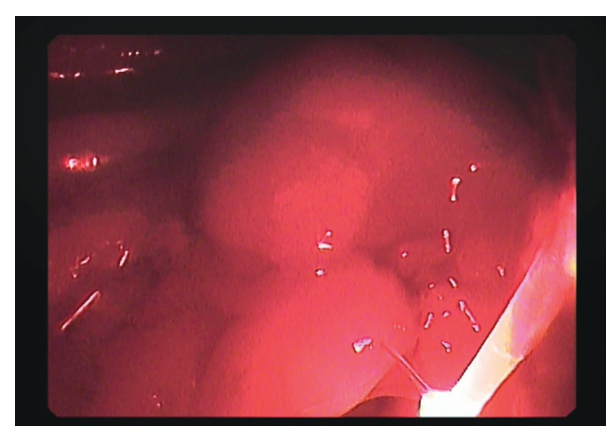


Рис. 3. Злокачественное новообразование БСДПК с наличием свободного просвета и следов желчи в двенадцатиперстной кишке.

Fig. 3. Malignant tumor of the major duodenal papilla with visualisation of free lumen and signs of bile in the duodenum.

identify the absence of clinically significant growth of the neoplasm into the lumen of the major duodenal papilla.

The patient underwent local PDT using a single technique similar to previous courses (Fig. 3) with recommendations for planned stenting.

From the moment of morphological verification of the diagnosis to the moment of discharge after the third course of PDT, 10 months have passed, outpatient monitoring of the patient continues. Of particular importance is the absence of side effects from the use of the photosensitizer on the urinary system and the absence of negative dynamics of clinical and laboratory

markers of chronic renal failure against the background of multiple courses of PDT before and after surgery.

Conclusion

At the present stage, a number of studies of the effectiveness of PDT of malignant neoplasms of the bile ducts have been conducted, summarized in two meta-analyses: a meta-analysis of Moole H. et al. [7], which presents the main outcomes of heterogeneous studies, some of which used only PDT, while most patients underwent combined treatment (PDT and chemotherapy); and a meta-analysis of Tseimakh A.E. et al., which analyses homogeneous studies that assessed only the effectiveness of PDT without the influence of other methods of specific treatment. Despite significant difficulties in the combined assessment of PDT studies due to significant variability between photosensitizers, different regimens and treatment plans for patients, both meta-analyses equally show an increase in survival when using PDT in patients with malignant neoplasms of the bile ducts by more than 8 months (240 [7] and 256 [8] days, respectively) with the elimination of the clinical picture of mechanical jaundice and the prevention of its relapses. Thus, course PDT is a promising method for treating mechanical jaundice and subsequent prevention of its recurrence in patients with malignant neoplasms of the major duodenal papilla, which allows, in the absence of significant side effects, to improve survival, which is especially important for older patients with multimorbid pathology.

REFERENCES

- Status of oncological care for the population of Russia in 2023 / ed. Kaprin A.D., Starinskogo V.V., Shachzadova A.O. – M.: MSIOI named after. P.A. Herzen, branch of the FSBI «NMICR» of the Russian Ministry of Health, 2024, pp. 262.
- Zhang X. et al. Comparison of current guidelines and consensus on the management of patients with cholangiocarcinoma: 2022 update. *Intractable Rare Dis Res*, 2022, vol. 11(4), pp. 161-172.
- 3. Russian Oncology Association. Biliary cancer. *Clinical guidelines*, 2020, pp. 51.
- Nazarova D.V., Rasulov R.I., Zubrinsky K.G., Sogolov G.I. Evolution of treatment of cancer of the major duodenal papilla. Siberian Journal of Oncology, 2021, vol. 20(1), pp. 141-148. doi: 10.21294/1814-4861-2021-20-1-141-148 (In Russian)
- Shah R., John S. Cholestatic Jaundice. In: StatPearls [Internet]. Treasure Island (FL): StatPearls Publishing. – 2022. PMID: 29489239.
- Tseimakh A.E. et al. Method for complex mini-invasive treatment of obstructive jaundice, cholangitis, intrahepatic abscesses of tumor genesis using local and systemic photodynamic therapy. *Patent RF*, N. 2704474, 2019.
- 7. Moole H. et al. Success of Photodynamic Therapy in Palliating Patients With Nonresectable Cholangiocarcinoma: A Systematic Review and Meta-Analysis. World J Gastroenterol, 2017, vol. 23(7), pp. 1278-88. doi: 10.3748/wjg.v23.i7.1278
- 8. Tseimakh A.E., Mitshenko A.N., Kurtukov V.A. et al. Effectiveness of palliative photodynamic therapy for unresectable biliary cancer. systematic review and meta-analysis. *Biomedical Photonics*, 2024, vol. 13 (2), pp. 34-42. doi 10.24931/2413-9432-2024-13-2-34-42.

ЛИТЕРАТУРА

- Состояние онкологической помощи населению России в 2023 году / под ред. А. Д. Каприна, В. В. Старинского, А. О. Шахзадовой – М.: МНИОИ им. П.А. Герцена - филиал ФГБУ «НМИРЦ» Минздрава России, 2024. – 262 с.
- Zhang X. et al. Comparison of current guidelines and consensus on the management of patients with cholangiocarcinoma: 2022 update // Intractable Rare Dis Res. – 2022. – Vol. 11(4). – P. 161-172.
- Общероссийский национальный союз «Ассоциация онкологов России». Рак желчевыводящей системы // Клинические рекомендации. – 2024. – С. 51.
- Назарова Д.В., Расулов Р.И., Зубрински К.Г., Сонголов Г.И. Эволюция лечения рака большого сосочка двенадцатиперстной кишки // Сибирский онкологический журнал. – 2021. – Т. 20, №1. – С. 141-148. doi: 10.21294/1814-4861-2021-20-1-141-148
- Shah R., John S. Cholestatic Jaundice // In: StatPearls [Internet]. Treasure Island (FL): StatPearls Publishing. – 2022. – PMID: 29489239.
- Цеймах А.Е., Лазарев А.Ф., Куртуков В.А. и соавт. Способ комплексного мини-инвазивного лечения механической желтухи, холангита, внутрипеченочных абсцессов опухолевого генеза с применением локальной и системной фотодинамической терапии. Патент РФ №2704474, 2019.
- Moole H. et al. Success of Photodynamic Therapy in Palliating Patients With Nonresectable Cholangiocarcinoma: A Systematic Review and Meta-Analysis // World J Gastroenterol. – 2017. – Vol. 23(7). – P. 1278-88. doi: 10.3748/wjg.v23.i7.1278
- Цеймах А.Е., Мищенко А.Н., Куртуков В.А. и соавт. Эффективность паллиативной фотодинамической терапии нерезектабельных злокачественных новообразований желчевыводящей системы. Систематический обзор и метаанализ // Biomedical Photonics. – 2024. – Т. 13, № 2. – С. 34-42. doi 10.24931/2413-9432-2024-13-2-34-42.

PHOTODYNAMIC THERAPY WITH 5-AMINOLEVULINIC ACID FOR CUTANEOUS BASAL CELL CARCINOMA

Filonenko E.V.¹, Ivanova-Radkevich V.I.²

¹P.A. Herzen Moscow Oncology Research Center – branch of FSBI NMRRC of the Ministry of Health of the Russian Federation, Moscow, Russia ²Peoples' Friendship University of Russia (RUDN University), Moscow, Russia

Abstract

The aim of the study was to collect and analyze published data from clinical trials on the efficacy of photodynamic therapy (PDT) using 5-ALA-based drugs and its esters in patients with basal cell carcinoma (BCC). The review was conducted using the PubMed and ClinicalTrials.gov databases for the period from 1995 to 2025. Large prospective and retrospective studies with more than 20 patients were included in the analysis. The efficacy of PDT was examined and compared with traditional treatment methods. The analysis demonstrated significant efficacy of PDT in the treatment of BCC. The complete regression rate ranged from 84% to 99% after 3 months of therapy, from 62% to 96% after 12 months, and from 70% to 91% after 5 years. A significantly better cosmetic outcome was recorded compared with surgical methods. Studies have confirmed that PDT has a high safety profile, with severe side effects rare. The most common adverse effects include mild skin irritation, redness, and mild discomfort, which resolve on their own.

Key words: photodynamic therapy, cutaneous basal cell carcinoma, 5-aminolevulinic acid, 5-aminolevulinic acid methyl ester.

Contacts: Filonenko E.V., e-mail: elena.filonenko@list.ru

For citations: Filonenko E.V., Ivanova-Radkevich V.I. Photodynamic therapy with 5-aminolevulinic acid for basal squamous cell carcinoma, *Biomedical Photonics*, 2025, vol. 14, no. 3, pp. 43–51. doi: 10.24931/2413–9432–2025–14–3 –43–51

ФОТОДИНАМИЧЕСКАЯ ТЕРАПИЯ С 5-АЛК БОЛЬНЫХ БАЗАЛЬНОКЛЕТОЧНЫМ РАКОМ КОЖИ

Е.В. Филоненко¹, В.И. Иванова-Радкевич²

¹Московский научно-исследовательский онкологический институт им. П.А. Герцена — филиал ФГБУ «Национальный медицинский исследовательский центр радиологии» Министерства здравоохранения Российской Федерации, Москва, Россия ²Российский Университет дружбы народов, Москва, Россия

Резюме

Целью нашей работы были сбор и анализ опубликованных данных клинических исследований эффективности фотодинамической терапии (ФДТ) с препаратами на основе 5-АЛК и ее эфиров у пациентов с базальноклеточным раком кожи (БКРК). Анализ литературы проводился на основе базы данных PubMed и ClinicalTrials.gov за период с 1995 по 2025 гг. В анализ были включены крупные проспективные и ретроспективные исследования с количеством пациентов свыше 20 человек. Рассматривалась эффективность ФДТ, было выполнено сравнение с традиционными методами лечения. Проведенный анализ показал значительную эффективность ФДТ при лечении БКРК. Частота полных регрессий достигала от 84% до 99% через 3 мес после начала терапии, от 62% до 96% через 12 мес и от 70% до 91% через 5 лет. Зарегистрирован значительно лучший косметический результат по сравнению с хирургическими методами. Исследования подтвердили, что ФДТ обладает высоким профилем безопасности с редким развитием тяжелых побочных эффектов. Наиболее частые негативные последствия включают легкое раздражение кожи, покраснения и небольшой дискомфорт, проходящие самостоятельно.

Ключевые слова: фотодинамическая терапия, базальноклеточный рак кожи, 5-аминолевулиновая кислота, метиловый эфир 5-аминолевулиновой кислоты.

Контакты: Филоненко E.B., e-mail: elena.filonenko@list.ru

Для цитирования: Филоненко Е.В., Иванова-Радкевич В.И. Фотодинамическая терапия с 5-АЛК больных базальноклеточным раком кожи // Biomedical Photonics. -2025. - T. 14, № 3. - C. 43–51. doi: 10.24931/2413–9432–2025–14–3–43–51

Introduction

Basal cell carcinoma (BCC) is the most common nonmelanocytic skin tumor. It is a slow-growing skin tumor. While it rarely metastasizes, it often occurs in multiple forms and recurs on exposed skin areas, leading to significant treatment challenges. BCC is a heterogeneous group of tumors with histopathological and clinical characteristics ranging from superficial lesions to very extensive and destructive tumors [1].

Epidemiology

In the Russian Federation, when analyzing cancer incidence statistics, BCC is not separately considered from other non-melanocytic skin tumors. However, according to some data, BCC accounts for 75-97% of malignant epithelial skin neoplasms [2,3]. In 2024, the incidence of non-melanoma skin cancer in Russia was 313.9 cases per 100,000 population [3]. Thus, according to indirect estimates, the incidence of non-melanoma skin cancer is approximately 235-305 cases per 100,000 population.

In 2024, the number of newly diagnosed malignant neoplasms in the Russian Federation was 698,693. Of these, approximately 72,000 (10.3% of the overall cancer incidence) were cases of malignant skin cancer (excluding melanoma) [2]. Thus, according to indirect estimates, the number of newly diagnosed cases of nonmelanoma skin cancer annually ranges from 54,000 to 70,000.

The incidence of BCC varies greatly depending on the geographic region. The highest incidence is recorded in Australia (up to 1,000 per 100,000 inhabitants per year), followed by the United States (approximately 210-410 per 100,000 inhabitants per year) and Europe (approximately 75-160 per 100,000 inhabitants per year) [1].

The risk of developing BCC is higher in older people and in women (approximately 2 times more often than in men) [1].

Risk factors

The most significant risk factor for developing BCC is sun exposure, both in childhood and in adulthood. The development of BCC is provoked by ultraviolet rays of the UVA and UVB spectrum (the latter to a greater extent). This explains why most BCC lesions occur on sun-exposed areas of skin and are more common in people with fair skin [1]. The cause of it may be mutations caused by UV radiation. BCC is generally characterized by a high mutational tumor load (tumor mutational burden (TMB)), which is 65 mutations/megabases (compared to 14 mutations/megabases for melanoma) and contains a high percentage of mutations induced by UV radiation [4]. Indirect confirmation of the risk associated with UV radiation may also be the results of studies demonstrating an increased risk of developing

BCC in patients using solariums, with a confirmed doseresponse relationship. Other risk factors include fair skin color, red hair, blue eyes, and older age. A number of authors also associate increased risks of developing BCC with existing hematological neoplasms in the patient [4]. Immunodeficiency, including iatrogenic immunosuppression, can provoke the development of BCC [4]. According to some authors, the risk of developing BCC increases more than 10-fold with tissue and organ transplantation [5].

Classification, Staging, and Clinical Manifestations

The 8th version of the American Joint Committee on Cancer (AJCC) TNM staging system is currently used for BCC staging [6]. Morphological confirmation is mandatory; lymph node status is assessed for staging using clinical examination and instrumental studies [6].

BCC originates from follicular and interfollicular keratinocyte stem cells [1].

BCC is characterized by a variety of clinical forms. The main ones are superficial, nodular, and sclerodermalike

Superficial BCC is characterized by an erythematous, irregularly shaped lesion with clearly defined borders, often with serous and hemorrhagic crusts on the surface. This form is most often localized on the skin of the trunk [6].

Nodular form of BCC is characterized by a hemispherical nodule with a smooth surface, typically gray-pink in color with a pearly hue. This form is most often found on the face and scalp. One variant of this form is the *pigmented* form, which appears as a pigmented spot or nodule of gray-black color [6].

Scleroderma-like form of BCC is characterized by a whitish, scar-like area with no clear boundaries and peripheral "pearlescent" papules. The central portion of this area may contain punctate areas of hyperpigmentation, erosions of varying sizes, atrophic changes, and dyschromia [6].

Diagnosis

The primary method for the initial diagnosis of BCC is dermatoscopy. Compared to eye examination, dermatoscopy increases the sensitivity and specificity of diagnosis from 66.9% to 85.0% and from 97.2% to 98.2%, respectively [7]. Dermatoscopy can also determine the histopathological subtype of BCC [1].

According to most clinical guidelines, a biopsy is required for the diagnosis of BCC; however, in some cases, cytological diagnosis is acceptable for medical facilities with the appropriate technology [1,8].

Medical imaging, such as magnetic resonance imaging and ultrasound, is often required to determine the extent of locally advanced tumor spread [1].

BCC Prognosis

As noted above, BCC rarely metastasizes. Some researchers estimate the metastasis rate to be 0.0028–0.55% [9]. The development of metastases (especially distant ones) significantly worsens the prognosis of BCC. For example, in a study by McCusker M. *et al.*, the median survival was 87 months for regional metastases and 24 months for distant metastases, with every third patient receiving systemic chemotherapy [10].

The main problems with BCC are local tissue destruction, sometimes quite extensive, and a high recurrence rate. The risk of recurrence depends on the tumor location (e.g., zone H on the face, characterized by a high recurrence rate), histological subtype, perineural invasion, immunosuppression, and previous recurrences [1].

Severe forms of BCC are rare and heterogeneous. Data on the proportion of severe forms in the overall BCC structure vary significantly between studies and average between 0.01% and 0.8% [11-12].

Therapy

Surgical Treatment

Surgical treatment is the standard treatment for patients with BCC. Depending on the tumor characteristics (size, location, presence of recurrence, histology) and the surgeon's qualifications, standard excision or Mohs micrographic surgery may be used. The latter surgical treatment option is used for highrisk tumors, recurrent BCC lesions, and BCC located in critical anatomical zones [1]. Van Loo E. *et al.* showed that the 10-year cumulative risk of BCC recurrence after Mohs surgery is three times lower than after standard surgical treatment (4.4% and 12.2%, respectively), and for recurrent BCC, this difference is even higher (3.9% versus 13.5%) [13]. The main adverse effect of surgical treatment is the possibility of scarring [14].

Radiation Therapy

In elderly patients, with severe comorbidities, or those who refuse surgical treatment, radiation therapy may be an alternative to surgery. For BCC, external beam therapy, brachytherapy, or localized radiation therapy are used. The choice of radiation therapy depends on the tumor size, location, team experience, and resources. Radiation therapy can also be used as adjuvant therapy when re-excision of incompletely resected BCC lesions is not possible. Radiation therapy is comparable to surgical treatment in terms of recurrence-free survival [1]. However, radiation therapy may be associated with a risk of tissue fibrosis and secondary malignancies [14].

Local Drug Therapy

Local drug therapy is also an alternative to surgery [14]. This treatment is non-invasive but may cause local

skin reactions including erythema, swelling, itching, hypopigmentation, crusting/scabbing/desquamation, erosions and pain. Topical drug therapy is also associated with lower complete cure rates compared with other treatments [14].

Imiquimod is an immune response modifier used to treat superficial and small nodular BCC in immunocompetent adults. Imiquimod's action is associated with the activation of antitumor immunity. Imiquimod promotes the production of proinflammatory cytokines, chemokines, and other mediators that activate antigen-presenting cells and other components of the innate immune system [1].

According to some authors, the efficacy of imiquimod in BCC is comparable to that of surgical intervention. For example, in a study by Williams H.C. *et al.*, in the treatment of BCC lesions, a positive outcome 5 years after treatment was achieved in 82.5% of cases using imiquimod, compared to 97.7% with surgery [15].

Applications with 5% 5-fluorouracil are also used for BCC. Studies show that 5-fluorouracil is inferior to imiguimod in efficacy in most cases [1].

Cryotherapy

Cryotherapy is indicated only for superficial, low-risk BCC lesions and is not recommended for tumors deeper than 3 mm [1,14]. Disadvantages of cryodestruction include lower efficacy compared to the methods described above, pain, and questionable cosmetic results (the procedure often leaves hypopigmented spots that can persist for years) [1].

Photodynamic Therapy

Photodynamic therapy (PDT) is another alternative treatment option for basal cell carcinoma [1,14,16]. Its high efficacy against a range of skin cancers and precancerous conditions has been demonstrated in numerous clinical and observational studies [17-20]. In particular, our recent reviews demonstrated that PDT can be considered as a first-line treatment option for non-invasive basal cell carcinoma [19,20].

We searched for published results of large randomized and observational clinical trials from 1995 to 2025 on the websites https://clinicaltrials.gov and https://pubmed.ncbi.nlm.nih.gov using the keywords "basal cell carcinoma" and "photodynamic therapy"/"5-aminolevulinic acid"/"MAL – 5-aminolevulinic acid methyl ester." The analysis included randomized controlled and observational studies with more than 20 patients. The table provides summary data on the effectiveness of PDT in patients with BCC.

Discussion

The studies reviewed demonstrated significant heterogeneity in the photosensitizer concentrations,



Таблица

Сводные данные результативности применения фотодинамической терапии у пациентов с базальноклеточным раком кожи

Table

Summary of the effectiveness of photodynamic therapy of basal cell carcinoma

Авторы Authors	Число пациентов / количество очагов / No. of patients/ No. of lesions	Форма БКРК ВСС	Фотосенси- билизатор Photosensitizer	Режим облуче- ния Light wave- length	Количество курсов ФДТ Number of PDT courses	Эффективность ФДТ PDT efficiency
Kessels et al., 2017 [21] Van Delft et al., 2022 [22]	80 пациентов 80 patients	Первичный БКРК Primary BCC	MЭ-АЛК за 4 ч до облучения MAL 4 hours before irradiation	75 Дж/cm ² 75 J/cm ²	2 курса с интервалом 8 дней. 2 courses with an interval of 8 days	Полная регрессия: 95% через 3 мес 89% через 12 мес 91% через 60 мес Complete regression 95% after 3 months 89% after 12 months 91% after 60 months
Kessels et al., 2017 [21] Van Delft et al., 2022 [22]	82 пациента 82 patients	Первичный БКРК Primary BCC	5-АЛК за 4 ч до облучения 5-ALA 4 hours before irradiation	75 Дж/см ² 75 J/cm ²	Дважды в 1 день с интервалом 2 часа Twice on day 1, interval 1 hours	Полная регрессия: 96% через 3 мес 96% через 12 мес 76% через 60 мес Complete regression 96% after 3 months 96% after 12 months 76% after 60 months
Salmivuori et al., 2020 [23]	26 пациентов 33 очага 26 patients 33 lesions	Поверхностный БКРК на теле, но не на лице и волосистой части головы Superficial BCC on the body area, not face and scalp	5-АЛК (нано- эмульсия) за 3 ч до облучения 5-ALA (nano emulsion) 3 hours before irradiation	37 Дж/см ² 37 J/cm ²	2 курса с интервалом 8-14 дней 2 courses with an interval of 8-14 days	Полная регрессия: 91% через 3 мес Complete regression 91% after 3 months
Salmivuori et al., 2020 [23]	27 пациентов 31 очаг 27 patients 31 lesions	Поверхностный БКРК на теле, но не на лице и волосистой части головы Superficial BCC on the body area, not face and scalp	МЭ-АЛК за 3 ч до облучения MAL 3 hours before irradiation	37 Дж/см ² 37 J/cm ²	2 курса с ин- тервалом 8-14 дней 2 courses with an interval of 8-14 days	Полная регрессия: 97% через 3 мес Complete regression 97% after 3 months
Salmivuori et al., 2020 [23]		Поверхностный БКРК на теле, но не на лице и волосистой части головы Superficial BCC on the body area, not face and scalp	ГЭ-АЛК за 3 ч до облучения HAL 3 hours before irradiation	37 Дж/см ² 37 J/cm ²	2 курса с интервалом 8-14 дней 2 courses with an interval of 8-14 days	Полная регрессия: 94% через 3 мес Complete regression 94% after 3 months
Arits et al., 2013 [24], Roozeboom et al., 2016 [25], Jansen et al., 2018 [26]	202 пациента 202 patients	Поверхностный БКРК Superficial BCC	МЭ-АЛК за 3 ч до облучения MAL 3 hours before irradiation	37 Дж/см ² 37 J/cm ²	2 курса с интервалом 1 нед 2 courses with an interval of 1 week	Полная регрессия: 84% через 3 мес 87% через 12 мес 92% через 36 мес 70% через 60 мес Complete regression 84% after 3 months 87% after 12 months 92% after 36 months 70% after 60 months
Morton C. A. et al., 2018 [27]	121 пациент 148 очагов 121 patients 148 lesions	Поверхностный и узелковый БКРК Superficial and nodular BCC	5-АЛК за 3 ч до облучения 5-ALA 3 hours before irradiation	37 Дж/см ² 37 J/cm ²	2 курса с интервалом 1 нед 2 courses with an interval of 1 week	Полная регрессия: 93% через 3 мес 92% через 12 мес Complete regression 93% after 3 months 92% after 12 months

Morton C. A. et al., 2018 [27]	110 пациентов 127 очагов 110 patients 127 lesions	Поверхностный и узелковый БКРК Superficial and nodular BCC	MЭ-АЛК за 3 ч до облучения MAL 3 hours before irradiation	37 Дж/см ² 37 J/cm ²	2 курса с интервалом 1 нед 2 courses with an interval of 1 week	Полная регрессия: 92% через 3 мес 91% через 12 мес Complete regression 92% after 3 months 91% after 12 months
Церковский Д.А. и со- авт., 2017 [28] Tserkovsky D.A. et al., 2017 [28]	130 пациентов 156 очагов 130 patients 156 lesions	Первичный и рецидивный БКРК Primary and recurrent BCC	Хлорин еб за 2,5- 3 ч до облучения Chlorin eб 2.5-3 hours before irradiation		1 курс 1 course	Полная регрессия при первичном БКРК: 91% через 1-3 мес Полная регрессия при рецидивном БКРК: 90% через 1-3 мес Complete regression in primary BCRC: 91% in 1-3 months Complete regression in recurrent BCRC: 90% in 1-3 months
Mosterd et al., 2008 [29] Roozeboom et al., 2013 [30]	83 ovara 83 lesions	Узелковый БКРК Nodular BCC	5-АЛК 5-ALA	_	2 сеанса облучения (интервал 1 ч) 2 irradiation sessions (interval 1 hour)	Полная регрессия: 73% через 60 мес Complete regression 73% after 60 months
Капинус В.Н. и соавт. [31] Каріпиз V.N. et al., 2013 [31]	127 пациентов 127 patients	Рецидивный БКРК Recurrent BCC	Хлорин еб за 3 ч до облучения Chlorin еб 3 hours before irradiation	100-600 Дж/см² 100-600 J/ cm²	1-4 courses	Полная регрессия: 68,5% (срок наблюдения 6-60 мес) У пациентов с рецидивами после лучевой терапии – 20,5% У пациентов с рецидивами после лучевой терапии – 20,5% У пациентов с рецидивами после крио-, электро-, лазеркоагуляции и хирургического лечения – 28,6-30,8% У пациентов с рецидивами после предшествующего комбинированного лечения – 47,2% Сотрете regression: 68.5% (observation period 6-60 months) In patients with relapses after radiation therapy - 20.5% In patients with relapses after rediation therapy - 20.5% In patients with relapses after cryo-, electro-, laser coagulation and surgical treatment - 28.6-30.8% In patients with relapses after cryo-, electro-, laser coagulation and surgical treatment - 28.6-30.8% In patients with relapses after previous combined treatment - 47.2%
De Haaset al., 2006 [32] de Vijlderet al., 2012 [33]	100 пациентов 243 oчагов 100 patients 243 lesions	Поверхностный БКРК Superficial BCC	MЭ-АЛК за 4 ч до облучения MAL 4 hours before irradiation	75 Дж/см ² 75 J/cm ²	1 сеанс облучения 1 irradiation session	Полная регрессия: 75% через 60 мес Complete regression 75% after 60 months
De Haaset al., 2006 [32] de Vijlderet al., 2012 [33]	55 пациентов 262 очагов 55 patients 262 lesions	Поверхностный БКРК Superficial BCC	MЭ-АЛК за 4 ч до облучения MAL 4 hours before irradiation	Дж/см ² 20 and	2 сеанса облучения (через 4 и 6 ч) 2 irradiation sessions (after 4 and 6 hours)	Полная регрессия: 88% через 60 мес Complete regression 88% after 60 months

Foley et al., 2009 [34]	66 пациентов 75 очагов 66 patients 75 lesions	Узелковый БКРК Nodular BCC	МЭ-АЛК за 3 ч до облучения MAL 3 hours before irradiation	75 Дж/см ² 75 J/cm ²	2 курса с интервалом 1 нед 2 courses with an interval of 1 week	Полная регрессия: 75% через 6 мес Complete regression 75% after 6 months
Basset- Seguin N. et al., 2008 [35]	60 пациентов 114 очагов 60 patients 114 lesions	Поверхностный БКРК Superficial BCC	МЭ-АЛК за 3 ч до облучения MAL 3 hours before irradiation	75 Дж/см ² 75 J/cm ²	1-3 курса в течение 3 мес 1-3 courses for 3 months	Полная регрессия: 88% через 3 мес 78% через 60 мес Complete regression 88% after 3 months 78% after 60 months
Smucler et al., 2008 [36]	286 пациентов 286 очагов 286 patients 286 lesions	Узелковый БКРК Nodular BCC	МЭ-АЛК за 3 ч до облучения MAL 3 hours before irradiation	75 Дж/см ² 75 J/cm ²	2 курса с интервалом 1 нед 2 courses with an interval of 1 week	Полная регрессия: 99% через 3 мес 95% через 12 мес Complete regression 99% after 3 months 95% after 12 months
Rhodes et al., 2004 [37] 2007 [38]	53 пациента 60 очагов 53 patients 60 lesions	Узелковый БКРК Nodular BCC	МЭ-АЛК за 3 ч до облучения MAL 3 hours before irradiation	75 Дж/см² 75 J/cm²	2 курса с интервалом 1 нед 2 courses with an interval of 1 week	Полная регрессия: 91% через 3 мес 83% через 12 мес 76% через 24 мес Complete regression 91% after 3 months 83% after 12 months 76% after 24 months
Berroeta et al., 2007 [39]	21 oyar 21 lesions	Узелковый БКРК Nodular BCC	5-АЛК 5-ALA	-	-	Полная регрессия: 62% через 12 мес Complete regression 62% after 12 months

*БКРК – базальноклеточный рак кожи, 5-АЛК – 5-аминолевулиновая кислота, МЭ-АЛК – метиловый эфир 5-аминолевулиновой кислоты, ГЭ-АЛК – гексиловый эфир 5-аминолевулиновой кислоты

light sources, incubation times, and pretreatment strategies used. This precludes a comparative analysis of the efficacy of different PDT regimens and the generalization of results to develop standardized approaches. However, based on the analyzed results, it can be confidently stated that PDT with 5-ALA and MAL-based photosensitizers demonstrates high efficacy against superficial BCC lesions with excellent cosmetic results [14].

The rate of complete regression of BCC lesions at 3 months after PDT averaged 84-99%, 62-96% at 12 months, and 70-91% at 5 years. No difference in efficacy was observed between 5-ALA and MAL [19,20,25-39]. Our search also identified one study involving more than 20 patients using HAL [23]. It should be noted that in most studies, patients with an incomplete response could undergo an additional course of PDT. However, the authors did not demonstrate a relationship between the treatment effect and the number of PDT courses [22,25,26,27,29,30,34-38].

It should be noted that in global clinical practice, photosensitizers based on 5-ALA and its esters are most often used for the treatment of BCC [22,23,24-27,29-30,32-39]. Russian studies also use photosensitizers based on chlorin e6 for the treatment of BCC [28,31]. The treatment efficacy in both cases is quite high.

In most studies, the light dose per irradiation session was approximately 37-75 J/cm². However, some authors

have demonstrated greater efficacy with fractionated irradiation (two irradiation sessions separated by 1-2 hours) [32,33].

A number of studies have assessed the efficacy of alternative treatments compared to PDT. PDT demonstrated similar complete response rates as most other treatments, with the exception of surgery and imiquimod, which demonstrated better results. The main disadvantage of surgery, especially compared with PDT, was unsatisfactory cosmetic results [22,23,24,37].

The most common adverse events associated with PDT are pain and discomfort. These may occur immediately or after completion of irradiation. Most patients tolerate the treatment well for BCC without the need for additional analgesics. Local adverse events such as mild to moderate erythema, local edema, pruritus, superficial crusting, and vesicular eruptions were also recorded during the observational studies. According to the data from the reviewed studies, all of these reactions were transient and self-limited. Based on these results, PDT has a favorable safety profile [22-39].

The main limitations of some of the reviewed studies included an observation period of less than 12 months, heterogeneity in the assessment of clinical outcomes, and the fact that not all studies reported treatment-related adverse events. The duration of the observation period was important for assessing the effectiveness of various treatments, as BCC can recur years after treatment [14].

^{*}BCC – basal cell carcinoma, 5-ALA – 5-aminolevulinic acid, MAL – 5-aminolevulinic acid methyl ester, HAL – 5-aminolevulinic acid hexyl ester.

Conclusion

Photodynamic therapy demonstrates high efficacy and good cosmetic results in patients with BCC. In some cases (eg, advanced age, severe comorbidities, patient refusal of surgery, contraindications to surgery), PDT can be considered as an alternative to surgery. Numerous

clinical studies and observational studies convincingly demonstrate that PDT with 5-ALA and its derivatives is effective, safe, and cosmetically favorable for patients with BCC. However, the variability of treatment protocols highlights the need for further randomized controlled trials to determine optimal treatment parameters.

REFERENCES

- Basset-Seguin N., Herms F. Update on the management of basal cell carcinoma. *Acta dermato-venereologica*, 2020, Vol. 100 (11), pp. 5750.
- Samulenko A., Mordovsky A., Polyakov A. Modern Treatment Strategy for Basal Cell Carcinoma of the Head and Neck. *Vrach*, 2017, No. 12, pp. 5-8.
- 3. Edited by A.D. Kaprin, V.V. Starinsky, A.O. Shakhzadova. The State of Cancer Care in Russia in 2024. Moscow: P.A. Herzen Moscow Research Institute of Oncology, a branch of the National Medical Research Radiological Center of the Ministry of Health of the Russian Federation, 2025, p. 275.
- Peris K. et al. European consensus-based interdisciplinary guideline for diagnosis and treatment of basal cell carcinoma – update 2023. European Journal of Cancer, 2023, Vol. 192, pp. 113254.
- Krynitz B. et al. Risk of basal cell carcinoma in Swedish organ transplant recipients: a population-based study. *British Journal of Der*matology, 2016, Vol. 174(1), pp. 95-103.
- Clinical Guidelines Basal Cell Skin Cancer 2020-2021-2022 (20.01.2023) – Approved by the Ministry of Health of the Russian Federation.
- Reiter O. et al. The diagnostic accuracy of dermoscopy for basal cell carcinoma: A systematic review and meta-analysis. *Journal of the American Academy of Dermatology*, 2019, Vol. 80(5), pp. 1380-1388.
- 8. Filonenko E.V., Grigoriev N.I. Photodynamic Therapy for a Patient with Basal Cell Carcinoma of the Lower Eyelid Skin (Clinical Case). *Biomedical Photonics*, 2023, Vol. 12(4), pp. 30-32. doi: 10.24931/2413–9432–2023–12-4-30–32.
- 9. Peris K. et al. Diagnosis and treatment of basal cell carcinoma: European consensus–based interdisciplinary guidelines. *European Journal of cancer*, 2019, Vol. 118, pp. 10-34.
- McCusker M. et al. Metastatic basal cell carcinoma: prognosis dependent on anatomic site and spread of disease. European journal of cancer, 2014, Vol. 50(4), pp. 774-783.
- 11. Morton C. et al. European Dermatology Forum Guidelines on topical photodynamic therap. *European Journal of Dermatology*, 2015, Vol. 25(4), pp. 296-311.
- 12. Schulten R. et al. Comparison of the uptake of 5-aminolevulinic acid and its methyl ester in keratinocytes and skin. *Naunyn-Schmiedeberg's archives of pharmacology*, 2012, Vol. 385(10), pp. 969-979
- 13. Van Loo E. et al. Surgical excision versus Mohs' micrographic surgery for basal cell carcinoma of the face: a randomised clinical trial with 10 year follow-up. *European Journal of Cancer*, 2014, Vol. 50(17), pp. 3011-3020.
- 14. Zeitouni N. C. et al. 5-aminolevulinic acid photodynamic therapy for the treatment of basal and squamous cell carcinoma: A systematic review. *Photodiagnosis and Photodynamic Therapy*, 2025, pp. 104649.
- 15. Williams H. C. et al. Surgery versus 5% imiquimod for nodular and superficial basal cell carcinoma: 5-year results of the SINS randomized controlled trial. *Journal of Investigative Dermatology*, 2017, Vol. 137(3), pp. 614-619.
- Wang J. Y. et al. Photodynamic Therapy: Clinical Applications in Dermatology. *Journal of the American Academy of Dermatology*, 2025.
- 17. Calzavara-Pinton P.G. et al. Methylaminolaevulinate-based photodynamic therapy of Bowen's disease and squamous cell carcinoma. *British Journal of Dermatology*, 2008, Vol. 159(1), pp. 137-144.
- Keyal U. et al. Present and future perspectives of photodynamic therapy for cutaneous squamous cell carcinoma.

ЛИТЕРАТУРА

- Basset-Seguin N., Herms F. Update on the management of basal cell carcinoma //Acta dermato-venereologica. – 2020. – Vol. 100 (11). – P. 5750.
- Самуленко А., Мордовский А., Поляков А. Современная стратегия лечения базальноклеточного рака кожи головы и шеи // Врач. 2017. №. 12. С. 5-8.
- 3. Под ред. А.Д. Каприна, В.В. Старинского, А.О. Шахзадовой. Состояние онкологической помощи населению России в 2024 году. Москва: МНИОИ им. П.А. Герцена филиал ФГБУ «НМИЦ радиологии» Минздрава России. 2025. С. 275.
- Peris K. et al. European consensus-based interdisciplinary guideline for diagnosis and treatment of basal cell carcinoma – update 2023 // European Journal of Cancer. – 2023. – Vol. 192. – P. 113254
- 5. Krynitz B. et al. Risk of basal cell carcinoma in Swedish organ transplant recipients: a population-based study // British Journal of Dermatology. 2016. Vol. 174(1). P. 95-103.
- 6. Клинические рекомендации Базальноклеточный рак кожи 2020-2021-2022 (20.01.2023) Утверждены Минздравом РФ.
- 7. Reiter O. et al. The diagnostic accuracy of dermoscopy for basal cell carcinoma: A systematic review and meta-analysis // Journal of the American Academy of Dermatology. 2019. Vol. 80(5). P. 1380-1388.
- 8. Филоненко Е.В., Григорьевых Н.И. Фотодинамическая терапия больной базальноклеточным раком кожи нижнего века (клиническое наблюдение) // Biomedical Photonics. 2023. Т. 12, № 4. С. 30-32. doi: 10.24931/2413–9432–2023–12-4-30–32.
- Peris K. et al. Diagnosis and treatment of basal cell carcinoma: European consensus-based interdisciplinary guidelines // European Journal of cancer. – 2019. – Vol. 118. – P. 10-34.
- McCusker M. et al. Metastatic basal cell carcinoma: prognosis dependent on anatomic site and spread of disease // European journal of cancer. – 2014. – Vol. 50(4). – P. 774-783.
- Morton C. et al. European Dermatology Forum Guidelines on topical photodynamic therapy // European Journal of Dermatology. – 2015. – Vol. 25(4). – P. 296-311.
- Schulten R. et al. Comparison of the uptake of 5-aminolevulinic acid and its methyl ester in keratinocytes and skin // Naunyn-Schmiedeberg's archives of pharmacology. – 2012. – Vol. 385(10). – P. 969-979.
- 13. Van Loo E. et al. Surgical excision versus Mohs' micrographic surgery for basal cell carcinoma of the face: a randomised clinical trial with 10 year follow-up // European Journal of Cancer. 2014. Vol. 50(17). P. 3011-3020.
- 14. Zeitouni N. C. et al. 5-aminolevulinic acid photodynamic therapy for the treatment of basal and squamous cell carcinoma: A systematic review // Photodiagnosis and Photodynamic Therapy. 2025. P. 104649.
- Williams H. C. et al. Surgery versus 5% imiquimod for nodular and superficial basal cell carcinoma: 5-year results of the SINS randomized controlled trial //Journal of Investigative Dermatology. – 2017. – Vol. 137(3). – P. 614-619.
- Wang J. Y. et al. Photodynamic Therapy: Clinical Applications in Dermatology //Journal of the American Academy of Dermatology. – 2025.
- Calzavara-Pinton P.G. et al. Methylaminolaevulinate-based photodynamic therapy of Bowen's disease and squamous cell carcinoma // British Journal of Dermatology. – 2008. – Vol. 159(1). – P. 137-144.
- Keyal U. et al. Present and future perspectives of photodynamic therapy for cutaneous squamous cell carcinoma // Journal of the



- Journal of the American Academy of Dermatology, 2019, Vol. 80(3), pp. 765-773.
- Filonenko E.V., Ivanova-Radkevich V.I. Photodynamic therapy of cutaneous squamous cell carcinoma. *Biomedical Photonics*, 2024, Vol. 13(4), pp. 33-39. doi: 10.24931/2413-9432-2024-13-4-33-39
- Filonenko E.V., Ivanova-Radkevich V.I. Photodynamic therapy of Bowen's disease. *Biomedical Photonics*, 2023, Vol. 12(4), pp. 22-29. doi: 10.24931/2413-9432-2023-12-4-22-29
- Kessels J.P.H.M. et al. Treatment of superficial basal cell carcinoma by topical photodynamic therapy with fractionated 5-aminolaevulinic acid 20% vs. two-stage topical methyl aminolaevulinate: results of a randomized controlled trial. *British Journal of Dermatol*ogy, 2018, Vol. 178(5), pp. 1056-1063.
- Van Delft L.C.J. et al. Long-term efficacy of photodynamic therapy with fractionated 5-aminolevulinic acid 20% versus conventional two-stage topical methyl aminolevulinate for superficial basal-cell carcinoma. *Dermatology*, 2022, Vol. 238(6), pp. 1044-1049.
- Salmivuori M. et al. Hexyl aminolevulinate, 5-aminolevulinic acid nanoemulsion and methyl aminolevulinate in photodynamic therapy of non-aggressive basal cell carcinomas: A non-sponsored, randomized, prospective and double-blinded trial. *Journal* of the European Academy of Dermatology and Venereology, 2020, Vol. 34(12), pp. 2781-2788
- Arits A.H.M.M. et al. Photodynamic therapy versus topical imiquimod versus topical fluorouracil for treatment of superficial basal-cell carcinoma: a single blind, non-inferiority, randomised controlled trial. *The lancet oncology*, 2013, Vol. 14(7), pp. 647-654.
- Roozeboom M. H. et al. Three-year follow-up results of photodynamic therapy vs. imiquimod vs. fluorouracil for treatment of superficial basal cell carcinoma: a single-blind, noninferiority, randomized controlled trial. *Journal of Investigative Dermatology*, 2016, Vol. 136(8), pp. 1568-1574.
- Jansen M.H.E. et al. Five-year results of a randomized controlled trial comparing effectiveness of photodynamic therapy, topical imiquimod, and topical 5-fluorouracil in patients with superficial basal cell carcinoma. *Journal of Investigative Dermatology*, 2018, – Vol. 138(3), pp.527-533.
- Morton C.A. et al. A randomized, multinational, noninferiority, phase III trial to evaluate the safety and efficacy of BF-200 aminolaevulinic acid gel vs. methyl aminolaevulinate cream in the treatment of nonaggressive basal cell carcinoma with photodynamic therapy. *British Journal of Dermatology*, 2018, Vol. 179(2), pp. 309-319.
- Tserkovsky D.A., et al. Photodynamic therapy of basal cell skin cancer with the photosensitizer Photolon. *Biomedical Photonics*, 2017, Vol. 6(1), pp. 12-19.
- Mosterd K. et al. Fractionated 5-aminolaevulinic acid-photodynamic therapy vs. surgical excision in the treatment of nodular basal cell carcinoma: results of a randomized controlled trial. *British Journal of Dermatology*, 2008, Vol. 159(4), pp. 864-870.
- Roozeboom M.H. et al. Fractionated 5-aminolevulinic acid photodynamic therapy after partial debulking versus surgical excision for nodular basal cell carcinoma: a randomized controlled trial with at least 5-year follow-up. *Journal of the American Academy of Dermatology*, 2013, Vol. 69(2). – P. 280-287
- 31. Kapinus V.N. et al. Possibilities of photodynamic therapy in the treatment of basal cell skin cancer relapses. *Oncology. Journal named after PA Herzen*, 2013, Vol. 1(4), pp. 40-44.
- de Haas E.R.M. et al. Fractionated illumination significantly improves the response of superficial basal cell carcinoma to aminolevulinic acid photodynamic therapy. *Journal of investigative dermatology*, 2006, Vol. 126(12), pp. 2679-2686
- De Vijlder H.C. et al. Light fractionation significantly improves the response of superficial basal cell carcinoma to aminolaevulinic acid photodynamic therapy: five-year follow-up of a randomized, prospective trial. Acta dermato-venereologica, 2012, Vol. 92(6), pp. 641-647.
- Foley P. et al. Photodynamic therapy with methyl aminolevulinate for primary nodular basal cell carcinoma: results of two randomized studies. *International journal of dermatology*, 2009, Vol. 48(11), pp. 1236-1245.

- American Academy of Dermatology. 2019. Vol. 80(3). P. 765-773
- 19. Filonenko E.V., Ivanova-Radkevich V.I. Photodynamic therapy of cutaneous squamous cell carcinoma // Biomedical Photonics. 2024. Vol. 13(4). P. 33-39.
- Filonenko E.V., Ivanova-Radkevich V.I. Photodynamic therapy of Bowen's disease // Biomedical Photonics. – 2023. – Vol. 12(4). – P. 22-29.
- Kessels J.P.H.M. et al. Treatment of superficial basal cell carcinoma by topical photodynamic therapy with fractionated 5-aminolaevulinic acid 20% vs. two-stage topical methyl aminolaevulinate: results of a randomized controlled trial //British Journal of Dermatology. – 2018. – Vol. 178(5). – P. 1056-1063.
- Van Delft L.C.J. et al. Long-term efficacy of photodynamic therapy with fractionated 5-aminolevulinic acid 20% versus conventional two-stage topical methyl aminolevulinate for superficial basal-cell carcinoma // Dermatology. – 2022. – Vol. 238(6). – P. 1044-1049.
- Salmivuori M. et al. Hexyl aminolevulinate, 5-aminolevulinic acid nanoemulsion and methyl aminolevulinate in photodynamic therapy of non-aggressive basal cell carcinomas: A non-sponsored, randomized, prospective and double-blinded trial // Journal of the European Academy of Dermatology and Venereology. – 2020. – Vol. 34(12). – P. 2781-2788
- Arits A.H.M.M. et al. Photodynamic therapy versus topical imiquimod versus topical fluorouracil for treatment of superficial basal-cell carcinoma: a single blind, non-inferiority, randomised controlled trial // The lancet oncology. – 2013. – Vol. 14(7). – P. 647-654.
- Roozeboom M. H. et al. Three-year follow-up results of photodynamic therapy vs. imiquimod vs. fluorouracil for treatment of superficial basal cell carcinoma: a single-blind, noninferiority, randomized controlled trial // Journal of Investigative Dermatology. – 2016. – Vol. 136(8). – P. 1568-1574.
- Jansen M.H.E. et al. Five-year results of a randomized controlled trial comparing effectiveness of photodynamic therapy, topical imiquimod, and topical 5-fluorouracil in patients with superficial basal cell carcinoma // Journal of Investigative Dermatology. – 2018. – Vol. 138(3). – P. 527-533.
- 27. Morton C.A. et al. A randomized, multinational, noninferiority, phase III trial to evaluate the safety and efficacy of BF-200 aminolaevulinic acid gel vs. methyl aminolaevulinate cream in the treatment of nonaggressive basal cell carcinoma with photodynamic therapy // British Journal of Dermatology. 2018. Vol. 179(2). P. 309-319.
- 28. Церковский Д. А. и др. Фотодинамическая терапия базальноклеточного рака кожи с фотосенсибилизатором фотолон // Biomedical Photonics. – 2017. – Т. 6, № 1. – С. 12-19.
- Mosterd K. et al. Fractionated 5-aminolaevulinic acidphotodynamic therapy vs. surgical excision in the treatment of nodular basal cell carcinoma: results of a randomized controlled trial // British Journal of Dermatology. – 2008. – Vol. 159(4). – P. 864-870.
- 30. Roozeboom M.H. et al. Fractionated 5-aminolevulinic acid photodynamic therapy after partial debulking versus surgical excision for nodular basal cell carcinoma: a randomized controlled trial with at least 5-year follow-up // Journal of the American Academy of Dermatology. 2013. Vol. 69(2). P. 280-287
- 31. Капинус В.Н. и др. Возможности фотодинамической терапии при лечении рецидивов базально-клеточного рака кожи // Онкология. Журнал им. ПА Герцена. 2013. Т. 1, №. 4. С. 40-
- de Haas E.R.M. et al. Fractionated illumination significantly improves the response of superficial basal cell carcinoma to aminolevulinic acid photodynamic therapy //Journal of investigative dermatology. – 2006. – Vol. 126(12). – P. 2679-2686
- De Vijlder H.C. et al. Light fractionation significantly improves the response of superficial basal cell carcinoma to aminolaevulinic acid photodynamic therapy: five-year follow-up of a randomized, prospective trial // Acta dermato-venereologica. – 2012. – Vol. 92(6). – P. 641-647.
- Foley P. et al. Photodynamic therapy with methyl aminolevulinate for primary nodular basal cell carcinoma: results of two randomized studies // International journal of dermatology. – 2009. – Vol. 48(11). – P. 1236-1245.

REVIEWS OF LITERATURE

- 35. Basset-Seguin N. et al. Topical methyl aminolaevulinate photodynamic therapy versus cryotherapy for superficial basal cell carcinoma: a 5 year randomized trial. European Journal of dermatology,
- 2008, Vol. 18(5), pp. 547-553.
 36. Šmucler R., Vlk M. Combination of Er: YAG laser and photodynamic therapy in the treatment of nodular basal cell carcinoma. Lasers in Surgery and Medicine: The Official Journal of the American Society for Laser Medicine and Surgery, 2008, Vol. 40(2), pp. 153-158.
- 37. Rhodes L. E. et al. Photodynamic therapy using topical methyl aminolevulinate vs surgeryfor nodular basal cell carcinoma: results of a multicenter randomized prospective trial. *Archives of dermatology*, 2004, Vol. 140(1), pp. 17-23.
- Rhodes L. E. et al. Five-year follow-up of a randomized, prospective trial of topical methyl aminolevulinate photodynamic therapy vs surgery for nodular basal cell carcinoma. *Archives of dermatology*, 2007, Vol. 143(9), pp. 1131-1136
- Berroeta L. et al. A randomized study of minimal curettage followed by topical photodynamic therapy compared with surgical excision for low-risk nodular basal cell carcinoma. *British Journal of Dermatology*, 2007, Vol. 157(2), pp. 401-403.

- 35. Basset-Seguin N. et al. Topical methyl aminolaevulinate photodynamic therapy versus cryotherapy for superficial basal cell carcinoma: a 5 year randomized trial //European Journal of dermatology. 2008. Vol. 18(5). P. 547-553.
- Šmucler R., Vlk M. Combination of Er: YAG laser and photodynamic therapy in the treatment of nodular basal cell carcinoma // Lasers in Surgery and Medicine: The Official Journal of the American Society for Laser Medicine and Surgery. – 2008. – Vol. 40(2). – P. 153-158.
- 37. Rhodes L. E. et al. Photodynamic therapy using topical methyl aminolevulinate vs surgeryfor nodular basal cell carcinoma: results of a multicenter randomized prospective trial //Archives of dermatology. 2004. Vol. 140(1). P. 17-23.
- 38. Rhodes L. E. et al. Five-year follow-up of a randomized, prospective trial of topical methyl aminolevulinate photodynamic therapy vs surgery for nodular basal cell carcinoma //Archives of dermatology. 2007. Vol. 143(9). P. 1131-1136
- 39. Berroeta L. et al. A randomized study of minimal curettage followed by topical photodynamic therapy compared with surgical excision for low-risk nodular basal cell carcinoma // British Journal of Dermatology. 2007. Vol. 157(2). P. 401-403.

ФОТОСЕНСИБИЛИЗАТОРЫ нового поколения для фотодинамической терапии

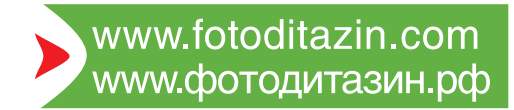


«ФОТОДИТАЗИН®» концентрат для приготовления раствора для инфузий — лекарственное средство (РУ № ЛС 001246 от 18.05.2012 г.) «ФОТОДИТАЗИН®» гель — изделие медицинского назначения (РУ № ФСР 2012/13043 от 03.02.2012 г.) «ФОТОДИТАГЕЛЬ®» — косметическое средство (ДС ЕАЭС № RU Д-RU.НВ42.В.06108/20 от 24.09.2020 г.)

Препараты применяются для флюоресцентной диагностики и фотодинамической терапии злокачественных новообразований, а также патологий неонкологического характера в следующих областях медицины:

- **С** гинекология
- урология
- нейрохирургия
- **У** торакальная хирургия
- офтальмология
- **У** травматология

- 🗸 ортопедия
- комбустиология
- У гнойная хирургия
- **У** дерматология
- косметология
- стоматология





123056, г. Москва, ул. Красина, д. 27, стр. 2 Тел.: +7 (499) 250-40-00, +7 (929) 971-44-46 E-mail: veta-grand@mail.ru









